UiT
THE ARCTIC
UNIVERSITY
OF NORWAY

Faculty of Science and Technology
Department of Physics and Technology

Case Study of a Large-Scale Solar, Wind and Hydro Power Hybrid System in Skibotndalen, Troms

Karoline Ingebrigtsen

EOM-3901 Master's thesis in Energy, Climate and Environment - June 2017

The front page image is from http://www.cmf-co.com/blog/

Abstract

The power company *Troms Kraft* is interested in the feasibility of a large-scale hybrid system in Skibotndalen in Troms. There are two existing hydro power stations in the area, and this thesis concerns the addition of an electric solar power plant of 20 MW and a wind power plant of 21 MW to these stations. As measured solar radiation is not available for one whole year at the location, solar radiation data is simulated by using the acknowledged Weather Research and Forecasting Model (WRF) tool for weather prediction. The technical performance of the hybrid system is simulated by using the software HOMER Pro, and by request from *Troms Kraft*, a simple economic analysis of the system is also done. The simulated solar radiation data overestimates the solar resource, but this is taken into account by scaling the data. However, correction of timing errors of the simulated data is not included.

In a hybrid system between several energy resources, a complementary nature between the resources is advantageous. Therefore, the anti-correlation between the solar and wind resource in the area is examined. Using simulated solar radiation values for 2016, a moderate negative correlation is found on longer time-scales such as weekly and monthly. Using measured values from the first four months of 2017, the anti-correlation is moderate on a weekly basis, and very high on a monthly basis. Using shorter time scales resulted in low to none anti-correlation. Both the solar and wind resource is found to be above what is required for feasibility for power production.

The results show that the technical feasibility of the system is good, but as there are large uncertainties in inter alia the simulated solar resource and because the losses in the power output due to turbulence are not included in the simulations, sensitivity analyses are done on these and other technical parameters. The interaction with the existing hydro power station is also examined. The economic analysis shows that the system is not profitable, but sensitivity analyses and a simulation of a future scenario with lower costs and higher efficiencies shows that the system can turn out to be profitable under certain conditions.

Acknowledgements

Writing my master's thesis may be one of the hardest and most stressful things I have ever done. But it has also been one of my most educational experiences! It has been a journey of ups and downs, of exasperations and revelations. It has inspired me to continue working with renewable energy. And it has now come to an end. I want to thank my supervisor, professor Tobias Boström, for advice, discussions and feedback, even if this semester happened to coincide with his parental leave. I appreciate all help from my co-supervisor at Troms Kraft, Svein Erik Thyrhaug, who answered my questions even late in the evenings, and provided me with the data I needed. A special thanks to Yngve Birkelund for simulating solar radiation data, without it this thesis would not be able to analyse the hybrid system during one whole year (quite essential for renewable energy feasibility, right?). Øystein Kleven at *Solbes* has offered his time to discuss the economics of photovoltaic systems in northern Norway, and I am grateful for that.

After five years of studying hard, I have gained an awful lot of knowledge, but also friends and unforgettable memories. Thanks to my fellow students for giving me five inspiring, exciting and fun years! A special thanks to my office mates, for discussions, coffee, dinner times, laughs, and always cheering each other on. To my "partner in crime", Charlotte Tiller, who has had the same struggles and inspiring moments as myself, and who shares my interests, thank you for useful (and non-useful) discussions, for good ideas, for asking the right questions, for inspiring me to always seek more knowledge, and for ditching the summer body together with me.

Finally, I want to thank family (thank you little sister Ingeborg for surprising me with that cinnamon bun when I needed it) and friends for bearing with me through five hectic years, and especially Morten, who has been standing by my side.

Karoline Ingebrigtsen
Tromsø, June 2017

Contents

List of Figures

List of Tables

Abbreviations

AC alternating current

AM Air Mass

BOSCO both sides collecting and contacted

BSF back surface field

DC direct current

DEM Digital Elevation Model

ECMWF European Centre for Medium-Range Weather Forecasts

EoT Equation of Time

GHI global horizontal irradiation

GIS Geographic Information Systems

GPS Global Positioning Systems

IRR Internal Rate of Return

LST Local Solar Time

LT Local Time

MPPT maximum power point tracking

NNM Non-hydrostatic Mesoscale Model

NOCT Nominal Operating Cell Temperature

NPV Net Present Value

PERT passivated emitter, rear totally diffused

PV photovoltaic

RMSE Root Mean Square Error

STC Standard Test Conditions

WRF Weather Research and Forecasting

WT wind turbine

Nomenclature

Symbol	Description	Unit
θ	Solar zenith angle	degrees
α	Solar elevation angle	degrees
Φ	Solar azimuth angle	degrees
δ	Declination angle	degrees
ϕ	Latitude	degrees
λ_{long}	Longitude	degrees
β	Tilt angle of PV modules	degrees
LT	Local Time	minutes
LST	Local Solar Time	minutes
LSTM	Local Standard Time Meridian	minutes
GMT	Greenwich Mean Time	hours
ΔT_{GMT}	Difference between LT in hours and GMT	hours
d	the number of day	
HRA	Hour Angle	degrees
V	Bias voltage	Voltage [V]
T	Temperature	$^{\circ}C$
I_0	Dark current	Ampere [A]
I_r	Recombination current	Ampere [A]
I_j	Net junction current	Ampere [A]
I	External circuit current	Ampere [A]
I_{sc}	Short-circuit current	Ampere [A]
V_{oc}	Open-circuit voltage	Voltage [V]
I_m	Maximum current	Ampere [A]
V_m	Maximum voltage	Voltage [V]
P_m	Maximum power	Watt [W]
η	Electrical conversion efficiency	unitless
P_{in}	Power input	Watt [W]

Symbol	Description	Unit
$P_{\text{available}}$	Available power in wind	Watt [W]
A	Spanned area of wind turbine blades	m^2
$P_{\text{available per unit area}}$	Available power in wind per unit area	W/m^2
u_{wind}	Wind speed	m/s
$u_{\text{wind}}*$	Friction velocity	m/s
z	Height above Earth's surface	meters [m]
z_0	Surface roughness length	meters [m]
z_r	Reference height	meters [m]
C_p	Power coefficient	unitless
P_{rated}	Rated power of wind turbine	Watt [W]
$P_{\text{theoretical}}$	Theoretical power from water reservoir	Watt [W]
H	Height of water reservoir	meters [m]
H_{eff}	Effective height of water reservoir	
Q	Volumetric flow rate	m^3/s
η_t	Hydro power turbine efficiency	unitless
i	discount rate	%
I_0	Initial investment cost	NOK
C_t	Costs in year t	NOK
R_t	Revenues in year t	NOK
E_t	Electricity generated in year t	Watt-hours [Wh]

Constants

Symbol	Description	Unit	Value
e_0	Electron charge	Coulomb [C]	$1.602 \cdot 10^{-19}$
k	Boltzmann constant	J/K	$1.381 \cdot 10^{-23}$
ρ_{air}	Density of air	kg/m^3	1.225 at STC
g	Gravitational acceleration	m/s^2	9.81
ρ_w	Density of water	kg/m^3	10^3 kg/m^3

1 Introduction

The energy demand in the world is increasing [(IEA), 2016], and the focus on renewable energy has increased drastically. In every year in the period 2010-2014, around 50% of the added energy capacity has been from renewables [IRENA, 2015].

A recognised challenge with renewable sources such as solar and wind energy is their variability [IEC, 2012]. Connecting renewable power plants to the grid can therefore cause controlling problems if the electricity network is not designed for handling such variations. A substantial amount of research is therefore being performed on hybrid systems, combining several renewable, and in some cases conventional, power plants. This has the advantage that the variability of the renewable sources can be decreased, because the variable power output can be levelled out either due to a complementary nature between renewable resources or by other energy sources that are easier to control, for example hydropower. It is the case in some locations that the solar and wind resource has an anti-correlation, complementing each other and giving a less variable output than each of the resources would if exploited independently [Diaf et al., 2008].

The power company *Troms Kraft* has estimated that in the county of Troms, there has since 2002 been an electricity deficit of approximately 871 GWh each year [Troms Kraft, 2014]. Large-scale hybrid systems have not yet been constructed in Northern Norway, but can contribute to a decrease in this deficiency and to an electricity independence of Troms. *Troms Kraft* is interested

in the feasibility of hybrid systems in Troms, and this thesis is written in collaboration with *Troms Kraft*. The company is also interested in a hybrid system at another location in Northern Norway, namely *Fakken*, where the addition of a solar power plant to the wind power plant already existing at the location should be examined. A master's thesis is therefore also performed on the feasibility of this location by Charlotte Tiller [Tiller, 2017], and the results in the two theses are compared in the end of this thesis.

Skibotn is known to be one of the driest areas in Norway [Ovhed, 2016], which implies that there may be a superior solar resource here compared to other locations. This is a very interesting aspect, and will be examined in this thesis. In addition, the climate in northern Norway is cold, which is advatageous considering that the efficiency of PV modules increases with decreasing temperature [Solanki, 2015]. It also leads to a higher available energy in the wind, because the air density is higher at lower temperatures [Gipe, 2004]. Some of the mountains surrounding Skibotndalen has large wind resources compared to nearby locations [Kjeller Vindteknikk, 2009]. In addition, Skibotndalen has many snow days during the year, creating high reflectance of the solar radiation reaching the ground, which increases the amount of radiation reaching the PV modules.

1.1 Objective of the study

The objective of this thesis is to examine the technical performance and feasibility of a large-scale grid-connected hybrid system in Skibotndalen in Troms. The system consists of a 20 MW PV power plant and a 21 MW wind power plant, and will be operated in combination with two existing hydro power stations in Skibotn with a total capacity of 80.5 MW. The performance of the system is achieved by using the hybrid system simulation software HOMER Pro, and both stationary modules and tracking systems for the PV power plant are simulated. By request from *Troms Kraft*, also a simple economic analysis is done to assess the feasibility of the hybrid system.

Weather data is acquired from different sources, both measured and simulated. A solar sensor was installed at a location called Galgo in December 2016 at the site. However, as the system should be simulated over at least the period of one year to get an impression of its performance during all seasons, simulated solar data from 2016 at the same location as the solar sensor was installed is used. The data is simulated using the Weather Research and Forecasting (WRF) model, which is an acknowledged tool for weather prediction. A simulation of the solar resource is done for Holt at the island of Tromsø as well, so that the representativeness of the simulated data can be analysed. Wind resource data

is received from *The Norwegian Meteorological Institute* from a location nearby the solar sensor called Rieppi.

Because there are uncertainties in the weather data, a sensitivity analysis is done on these parameters both in the technical and economic analysis. Also parameters such as the efficiency and slope of the PV modules and wind turbine losses are varied to examine the change in performance of the system. Cost information on PV and wind components in northern Norway is not easily available, and the future development of electricity prices are very uncertain, hence these and other economic parameters are varied in the economic analysis.

1.2 Structure of the thesis

Excluding the introduction, the thesis consists of the following five chapters:

Chapter 2: a theoretical background is given for the components of the hybrid system, connecting a hybrid system to the grid, the WRF model and statistical and financial methods for analysing data

Chapter 3: describes the potential site for the hybrid system

Chapter 4: presents the methodology used in the thesis, including data and their sources, the simulation inputs and the processing of the simulation results

Chapter 5: the results from an examination of the representativeness of the simulated solar data, a comparison of the solar resource at different locations, a correlation analysis on the wind and solar resource at the site and the technical and economic results from the simulation are presented, and the results are discussed. Sources of errors are also discussed, and a comparison of the potential renewable resource at Fakken and in Skibotndalen is performed

Chapter 6: provides a summary of the most important findings and is closed by a section regarding further work which should be performed to improve this study and develop the project of a large-scale hybrid system in Northern Norway further

2

Theoretical background

2.1 Electrical solar energy

2.1.1 The solar resource

The amount of solar radiation at the top of the Earth's atmosphere is measured by satellites to be $1366 \pm 7\,\mathrm{W/m^2}$ [Sengupta et al., 2015]. This number is relatively constant (only varying slightly because of solar activity), but the radiation that reaches the Earth's surface is influenced by several factors.

As the radiation travels through the atmosphere, some of it is absorbed and some is scattered. Gas molecules change the *spectral content* of the radiation as specific gas molecules absorb specific wavelengths. Absorption by air molecules and dust, on the other hand, has a larger impact on the incident *radiation power* on the Earth's surface, depending on the length of the path which the radiation travels through the atmosphere [Honsberg and Bowden, 2015]. This path length is influenced by the position of the location on Earth and the position of the Sun in the sky and is also called AM [Sengupta et al., 2015]. AM is the path length standardised to the path length when the sun is at its highest [Honsberg and Bowden, 2015]:

$$AM = \frac{Y}{X} = \frac{1}{\cos(\theta)}$$

where X, Y and θ are as shown in Figure 2.1. The angle between X and Y is called the zenith angle [Honsberg and Bowden, 2015].

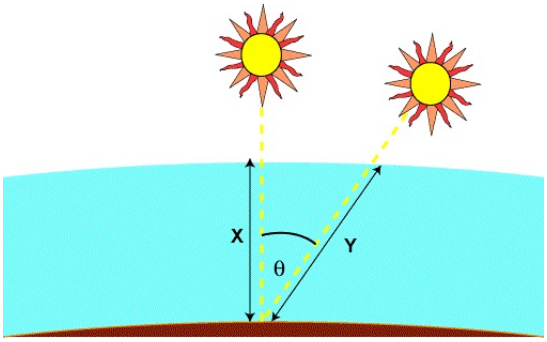

Figure 2.1: Calculating AM. From [Honsberg and Bowden, 2015]

Particles in the atmosphere in addition scatters a portion of the incident radiation; it spreads the radiation. The amount and wavelength scattered depends on the physical properties of the molecules and particles. The longer the path through the atmosphere, the more scattering occurs [Sengupta et al., 2015]. Clouds also scatter some of the incident radiation, and hence reduces the power reaching the surface of the Earth [Honsberg and Bowden, 2015]. In addition, the ground and other objects will reflect some radiation depending on their albedo (the percentage of incident solar radiation being reflected from a specific surface).

As a consequence of the scattering of solar radiation, there are two types of radiation: direct and diffuse. The direct radiation reaches the surface without being scattered or absorbed [Sengupta et al., 2015], whereas the diffuse light has no specific direction and hence it is observed as coming from all directions in the sky. In addition, the reflected light can be seen as a third component of the solar radiation.

The shorter-term variability caused by the effect of clouds in combination with their movement can change the radiation substantially in time periods of seconds and minutes, and is complicated to predict [Perez and Hoff, 2013].

2.1.2 Calculating the solar path

Also the rotation of the Earth has an effect on the variability of the solar resource; as the Earth rotates, the Sun occurs to be moving in the sky. This affects the angle in which the direct radiation impinge on the ground [Honsberg and Bowden, 2015]. However, this variability is relatively easy to predict, and has largest effect in a longer time interval (hours or days), and in particular during sunrise and sunset [Perez and Hoff, 2013].

Two parameters are needed to describe the solar path:

- Elevation angle α: The angle between the incident sunlight and the horizontal [Honsberg and Bowden, 2015].
- Azimuth angle Φ: the horizontal direction from which the sunlight is coming [Honsberg and Bowden, 2015].

Twelve noon in local time (LT) at a location is usually different than the time the Sun is highest in the sky, which is called twelve noon Local Solar Time (LST). This is inter alia because of the eccentricity of the Earth. In addition, there is variation within a time zone because longitude varies within a time zone. To correct for this, the LST can be written in hours as [Solanki, 2015], [Honsberg and Bowden, 2015]:

$$\text{LST} = \text{LT} + \frac{1}{15}\lambda_{long} - \Delta T_{GMT} + \text{EoT}$$

Where λ_{long} is longitude (longitudes to the west are negative) and ΔT_{GMT} is the difference between the Local Time (LT) and the Greenwich Mean Time (GMT) in hours. The Equation of Time (EOT) is an empirical equation which takes into account the eccentricity of the Earth. Several versions of the EOT has been developed, and the one relevant for this thesis is shown in Equation D.1 in Appendix D. The calculated LST can be converted from hours to the number of degrees the Sun moves by the following equation:

$$\text{HRA} = 15°(\text{LST} - 12) \tag{2.1}$$

Where HRA is called the hour angle, and it is zero at solar noon, and ranges from -180°to 180°. The Sun thus moves 15°each hour. The elevation angle is then calculated as:

$$\alpha = \sin^{-1}(\sin(\delta)\sin(\phi) + \cos(\delta)\cos(\phi)\cos(\text{HRA}))$$

Where ϕ is the latitude of the location in interest. δ is the declination angle; the tilt of the Earth. It varies from -23.45°in December solstice to +23.45°in June solstice and to -23.45°in December solstice again [Honsberg and Bowden, 2015]. The declination angle is zero twice during a year, in March and September [Solanki, 2015]. It is calculated by [Honsberg and Bowden, 2015]:

$$\delta = 23.45° \cdot \sin(\frac{360°}{365}(d + 284))$$

And the azimuth is calculated as [Honsberg and Bowden, 2015]:

$$\Phi = \cos^{-1}\left(\frac{\sin(\delta)\cos(\theta) - \cos(\delta)\sin(\theta)\cos(\text{HRA})}{\cos(\alpha)}\right)$$

Where in this formula, an azimuth angle of o°represents north. A method to calculate the the incident solar radiation on a tilted surface from the solar radiation incident on a horizontal surface is described in Appendix D.

2.1.3 Structure of a photovoltaic (PV) cell

PV cells are produced from semiconductors, which are materials that only conduct when electrons are excited to a higher energy level in the atoms of the material. When an electron is excited, it leaves behind a vacancy which is referred to as a *hole*. A semiconductor can be p-doped or n-doped, and these two types of semiconductors be combined in a p-n junction, which is what a solar cell is comprised of. Electrons are majority charge carriers in an n-doped material and the holes are minority charge carriers, and vice versa in a p-doped material [Nelson, 2003]. In a p-n junction, an electric field exists from the n-side to the p-side, resulting in a drift current of electrons to the n-side and holes to the p-side [Andrews and Jelley, 2007]. When light is shining on a solar cell, photons that possess an energy higher than the band gap of the silicon atoms have the opportunity to excite electrons.

The following IV-equation describes the current that flows through the external circuit of a PV cell under illumination:

$$I = I_{sc} - I_0[e^{\frac{e_0 V}{kT}} - 1] \tag{2.2}$$

Here, I_0 is called the dark current and I_{sc} is the short circuit current, which is the maximum current a PV cell can produce, and it depends on how large fraction of the incident photons have enough energy to excite electrons in the semiconductor [Solanki, 2015]. $e_0 = 1.602 \cdot 10^{-19}$ C is the electron charge and $k = 1.381 \cdot 10^{-23}$ is the Boltzmann constant [Kreith, 2014].

Figure 2.2 shows a typical curent-voltage (I-V) curve for a PV cell under illumination. When the junction is short-circuited $V = 0$ and $I = I_{sc}$, and when the junction is open-circuited $I = 0$ and $V = V_{oc}$ [Kreith, 2014]. The open-circuit voltage V_{oc} is the maximum voltage over the PV cell.

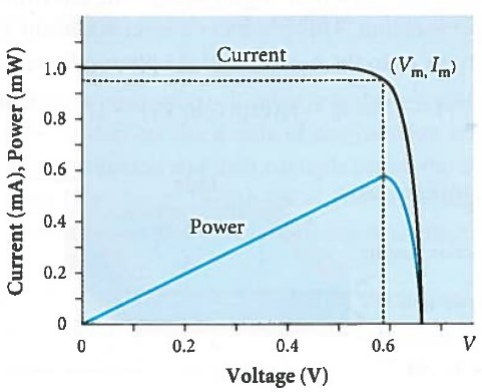

Figure 2.2: A typical current-voltage curve for a PV cell [Andrews and Jelley, 2007]

A power curve is also included in Figure 2.2. See that the power has a maximum, P_m, which occurs at $I = I_m$ and $V = V_m$.

The definition of electrical conversion efficiency at maximum power point operation is:

$$\eta = \frac{P_m}{P_{in}} \tag{2.3}$$

2.1.4 Efficiency and power of PV cells

In November 2016, the highest confirmed efficiency of a silicon solar cell was 26.3% [Green et al., 2017]. In [NREL, 2017], the best research-cell efficiency of silicon PV cells are given as approximately 22%-25%.

The efficiency of PV cells and modules are tested under Standard Test Conditions (STC): solar irradiation of 1000 W/m^2, a solar spectrum with AM equal to 1.5 and the temperature of the cell or module being 25 °C [Solanki, 2015]. The power output under these conditions is called the rated power output or peak power, denoted kW_p.

However, STC are not very realistic conditions, as the solar radiation is usually lower than this definition and the temperature of the cell or module is usually higher than 25 °C. Therefore, also a parameter called Nominal Operating Cell Temperature (NOCT) is used. It is the temperature a cell achieves when connected in an open circuited module (implying an efficiency of zero) that is mounted with open back side under a radiation of 800 W/m^2 and ambient temperature of 20 °C [Solanki, 2015].

The degradation factor of a PV module quantifies the maximum output power over the module's lifetime. PV modules always has a decline in maximum power output during its lifetime which can be due to the quality of the material, the way the p-n junction is structured etc, and a typical value is reported in [Jordan and Kurtz, 2012] to be 0.5% each year.

The degradation factor must not be confused with the derating factor. Because a PV module will not produce the same output in real conditions as in STC, a derating factor can be defined, which represents how large a fraction of the STC efficiency the module operates with under real conditions, when effects of soil and dust on the modules, shading, snow, aging and losses in wiring are included [HOMER Energy, 2016]. A typical derating factor for PV modules is in the range $0.62 - 0.92\,\%$ [Roberts et al., 2017].

The angle between the PV module and the ground (the tilt or slope angle) also has an effect on the power output, and it is claimed in [Honsberg and Bowden, 2015] that often a tilt angle equal to the latitude of the location is optimal.

There exists several models for calculating the power output from a PV cell or module under certain conditions, and the one relevant for this thesis is specified in Appendix D.

Effect of solar radiation and temperature on efficiency

In [Solanki, 2015] and [Honsberg and Bowden, 2015], the efficiency of solar cells is found to decrease with increasing temperature of the cell, and increase with amount of solar radiation. Even though increased radiation causes a higher temperature of the cell, the increase in efficiency because of increased radiation is larger than the effect of the increased temperature. A typical range for the temperature coefficient for silicon PV modules is $-0.5\,\%\text{ change in efficiency}/^{\circ}\text{C}$ to $-0.4\,\%\text{ change in efficiency}/^{\circ}\text{C}$ [Hasanuzzaman et al., 2016]. A model for quantifying the temperature of the modules given the ambient temperature is given in Appendix D.

The fact that the efficiency of PV cells increases in colder climates is advantageous for the area considered in this thesis; northern Norway.

Effect of albedo on PV power output

The type of terrain in the area where PV systems are mounted can affect the power output from the cells. A higher albedo leads to a larger amount of reflected radiation which can reach the PV cells. An overview of the approximate

albedo of different types of vegetation is shown in Table 2.1.

Table 2.1: Approximate albedos of different vegetation types. From [Quaschning, 2005] and [Gerrard, 1990]

Vegetation	Albedo
Grass (summer)	0.25
High mountain grassland	0.12-0.25
Dry grass	0.28-0.32
Uncultivated fields	0.26
Soil	0.17
Heathland and sand	0.10-0.25
Bare rock	0.05-0.15
Fresh snow cover	0.80-0.90
Old snow cover	0.45-0.70
Water ($\alpha > 45°$)	0.05
Water ($\alpha > 30°$)	0.08
Water ($\alpha > 20°$)	0.12
Water ($\alpha > 10°$)	0.22

2.1.5 PV systems

Modules and arrays

Several single PV cells can be connected together to form modules [Honsberg and Bowden, 2015]. They are enclosed in different materials that act to protect the cells and electrical connections between them from the rough outdoor environment they may have to endure [Kalogirou, 2014]. For grid-connected systems a module typically consists of 60 to 72 cells [Howell,]. Modules can in turn be connected together to form arrays, having parallel branches with a pre-determined number of series connected modules in each branch. This is examined more thoroughly in Subsection 2.5.2.

Mismatch and shading

When solar cells of different characteristics are connected together, mismatch occurs, and the result may be a power loss. Mismatch can also be due to shading, which affects the output power of the shaded solar cell(s), and this will reduce the output power from the whole module [Honsberg and Bowden, 2015]. It is found in [Silvestre and Chouder, 2008] that the loss of power increases with increased radiation (W/m^2).

In a series connection of several solar cells, shading may lead to hot spot heating. The shaded cell will have a reduced short-circuit current. As explained in [Solanki, 2015] and [Wohlgemuth and Hermann, 2005], if the current of the unshaded cells becomes larger than the shaded cell's I_{sc}, the forward biased voltage of the unshaded cells will reverse bias the shaded cell which in turn will cause this cell to dissipate power. If this reverse bias is very large, the cell can become extremely warm and may be damaged and even melt. To prevent hot spot heating, bypass diodes can be installed, which are connected in parallel with each of the cells in the series connection, with the opposite polarity than the cell. The reverse bias across the shaded cell will thus forward bias the diode and the current is diverted away from the shaded cell.

Because the modules are enclosed and framed, the heat does not flow as easily away from the cells. Thus, a module may have a higher temperature than separate cells, causing the efficiency to decrease [Honsberg and Bowden, 2015]. Mismatch can occur in the case of arrays as well, and bypass diodes can be fitted to bypass whole modules [Honsberg and Bowden, 2015].

2.1.6 Methods for increasing the efficiency of PV cells and modules

Tracking system

By using a tracking system, solar modules can move so as to always face the Sun, increasing the direct solar radiation received and absorbed by the solar cells. The tracking system can either be vertical single-axis, in which movement is possible in the east-west direction, horixontal single-axis, where the tilt of the modules can change, or two-axis, where variation of both the east-west direction and tilt is possible [Al-Mohamad, 2004].

There are two main ways of implementing tracking systems; either sensors are used to direct the modules towards the brightest spot in the sky, or the position of the Sun can be calculated and the modules are always facing the calculated position of the Sun (astronomical tracking). For the simulations in this thesis, the astronomical method is used, and the calculations of the solar path are explained in more detail in Subsection 2.1.2 and Appendix D.

Because the direct radiation reaching the PV module increases when using tracking systems, there is an energy yield gain of PV systems with tracking. However, the gain varies drastically with latitude. A one-axis tracking system at middle European latitudes can typically result in a 20% increase in output compared with fixed tilted modules, and two-axis system an increase of 30%. On higher latitudes on days with a high amount of direct radiation the energy gain

can be of the order of 50% in summer and 300% in winter [Quaschning, 2005]. In [Mousazadeh et al., 2009], it is stated that of the energy gain that is achieved when employing tracking systems, approximately 2-3% of this is consumed by the tracking system motors themselves. It is also important to notice that on days with overcast weather, there may be a reduction in energy gain, as such weather causes higher amounts of diffuse radiation that comes from all directions in the sky and not just from the Sun's position. In such conditions it can be more expedient to place the modules horizontally.

Tracking systems inherit a large cost and have therefore not yet become widely used [Rizk and Chaiko, 2008]. Because one-axis tracking is less expensive and less complicated than two-axis tracking but still have a quite large energy gain, one-axis tracking may have the highest overall advantage from both the technical and economic perspective. But also this depends on both latitude and direct and diffuse radiation levels.

Bifacial modules

Bifacial PV modules absorb sunlight at both the front and rear side. Where the back side on regular PV cells is covered by a opaque contact surface, the bifacial ones have a similar structure on the back side as the front side. This can enhance the output power compared to monofacial PV cells, and give a higher efficiency using the same amount of silicon material, resulting in a lower cost of energy, as bifacial cells and monofacial cells are available at approximately the same cost [Joge et al., 2002].

The radiation received by the back surface comes from diffusive and reflective components of the solar radiation. The reflective radiation can either be reflected from the ground or from objects in near vicinity of the modules. The amount of radiation reflected from the ground depends on the albedo of the surface and the amount of radiation which is incident on the ground [Hansen et al., 2016]. If the Sun is low in the sky and is positioned behind the solar panel, direct radiation will also reach the back surface.

For northern areas, bifacial modules can be an especially effective solution to obtain a higher power output from a solar plant, as the area has large snow-covered areas (thus with high albedo) during a substantial portion of the year. In addition, the Sun does not set during the summer months, and bifacial modules can exploit this direct radiation.

2.2 Electrical wind energy

2.2.1 The wind resource

As the Sun shines on the Earth, the radiation hits the surface at different angles depending on the latitude. Hence, an horizontal area near the equator receives more radiation than horizontal areas at higher latitudes. This uneven heating causes the air near the equator to be less dense than the surrounding air, resulting in a low-pressure region as the air rises to the tropopause [Taylor, 2012]. This air will then move north- and southwards, and at approximately latitude ±30°, it becomes unstable and sinks [Andrews and Jelley, 2007]. In [Taylor, 2012], the formation of three different cells are explained:

Some of the sinking air that reaches the surface at ±30° latitude moves back towards the equator, creating what is called the "trade winds". The circulation of air from the equator and back to the equator is often called the Hadley cell. The rest of the air at the surface at ±30° is pushed towards the poles. Because this air is warmer and less dense than the air near the poles, it rises at approximately ±60° latitude. A portion of this air moves towards latitude ±30° again, resulting in another cell, called the Ferrel cell. The rest of the rising air at ±60° will move towards the poles, closing the circulation of the polar cell.

Rising and sinking air causes pressure gradients, in which the direction of the force is towards lower pressure. Figure 2.3 shows the structure of the cells as blue circles just above the surface of the Earth.

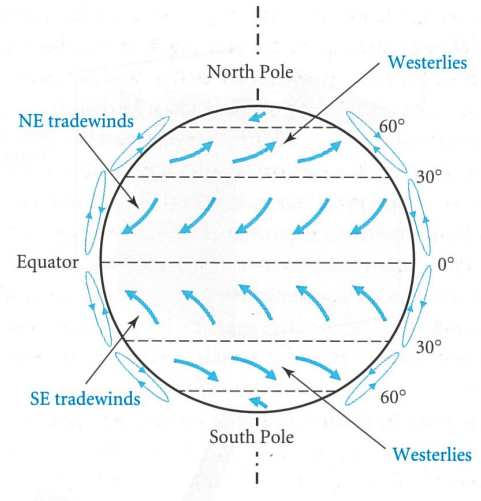

Figure 2.3: A simplified model of the wind in the atmosphere. From [Andrews and Jelley, 2007]

A more realistic model of the global wind pattern is obtained by including the effects which the rotation of the Earth has on the movement of air; the Coriolis force. The rotation causes the eastward velocity of a fixed point on Earth's surface to be largest at the equator and decreasing towards the poles [Andrews and Jelley, 2007]. Hence, because of conservation of angular momentum, as air flows from the equator in the direction of one of the poles, the distance to the axis of rotation decreases and hence the velocity in the eastward direction must increase, and the parcel is deflected eastwards. The air is similarly deflected in the westward direction when flowing towards the equator. The net result of this is shown by blue arrows in Figure 2.3. The direction of the Coriolis force is always normal to the direction the air is moving.

When the pressure force and Coriolis force balance each other, the result is called geostrophic wind, and the result is a wind parallel to the isobars in the atmosphere. See Figure 2.4 for the development of such a balance.

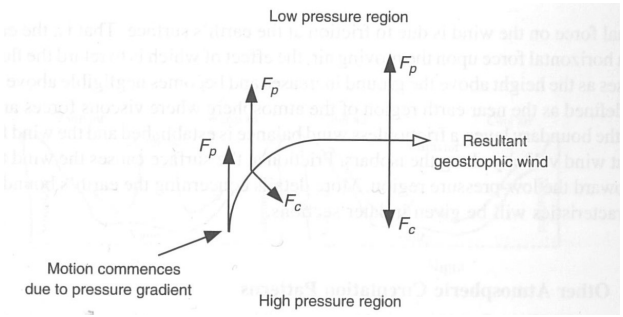

Figure 2.4: The development of geostrophic wind. From [Manwell et al., 2009]

Another fictive force that is important for the global wind pattern is the centrifugal force. In reality isobars are curved, and the consequence of this is that a parcel moving parallel to the isobars experiences a centrifugal force outwards from the curve. The balance between the pressure force, Coriolis force and centrifugal force results in a wind called gradient wind, parallel to the curved isobars [Manwell et al., 2009], as shown in Figure 2.5.

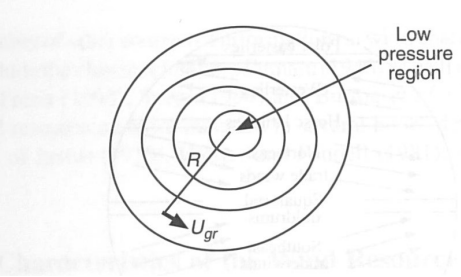

Figure 2.5: The gradient wind. From [Manwell et al., 2009]

Finally, the friction between the wind and Earth's surface will influence the global wind pattern. The friction force is directed in the opposite direction of the air flow and acts near the surface, diminishing at higher altitudes [Manwell et al., 2009].

Considering the mentioned four forces gives a good approximation for the wind pattern on Earth, but it is important to remember that the topography and landscape along with local temperature changes and other local phenomena will have a considerable effect on this idealised model. Therefore local and short-term wind conditions are difficult to predict.

Available power in the wind

The available power in wind with speed u incident at a turbine with area A is [Andrews and Jelley, 2007]:

$$P_{\text{available}} = \frac{1}{2}\rho_{\text{air}} A u_{\text{wind}}^3$$

Where ρ_{air} is the density of air, which is $1.225\ ^{\text{kg}}/_{\text{m}^3}$ at STC, and increases with decreasing temperature [Gipe, 2004]. See that the power available in the wind is proportional to the cubed wind speed, and thus a small increase in the wind speed will cause large changes in the power. To calculate the available power per unit area ($^{\text{W}}/_{\text{m}^2}$), the following equation can be used:

$$P_{\text{available per unit area}} = \frac{1}{2}\rho_{\text{air}} u_{\text{wind}}^3 \tag{2.4}$$

It is stated in [Aarrestad and Hatlen, 2015] that an average wind speed of $6.5\ ^{\text{m}}/_{\text{s}}$ at hub height is considered a rule of thumb for classifying the feasibility of electrical wind power at a location as good.

2.2.2 Vertical wind speed profile

The wind speed increases with height in the lower atmosphere, and there exists several models for the vertical wind speed gradient. The logarithmic profile is used in this thesis, and hence explained here.

Logarithmic profile

Can be derived in a number of ways from theoretical fluid mechanics and empirical research. Assumptions in the derivation is that the pressure is independent of height and the pressure gradient is very small near the surface and that the surface is smooth. The resulting model for wind speed at a height z is [Manwell et al., 2009]:

$$u_{\text{wind}}(z) = \frac{u_{\text{wind}}*}{K}\ln\left(\frac{z}{z_0}\right) \tag{2.5}$$

Where $u_{\text{wind}}*$ is defined as friction velocity, K is called von Karman's constant and has a value of 0.4, and z_0 is a characterisation of the roughness of the terrain on the ground, called the roughness length. Typical roughness lengths are shown in Table 2.2.

Table 2.2: Typical roughness lengths for different terrain types. From [Manwell et al., 2009]

Terrain type	Roughness length (m)
Ice, mud	0.00001
Calm open sea	0.0002
Blown sea	0.0005
Snow surface	0.003
Lawn grass	0.008
Rough pasture	0.01
Fallow field	0.03
Crops	0.05
Few trees	0.1
Many trees	0.25
Forest and woodlands	0.5
Suburbs	1.5
Cities, tall buildings	3.0

To find the friction velocity $u_{\text{wind}}*$, Equation 2.5 can be written as:

$$ln(z) = \left(\frac{k}{u_{\text{wind}}*}\right)u_{\text{wind}}(z) + ln(z_0)$$

In this form, the equation can be plotted on a graph with log scale using experimental data, and from the slope of the curve, $u*$ can be found, since the slope is $\frac{k}{u_{\text{wind}}*}$. To find the wind speed from the known wind speed at another height z_r, the following formula is used [Manwell et al., 2009]:

$$\frac{u_{\text{wind}}(z)}{u_{\text{wind}}(z_r)} = \frac{ln(\frac{z}{z_0})}{ln(\frac{z_r}{z_0})}$$

A plot of wind speed versus height above ground is shown in Figure 2.6 for different surface roughness lengths, given a measured wind speed of 5 m/s at 10 m height.

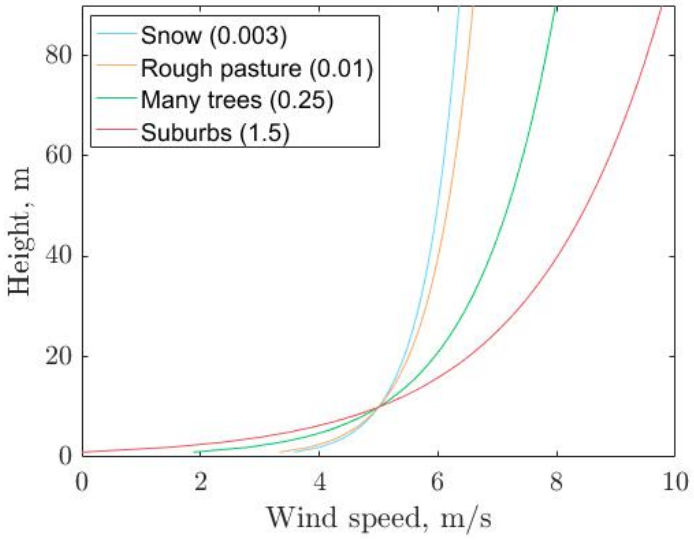

Figure 2.6: Plot of the logarithmic vertical wind speed profile with different roughness lengths, given a measured wind speed of 5 m/s at 10 m height

2.2.3 Betz limit and power coefficient

As the wind travels through a wind turbine, its velocity decreases. Because accumulation of air behind the turbine will cause the turbine to eventually stall, the wind cannot lose all its velocity. Assuming that the air flow is homogeneous, incompressible and steady, that there is no frictional drag, that the number

of blades is infinite, the thrust is evenly spread out over the rotor area, and that the air flow in the wake after the turbine does not rotate, the available power in the can be derived wind by use of one-dimensional momentum theory [Manwell et al., 2009]. The result is that the power coefficient, $C_p = \frac{\text{power extracted by turbine}}{\text{power in the wind}} = \frac{P}{\frac{1}{2}\rho u^3 A}$ has its maximum at $C_{\text{p,max}} = \frac{16}{27}$. This is called the Betz limit and is shown as a solid line in Figure 2.7.

By not making the assumption that the wake behind the turbine does not rotate, the result is calculated in [Manwell et al., 2009] to be as illustrated by the dotted curve in Figure 2.7.

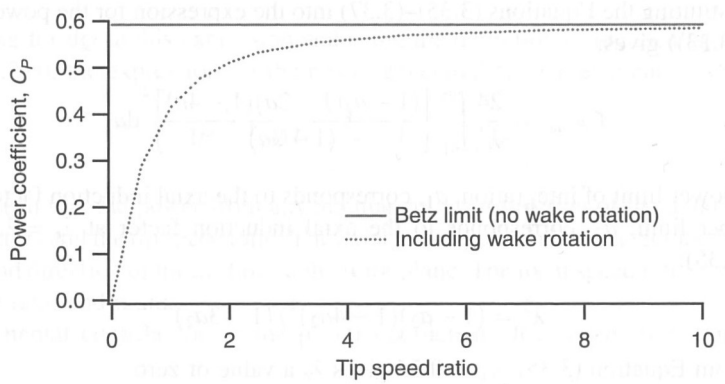

Figure 2.7: Betz limit with and without wake rotation [Manwell et al., 2009]

2.2.4 Operating and controlling the wind turbine

As the wind direction changes continuously, the turbine can possess a yaw control to always face the wind [Andrews and Jelley, 2007]. This can either be done by an electric motor or by a guide vane (making the wind itself the cause of the movement).

If the turbine is designed to operate at a fixed rotor speed, but has a variable blade pitch, the pitch is varied so that the rotor speed is constant. But this has the consequence that the turbine is not operating at the maximum power coefficient when the wind speed is much lower or much higher than the mean wind speed the turbine is designed for [Kreith, 2014]. Turbines that have both variable pitch and speed can vary the blade speed to always operate at maximum power coefficient [Kreith, 2014]. This is the most widely used topology today.

The power output from a wind turbine at different wind speeds is illustrated in

Figure 2.8. Such a curve is called a power curve, and its exact form depends on the wind turbine type. The wind speed must reach a certain level, $u_{\text{cut-in}}$ before the rotor starts to rotate. When the wind speed reaches what is called the rated wind speed, u_{rated}, the pitch (and rotor speed, if applicable) is changed so that the power output is constant at its rated power.

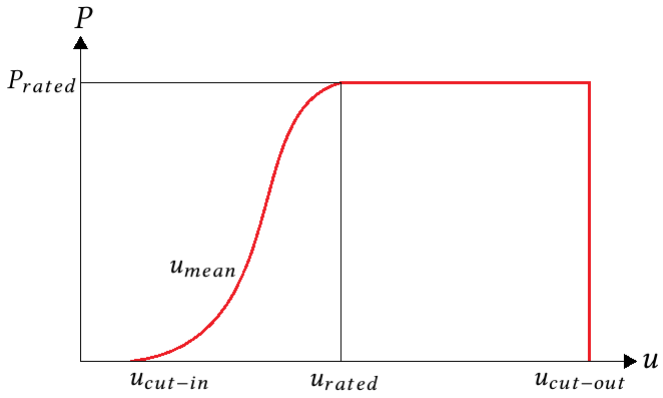

Figure 2.8: Power output for wind turbines with constant speed and variable pitch versus wind turbines with variable speed and variable pitch. Inspired by [Kreith, 2014] and [Andrews and Jelley, 2007]

2.2.5 Wind turbine systems

Several wind turbines can be sited adjacent to each other in a wind farm. The most important aspect to take into account is that wake effects of each turbine will decrease the incident wind speed for the turbine behind it. This causes array losses. Array losses also arises from the type of the turbines, the size of the wind farm, the amount of turbulence at the site and the variation in wind direction [Manwell et al., 2009]. In addition, it depends on the terrain [Patel, 2006]. It is stated in [Niayifar and Porté-Agel, 2016] that wake effects can cause power losses up to 25%. To obtain turbulence losses, a turbulence analysis should be performed on the location.

Thus, the optimum distance between the array of wind turbines must be calculated. This can be done using wake models of different complexity. According to [Manwell et al., 2009] a general rule is that the turbines should have a distance between them of 8-10 rotor diameters in the downwind direction and 5 rotor diameters between each turbine in the other direction.

2.3 Hydroelectric energy

Water at an elevated height in for example a reservoir inherits potential energy, and this energy is exploited in a hydropower plant. The different parts of a hydropower plant is shown in Figure 2.9.

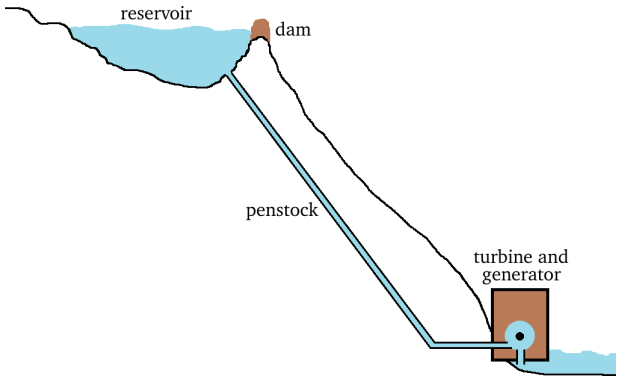

Figure 2.9: A typical hydropower plant. Inspired by [Taylor, 2012]

2.3.1 Available power of a dam

The theoretically possible power output available from a water reservoir at height H with volumetric flow rate Q (in m^3/s) out from the reservoir is [Andrews and Jelley, 2007]:

$$P_{\text{theoretical}} = \rho_w g H Q \tag{2.6}$$

Where g is the gravitational acceleration $g \approx 9.81\ \mathrm{m}/\mathrm{s}^2$ and ρ_w is the density of water; $\sim 10^3\ \mathrm{kg}/\mathrm{m}^3$.

This is the power that is available theoretically. But some energy will be lost due to friction in the penstock that leads the water to the generator. Furthermore, some energy will be lost as the water flows through the turbine, also mainly due to friction. The effect of this can be represented by a loss of head. The resulting head is then called the effective head. Loss of head due to friction is in steady flow determined by the empirical Darcy-Weisbach equation [Massey and Ward-Smith, 2006] shown below, but is outside the scope of this thesis.

$$h_f = \frac{\Delta p*}{\rho g} = \frac{4fl}{d}\frac{\bar{u}^2}{2g} \tag{2.7}$$

2.3.2 Efficiency of hydro power plants

Because turbines cannot have an efficiency of 100%, Equation 2.6 must be written as follows to determine the maximum possible delivered power:

$$P = \eta_t \rho_w g H_{\text{eff}} Q \tag{2.8}$$

where η_t is the efficiency of the turbine and $H_{\text{eff}} = H - h_f$ is the efficient head, given by Equation 2.7.

2.4 Hybrid systems

As discussed in the two previous sections, both the solar resource and the wind resource are highly variable, and varies in time intervals from seasons to minutes, and even seconds. Both resources can be predicted to some extent in near future, but the short-term variation is often difficult to predict. Hence, a system that can quickly respond to changes in these resources is necessary to be able to produce an amount of energy in accordance with the consumption.

These reasons are some of the driving forces for performing research on hybrid systems, which combines two or more energy sources. The combination of several renewable energy sources and in many cases also storage solutions can reduce some of the challenges the sources has when being exploited separately.

A great advantage of hybrid systems is that some of the different energy sources can complement each other. In some locations, it is found that the solar and wind resources are complementary (see e.g. [Diaf et al., 2008]).

Storage solutions for energy is advantageous to use together with renewable resources to balance the system when production is larger than consumption and vice versa. This project considers the solar and wind resource exploited together with the hydro resource in the area. Then the hydro power plant can be used as a sort of storage option: if the production is larger than the consumption, the energy from the PV and/or wind plants can be used, because this energy must be exploited when there is sunlight and/or wind apparent.

The water is kept in dams, so this can be stored there until the consumption increases above the production from the PV and wind components again, and used. However, the level of the dams must be controlled so they are within their allowed limits. The inclusion of pumped storage is also possible when there is excess electricity from the PV and wind plants.

A literature review on existing and simulated large-scale hybrid systems is included in Appendix A.

2.5 Connection to the grid

2.5.1 Existing grid, challenges and options

The electricity grid in Norway is divided into three types [Statnett, 2014]:

- Central network: This is the network that transports electricity across the country, and also to neighbouring countries. It has high voltage (132, 300 or 420 kV) so that there are low losses in terms of heat.

- Distribution network: The network which transports electricity to residential areas. It has a voltage of 22 kV, and the voltage is transformed down to 230 V before it is delivered to buildings.

- Regional network: Connects the central network and distribution network. Has a voltage between 66 and 132 kV.

When connecting variable energy sources to the grid, there are several factors that must be controlled, some of which are [Kropopski et al., 2006]:

- **Voltage regulation**: the voltage injected into the grid should be approximately constant

- **Synchronisation**: The frequency, the phase angle and the magnitude of the voltage waveform injected to the grid must have the same values as what is specified for the grid

- **Response to voltage and frequency disturbance**: If there are disturbances in the voltage or frequency, mechanisms must be in place to stabilise these at the appropriate level again

- **Disconnection for faults and fault-ride-through**: If the voltage, frequency or current becomes larger or smaller than what is recommended

and/or safe, the energy source should be disconnected from the grid. But on the other hand, if there is only a small disturbance that lasts only for a very short time interval, there should be a ride-through of this fault

- **Minimising harmonics**: the alternating current injected to the grid is sinusoidal, and then harmonic distortion will occur due to power electronic components. Harmonics have a frequency that is a multiple of the frequency wanted into the grid, and should be minimised

- **Power regulation**: power electronics used in the interface between the energy source and the grid produce both reactive and active power, and the ratio of these must be controlled [Farret and Simões, 2006]

2.5.2 Connecting a photovoltaic plant to the grid

Photovoltaic cells deliver direct current (DC) voltages. As the grid has alternating current (AC) voltage, the electricity from the PV cells must be converted to three-phase AC before connected to the grid. This can be done using inverters.

In a DC-AC converter, several control regimes are usually implemented. Firstly, to control the factors previously mentioned, the DC-AC converter itself comprises control regimes [Hassaine et al., 2014]. There exist a large number of algorithms for the schemes, which are not discussed in further detail here. Secondly, for a PV plant, often a maximum power point tracking (MPPT) is employed. As shown in Figure 2.2, there is a maximum for the power produced by a solar cell. The MPPT tracks the power output from the PV modules and extract the maximum. A number of methods can be used for this purpose [Hassaine et al., 2014].

There are several topologies for connecting PV modules to the grid in use today, and the most widely used are described below. The four first topologies are shown in Figure 2.10, and the last is shown in Figure 2.11:

- **Central configuration**: PV modules are connected in several series connections, where each series is connected in parallel forming an array which is then connected to one common DC-AC converter [Hassaine et al., 2014]. This is used for large PV plants with a large number of panels [Romero-Cadaval et al., 2013]. Disadvantages of this setup is that DC cables with high voltage must be used between the modules and inverters, mismatches between the modules will have large effects, and the MPPT and inverter control regimes in the DC-AC converter control the whole plant simultaneously [Hassaine et al., 2014]

- **String configuration**: Each series connection (string) of PV modules is connected to a separate DC-AC converter [Romero-Cadaval et al., 2013]. This method decreases the impact of mismatch between modules and each string can be controlled separately [Hassaine et al., 2014]

- **Multi-string configuration**: A mixture of the two first topologies. Each string is connected to a DC-DC converter, and then a centralised DC-AC converter is used to connect to the grid. The control regimes can here be applied separately to each string by the DC-DC converters [Hassaine et al., 2014]

- **Individual or paired configuration**: Similar to the multi-string configuration, but there is a DC-DC converter connected either to each individual module or for two parallel connected modules. The solution with two modules on each DC-DC converter is used for modules which has a high rated power (either higher than 405 W or higher than 800 W, depending on the converter model). The modules are typically series connected to an inverter. The DC-DC converter inhibits an MPPT tracker. It is also possible to buy PV modules with an integrated DC-DC converter [SolarEdge Corporate,]. In Figure 2.10, only the individual setup is shown, but the paired setup is easily achieved by replacing the single PV module by two connected in parallel with the DC-DC converter. Several strings can also be connected to the DC-AC inverter

- **Modular configuration**: Each string is connected with a DC-DC converter to a common DC bus, whereafter AC-DC inverters connects the bus to the grid [Romero-Cadaval et al., 2013]

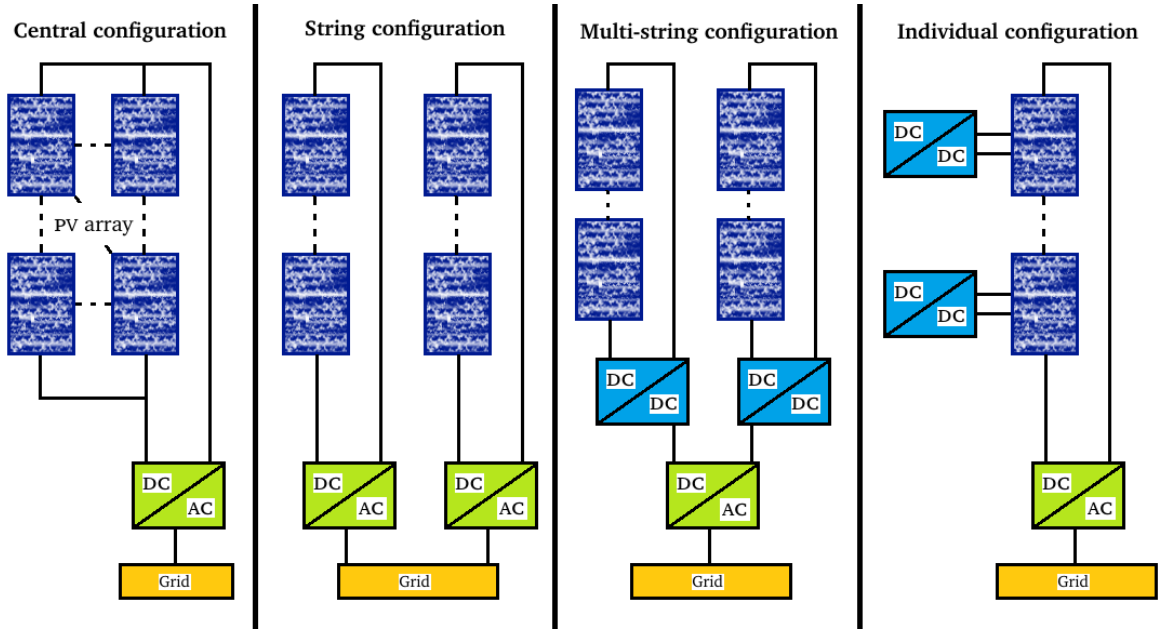

Figure 2.10: Four topologies for connecting PV systems to the grid. Inspired by [Romero-Cadaval et al., 2013] and [SolarEdge Corporate,]

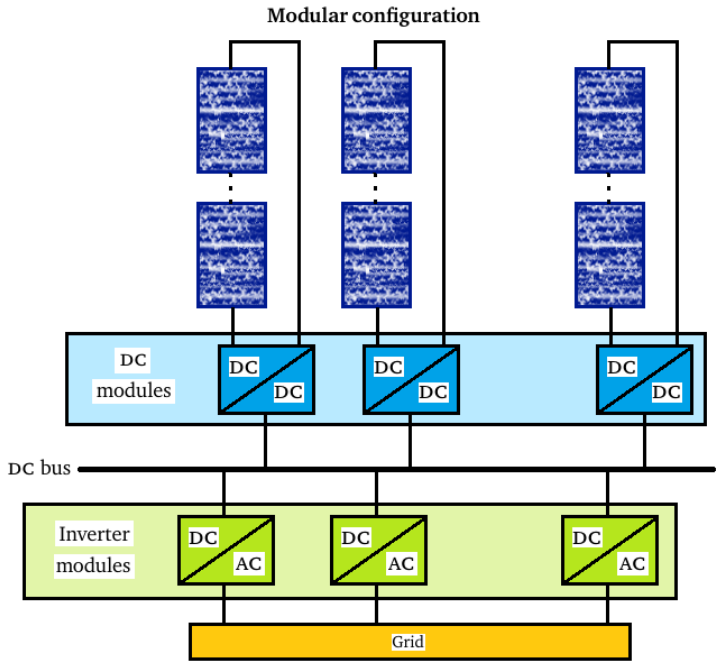

Figure 2.11: Modular topology for connecting PV systems to the grid. Inspired by [Romero-Cadaval et al., 2013]

In [Rodrigo et al., 2016], inverters with an efficiency of 97-98% are used, and the company *SMA* has made a commercialised celtralised inverter with an efficiency of 98% [SMA Solar Technology AG,]. In [Zipp, 2015], it is stated that the new age of PV inverter efficiencies was 99%. Multilevel inverters are also being researched and developed, as they can achieve higher efficiency and less distortion of the AC waveform injected into the grid [Romero-Cadaval et al., 2013].

2.5.3 Connecting a wind turbine plant to the grid

As a wind turbine is rotating, the resulting electricity is AC. But for the produced AC to be synchronous with the specifications of the grid, it is common practice to use power converters.

The interface between the wind turbine and the grid depends on the generator used in the wind turbine. Some widely used setups are described below:

- **Doubly fed induction generator (DFIG)**: Shown in the top panel in Figure 2.12. This is a setup with semi-variable speed (±30%). There is a power converter (AC-DC and DC-AC) connected to the rotor, which supplies approximately 30% of the total power delivered from the wind turbine. Because the power converters are only connected to 30% of the supply, only this amount of the power can be controlled [Yaramasu et al., 2015]. However, this setup has shown to provide flexible voltage control, fault ride-through and quick recovery from voltage disturbances [IEC, 2012]. This setup also makes use of a MPPT with the same principle as with PV systems [Yaramasu et al., 2015].

- **Squirrel cage induction generator (SCIG), permanent magnet synchronous generator (PMSG) or wound rotor synchronous generator (WRSG)**: Shown in the bottom panel of Figure 2.12. In this setup, all power from the wind turbine is directed from the stator through a power converter [IEC, 2012]. This implies that the generator can run at all speeds, because it is totally separated from the grid. But, the converters must have the same specifications as the generator, which increases the cost and size of the system compared to the previous system. As there are always losses in power converters, this setup may have a somewhat lower efficiency than the previous. However, all power from the wind turbine is controlled to achieve the appropriate voltage, frequency and synchronisation [Yaramasu et al., 2015]

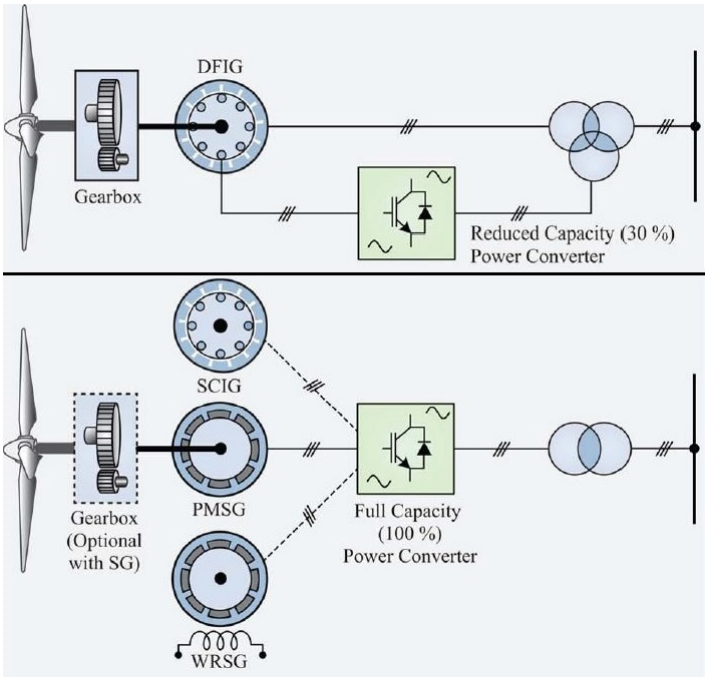

Figure 2.12: Topologies for connecting wind turbine systems to the grid. From [Yaramasu et al., 2015]

Induction generators require some reactive power [Farret and Simões, 2006]. Power converters are hence very advantegous to use with such generators, as they allow a bidirectional flow, which makes reactive power compensation possible [Yaramasu et al., 2015].

2.5.4 Connecting a hybrid system to the grid

This section about connecting a hybrid system to the grid is accomplished in collaboration with Charlotte Tiller, but as the hybrid systems in our theses are not identical, our sections about connecting a hybrid system to the grid are not identical either. There are several ways of connecting a hybrid system to the grid, and after conversations with *Troms Kraft*, it is chosen that only a simple model is presented in this thesis.

After the PV modules have been connected together by using power converters as explained in Subsection 2.5.2, the wind turbines have been connected together using power converters as explained in Subsection 2.5.3 and the output from the hydro power plant also has the correct power characteristics, they are connected together and controlled by using a regulator that by using in-

formation about the components of the system decides the optimal energy balance between the different power sources. If the hybrid system includes a storage unit, this is also converted to the correct power characteristics before connected to the regulator.

A simple model of a typical regulator for the type of hybrid system considered in this thesis is constructed, and it is shown in Figure 2.13. There are three different types of inputs: data, constraints and priorities. Data inputs include the renewable resources, i.e. the available solar radiation, water in the reservoir and available wind. It also includes the available power in a potential storage unit. To be able to put constraints on the total power output from the hybrid system, the electricity demand and maximum grid capacity is given as inputs, and the total output power must not exceed these values.

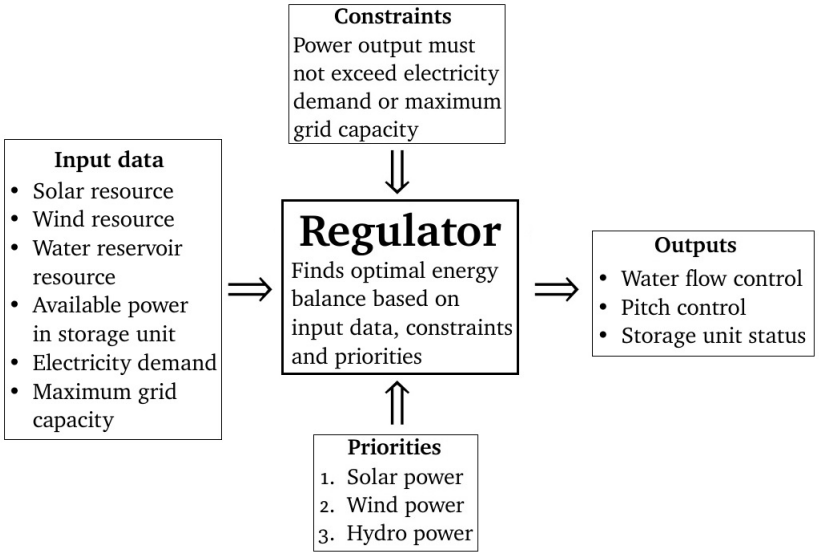

Figure 2.13: A simple model of a regulator used to control a large-scale hybrid system between PV, wind, hydro and a potential storage unit

As the PV power output is difficult to control, this power source is prioritised in the calculation of an optimal energy balance, and should ideally not be curtailed, as unused solar radiation can not be stored. If exploiting the available renewable resources 100% causes the total power output to exceed one of the constraints, the wind power is prioritised over the hydro power. The reason for this is that the water not being exploited for electricity production can be stored in the reservoir, while the portion of available wind not being exploited will remain unused.

The regulator gives as output the degree of control of the wind and hydro

power stations that must be performed to give an output in correspondence to the given constraints. Hence the pitch control of the wind turbines to increase/decrease the wind power production and the amount of water flowing to the turbine is decided. In addition, the status of the storage unit is given. If there is excess output power, the storage unit will be set to charging if it is not completely charged, and if there is deficit of output power the available power in the unit will be fed into the grid together with the output from PV, wind and hydro. If there is neither deficit nor excess of output power and the storage unit is fully charged, the unit is set to neutral.

2.6 Weather Research and Forecasting (WRF) Model

In situ weather measurements are not always available at a site. Therefore weather conditions are often simulated by using models. One of the available models is the *WRF*, which is a numerical model for prediction of weather at mesoscale and simulation of the atmosphere. It is developed by collaboration between several institutions, laboratories and university scientists, and is designed as an open source model [Skamarock et al., 2008]. The WRF system consists of two phases: a preprocessing system and the actual WRF simulation, illustrated in Figure 2.14.

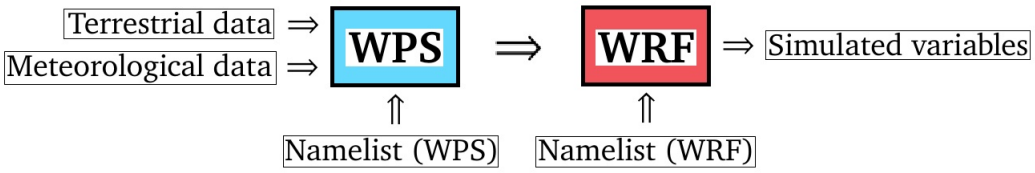

Figure 2.14: A simplified chart of the WRF model. Inspired by [Blæsterdalen, 2016]

The preprocessing phase takes user-defined terrestrial data (topography, vegetation, albedo etc.) and meteorological data as its inputs [Blæsterdalen, 2016]. The preprocessing then defines the domains of the simulation, interpolates the terrestrial data and horizontally interpolates the meteorological data to the domains defined [Wang et al., 2014]. The simulation parameters for the preprocessing step are read from a file called *namelist* [Blæsterdalen, 2016].

The simulation phase receives inputs from the preprocessing system, and in the same way as for the preprocessing programs, simulation parameters are defined

in a *namelist*-file. The first step is a program which vertically interpolates the meteorological data to the simulation domain, and outputs a 4-dimensional simulation domain (space and time dependent) [Blæsterdalen, 2016].

The next step is the actual simulation, which exploits dynamic solvers in its calculations; either the Advanced Research WRF or the Non-hydrostatic Mesoscale Model (NNM) [Skamarock et al., 2008]. The simulation phase also inter alia includes parametrisation schemes for time-integration, vertical coordinates, microphysics (water vapour processes etc), convective and shallow clouds, long- and shortwave radiation, interaction between surface and atmosphere and the boundary layer between them [Blæsterdalen, 2016]. The outputs from the simulation are files with all the simulation variables. The number of variables exceeds 150, and an extraction and analysis can then be done.

In this thesis, the radiation parametrisation scheme is of special interest. For shortwave radiation from the Sun, the solar fluxes for clear sky and cloudy sky are calculated, and it takes into account annual and diurnal changes in the solar radiation [Dudhia, 2017]. This can be done by using the local solar time calculations. Some of the parametrisation schemes also takes into account reflected shortwave radiation. Longwave radiation fluxes emitted from the Earth itself and other objects are also calculated. In many of the parametrisation schemes for radiation also cloud fields and precipitation, the absorption of radiation by gases in the atmosphere, aerosols and the effect slopes has on shortwave radiation (e.g. shading from mountains) are included [Dudhia, 2017].

The European Centre for Medium-Range Weather Forecasts (ECMWF) provides a dataset with meteorological data called ERA-Interim that can be used in WRF simulations. The data set is created by combining historical and present measured data into a global model for weather forecasting. A typical time resolution of the data is 3 hours and spatial resolution is 80 km horizontally. It contains 60 vertical levels [Blæsterdalen, 2016]. Other data sources that can be used are online resources, in situ measurements etc.

2.7 Statistical analysis of data

2.7.1 Fundamental statistics

The numerical value of the outcomes from an experiment constitute a random variable. If the outcomes can take any value in a continuous interval, the random variable is referred to as continuous. Random variables are denoted by capital letters, e.g. X.

If the random variable is measured n times, its measured values are denoted by x_i, where $i = 1, 2, \ldots, n$. The sample mean of the data set of measured values of X is defined as [Ross, 2014]:

$$\bar{x} = \frac{1}{n} \sum_{i=1}^{n} x_i$$

And the variation of the measured values is represented by the sample variance:

$$s^2 = \frac{1}{n-1} \sum_{i=1}^{n} (x_i - \bar{x})^2 = \sum_{i=1}^{n} {x_i}^2 - n\bar{x}^2$$

The square root of the sample variance is called the sample standard deviation, s. If a random variable is normally distributed, it peaks at the sample mean and is symmetrically decreasing on each side. It is empirically shown that $\sim 68\%$ of the measurements of a normally distributed random variable is located within one sample standard deviation of the mean [Ross, 2014].

2.7.2 Comparing two data sets

Root Mean Square Error (RMSE)

To calculate the average distance between two data sets, the Root Mean Square Error (RMSE) can be used. It is given by:

$$\text{RMSE} = \sqrt{\frac{1}{n} \sum_{i=1}^{n} (x_i - y_i)^2} \tag{2.9}$$

It is common to use this measure for two data sets where one contains observed values (y_i) and the other contains simulated values (x_i) of the same variable.

Bias

Another measure used to compare two data sets is the bias, which represents the data tendency and is given by [Carvalho et al., 2012]:

$$\text{bias} = \frac{1}{n}\sum_{i=1}^{n}(x_i - y_i) \tag{2.10}$$

If simulated values are set to be x_i and measured values are set to be y_i and the bias is positive, the tendency of the simulated values is to overestimate the variable, and if it is negative, the tendency is to underestimate.

Pearson correlation coefficient

To investigate the relationship between two data sets, correlation analysis can be used. One of the most widely used methods is to calculate the Pearson correlation coefficient [Osborne, 2008]. Its formula is [Sharma, 2005]:

$$r = \frac{\sum_{i=1}^{n}(x_i - \bar{x})(y_i - \bar{y})}{\sqrt{\sum_{i=1}^{n}(x_i - \bar{x})^2}\sqrt{\sum_{i=1}^{n}(y_i - \bar{y})^2}} \tag{2.11}$$

The Pearson coefficient lies between -1 and $+1$, and its magnitude represents the degree of correlation. If $r = -1$, there is a perfect negative correlation (anti-correlation) between the two variables and if $r = +1$, there is a perfect positive correlation. Furthermore, a typical classification of degree of correlation [Jain and Jhunjhunwala, 2007] is shown in Figure 2.15. However, the magnitude of the coefficient is not proportional to the degree of correlation. A twice as large coefficient does not imply a twice as large correlation, but actually describes a substantially larger correlation [Sharma, 2005].

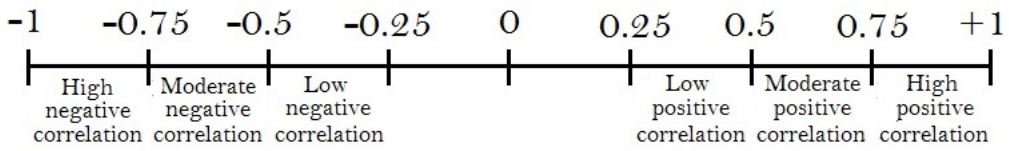

Figure 2.15: Degree of correlation for Pearson coefficient. Created with values from [Jain and Jhunjhunwala, 2007]

2.8 Economic analysis

2.8.1 Net Present Value (NPV)

NPV is a method for calculating an indicator of the profitability of an investment, and it considers all cash flows in the lifetime of the project. The NPV takes into account that the value of money is not constant in time, and costs and benefits occurring in the future must be transformed to their present values. This is done in the following way:

$$\text{present value} = \frac{\text{future value}}{(1+i)^t}$$

where i is the discount rate and t is the number of years from present the cost or benefit occurs. The discount rate is the predicted value with which money will change its value in time. A disadvantage of the NPV is that it assumes a constant discount rate, which may not be realistic. The factor $\frac{1}{(1+i)^t}$ is called the discount factor.

The NPV is calculated by [Bhattacharyya, 2011]:

$$\text{NPV} = \sum_{t=1}^{n} \left(\frac{R_t - C_t}{(1+i)^t} \right) - I_0 \tag{2.12}$$

Here, R_t represents the revenues in year t, C_t represents the costs in year t and I_0 is the initial investment (in year 0). n is the lifetime of the project. A positive NPV is desired for any project.

2.8.2 Levelised Cost of Energy (LCOE)

To find the average cost per kWh produced by a power plant, the LCOE can be used. Its formula is [Hernández-Moro and Martínez-Duart, 2013]:

$$LCOE = \frac{I_0 + \sum_{t=1}^{n} \frac{C_t}{(1+i)^t}}{\sum_{t=1}^{n} \frac{E_t}{(1+i)^t}} \tag{2.13}$$

Where E_t is the electricity generated in year t in kWh. The LCOE represents the electricity price which is required for a power plant to be profitable.

3

Location

Skibotn is a settlement in the bottom of the valley Skibotndalen in Troms. Its location is shown in Figure 3.1. The square in the map to the right shows which area Figure 3.2 below is viewing, which is a close view of Skibotndalen. The valley extends all the way from the sea up to the national border towards Finland and the Skibotn River runs through the valley. A main road also exists in the valley, shown with a red line in the two figures.

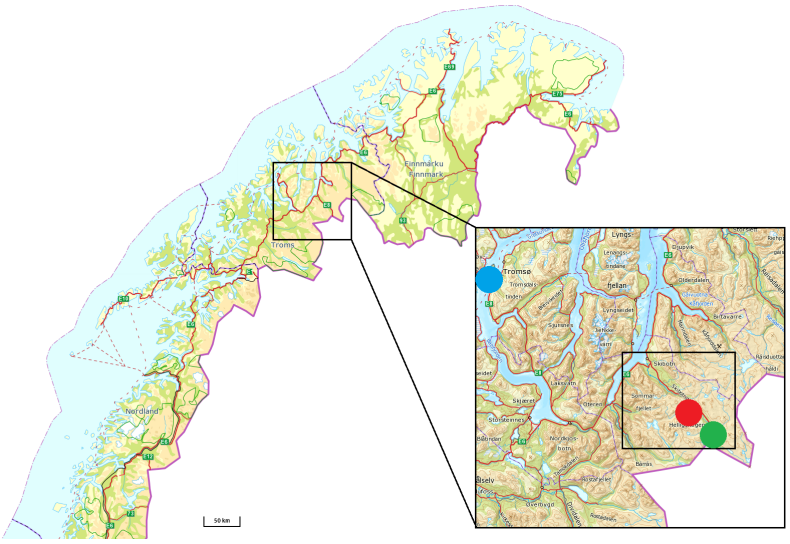

Figure 3.1: Map of Northern Norway showing the location of Skibotn. From `www.norgeskart.no`

Figure 3.2: Map of Skibotndalen. From `www.norgeskart.no`

3.1 Vegetation, albedo and snow cover

The vegetation in the area of Skibotn for the year 2012 is obtained from *NIBIO* (Norwegian Institute of Bioeconomics). It is from the *Corine programme* (coordination of information on the environment) in the *EU*. Figure 3.3 show the vegetation in the area of Skibotndalen. The colour codes for each vegetation type are the ones defined by the Corine programme itself.

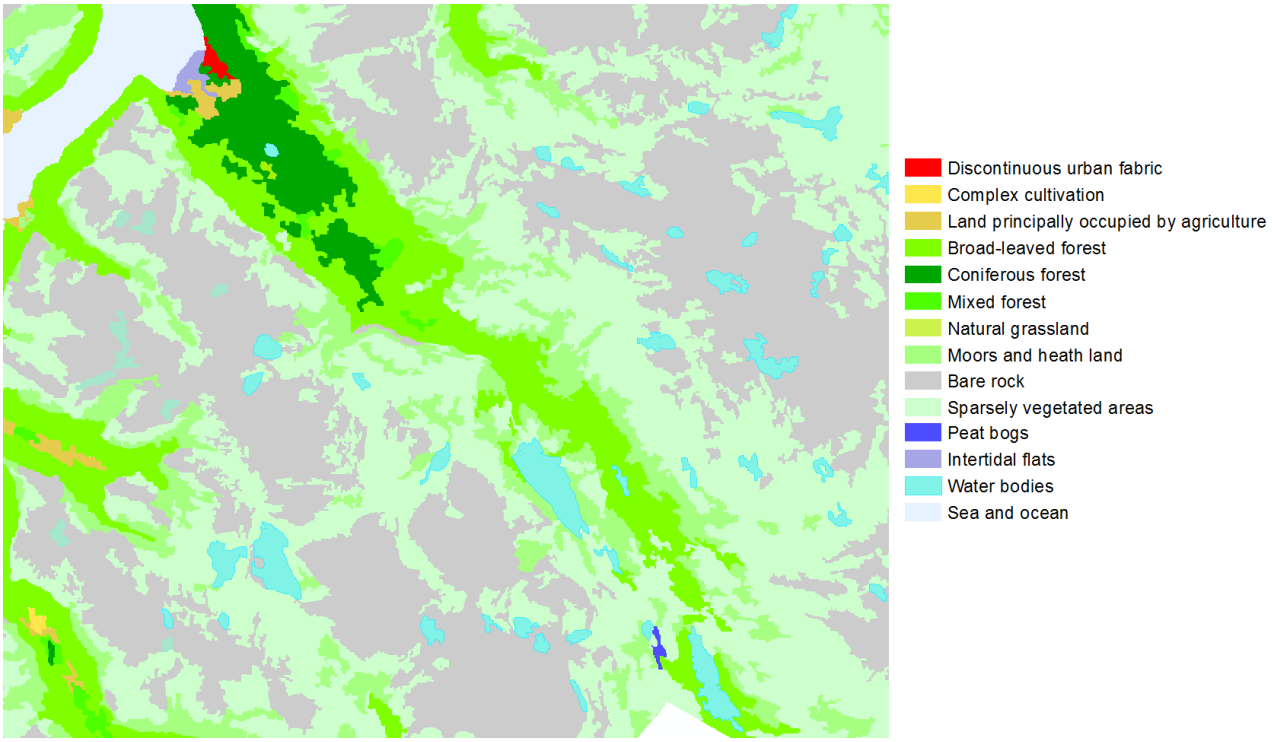

Figure 3.3: Vegetation types in Skibotndalen. From `http://www.skogoglandskap.no/kart/corine_landcover/artikler/2013/nedlasting_corine`

It can be seen that in the bottom of Skibotndalen, the vegetation is mostly forest. Up the valley sides there are moors and heath land in addition to sparsely vegetated areas, and on the mountain tops there is bare rock. From Table 2.1, the approximate albedo of Skibotndalen is 0.25 in the bottom of the valley, $0.10 - 0.25$ up the valley sides and $0.05 - 0.15$ at the highest elevations. The lakes in the area also reflects a portion of the incident solar radiation, namely between 0.05 and 0.22 depending on the elevation angle of the sun, α.

A snow cover map of Skibotn showing the typical number of days per year which has snow depth above 5 cm in the period 1971-2000 is found at `senorge.no`. It is shown in Figure 3.4. It is evident that the bottom of the valley usually

has 100-200 days and that the areas of higher elevation has 200-350 days with snow depth above 5 cm.

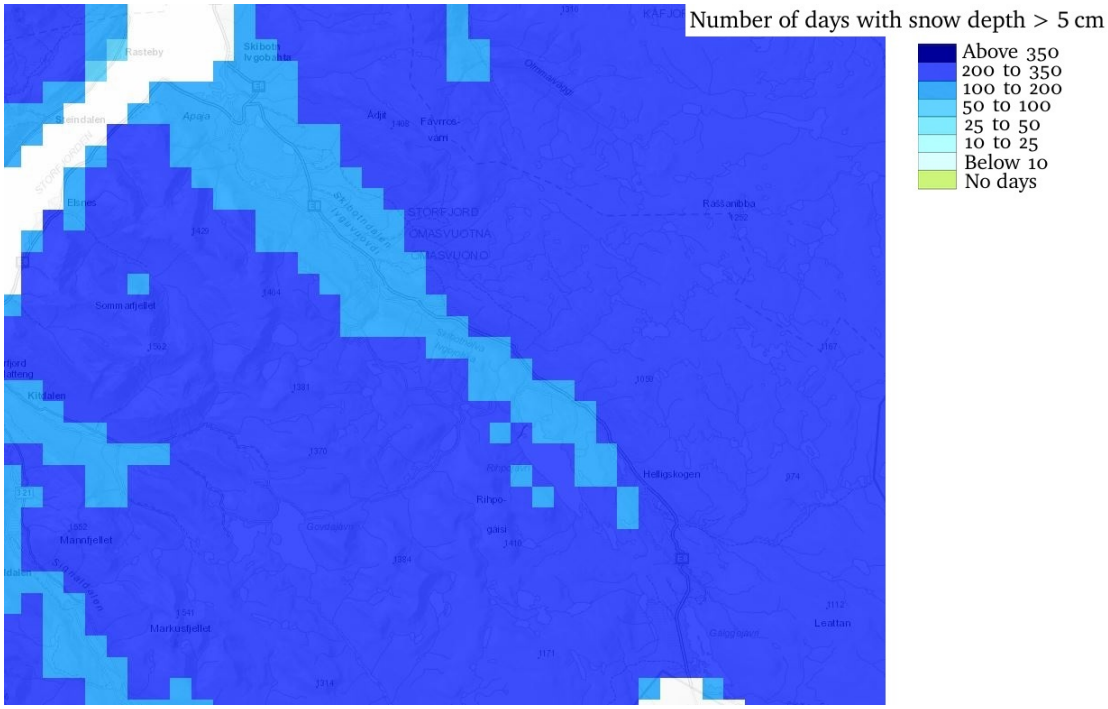

Figure 3.4: Snow cover map of Skibotndalen. From `http://www.senorge.no/?p=klima`

3.2 Existing power stations

The hydro power facility already existing in Skibotn consists of two hydro power stations; Skibotn and Lavkajokka. They are both shown in the map in Figure 3.5. Lavkajokka has a production of 25.7 GWh with a head of 127 m, the Skibotn power station has a production of 370.8 GWh with a head of 430 m, and they both have Francis turbines [TromsKraft,]. Production values are given as an average of the last seven years up to 2015. *Troms Kraft* has stated that the capacity of the turbine at Lavkajokka station is 8.5 MW and the capacity of the turbine at Skibotn station is 72 MW. They are operated depending on the electricity price, thus when the electricity price is high, they have a high power production, and when the electricity price is low, the production is low.

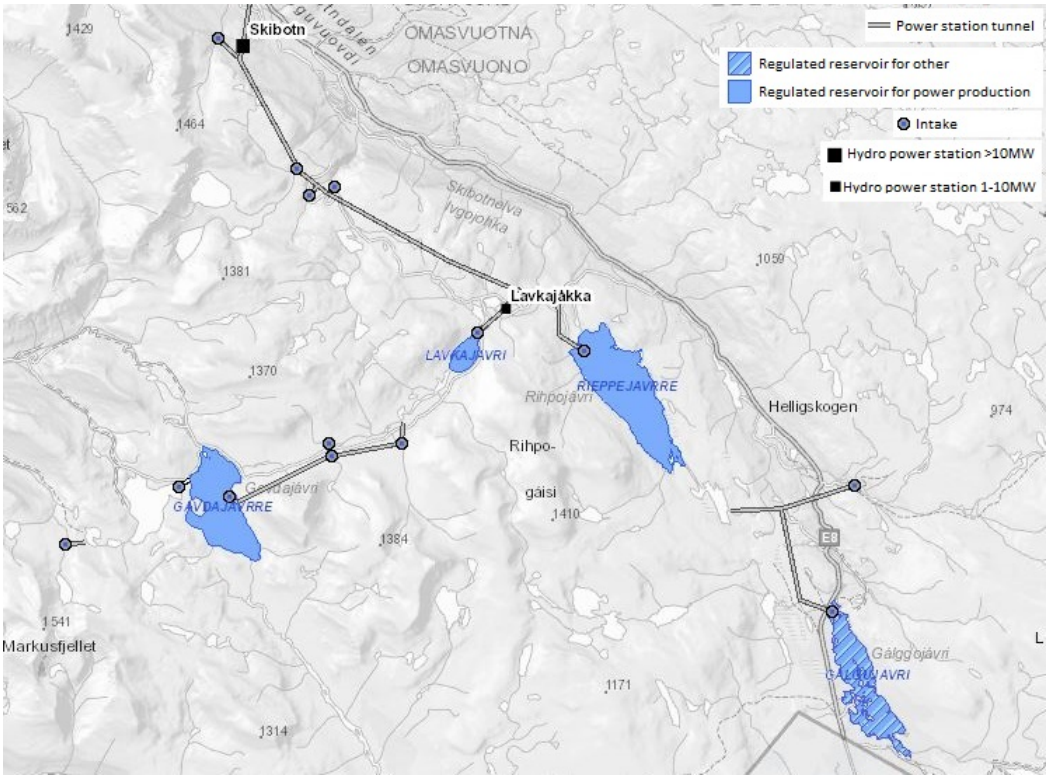

Figure 3.5: The two hydro power stations in Skibotn. From [NVE, b]

The following paragraphs primarily contains information received from *Troms Kraft*.

The Lavkajokka is the highest station. The reservoirs for Lavkajokka are Lavkajavri and Govdajavri, and the main reservoir for Skibotn is Rihpojavri [Rosvold, 2016]. In addition the water from Lavkajokka can either be channelled down to the Skibotn station or to Rihpojavri. The two power stations can thus be operated individually, but most often they are coordinated (all run-off water from Lavkajokka is used as input for the Skibotn station) to give an optimised power output (e.g. exploiting as much as possible of the potential energy in the water when the electricity price is high).

The generator at Skibotn power station is a synchronous generator, and the turbine is controlled by a regulation system with an analogue frequency regulator. The Lavkajokka power station also has a synchronous generator, but not a frequency regulator. It operates as a load regulator, producing a constant pre-defined output power. The output voltage can in both stations be controlled by changing the voltage on the rotor windings of the generator.

3.3 Existing electricity grid

The network in the area in the vicinity of Skibotn is shown in Figure 3.6. The red lines are central networks, the blue lines are regional networks and the green lines are distribution networks. The red squares are transformers.

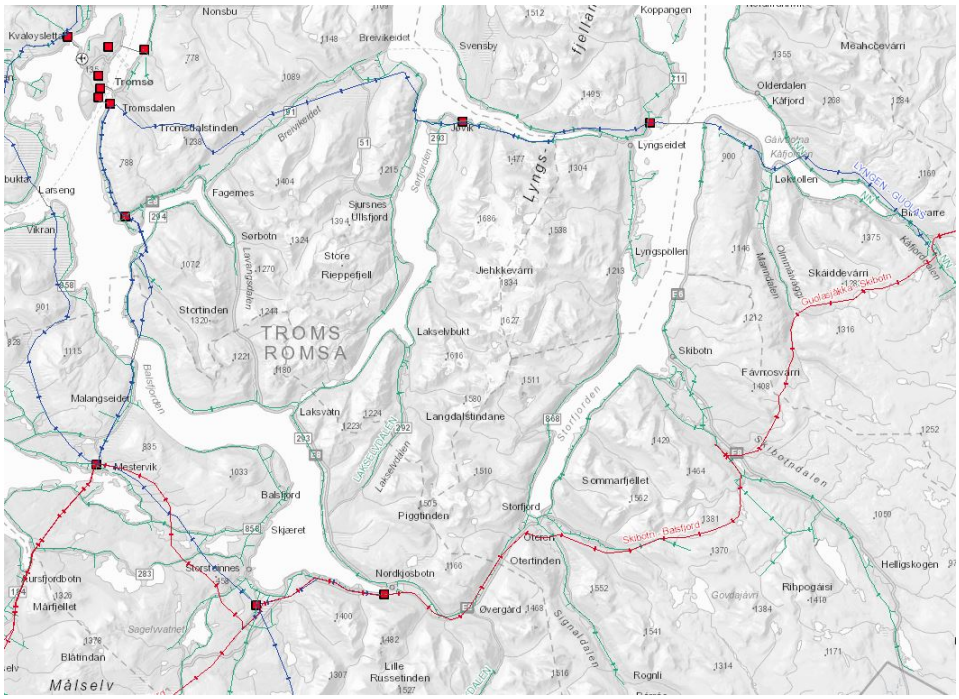

Figure 3.6: The electricity network in the Skibotn and Tromsø area. From [NVE, a]

3.4 Limitations

The electricity network in northern Norway does have some bottleneck-problems. The network does not have the capacity to transport more than 100 MW of power from Skibotn to other areas. However, two new central electricity lines are being built. One is between Ofoten in Nordland and Balsfjord in Troms, with a voltage of 420 kV. It is expected to be finished in 2017, and will enhance the security of supply in the central network between Nordland and Troms, with respect both to increased production and consumption in the northern part of Norway [Statnett, 2016b]. The second is a 420 kV line between Balsfjord in Troms and Skaidi in Finnmark, which is planned finished in 2021, and also enhances the security of supply in northern Norway [Statnett, 2016a]. The new lines also better connects the networks in northern regions to the larger networks in southern Norway.

4

Methodology

In this section, data and their sources in addition to a brief description of the simulation software is presented. Finally, the procedure used for statistical analysis of data and the hybrid system simulations are given. Note that for weather measurements from 2016, the leap day is removed from the data series, as the simulation software only takes as input time series with data for 365 days.

4.1 Solar resource data

4.1.1 In situ solar measurements

Galgo

As part of the preparations for this study, a solar sensor was installed at a weather station owned by the Norwegian road administration *Vegvesenet* in December 2016. It is located by the lake Galgojavri in upper Skibotn, near the Finnish border. A significant advantage of this location is that the station, which is a high mast, is raised very near the road E8 and is hence easy to access. A data logger in addition to a GSM-modem is utilised to transmit the data. The location of the sensor is shown in Figure 4.1 by the green circle in the bottom right of the image. It is also shown in Figure 3.1 by a green circle.

Figure 4.1: The location of the solar sensor at Galgo is shown with a green circle. From `www.norgeskart.no`

The solar sensor is delivered by *Apogee Instruments*. The model is called *SP-230*, and in the owner's manual received from *Apogee Instruments* [Instruments, 2016], it is stated that it measures both direct and diffuse shortwave radiation incident on a horizontal surface in W/m^2 (hence global radiation), and must therefore be mounted on a horizontal surface. The sensor consists of a silicon cell, and thus is sensitive to wavelengths between 350 nm and 1100 nm. It does not sense all these wavelengths identically, but is calibrated to give an estimate of the radiation in the complete solar spectrum, calibration uncertainty being 5%. Errors can arise when the conditions the sensor operates in are different than the calibration conditions (clear sky and zenith angle 45°).

This pyranometer differs from the other models from *Apogee Instruments* in that it inherits a heater. This makes it very suitable for cold environments such as Skibotn, and it prevents problems of snow and frost. The temperature of the environment can be as low as -40°C and as high as 70°C [Instruments, 2016]. The sensor itself does not need an external power source, but the heating

facility does need a 12 V source.

The sensor itself is mounted vertically. The aluminium rod it is mounted on should optimally point southwards, because this will give less shadowing from the mast on the sensor. Then there will only be shadow on the sensor when the sun is shining from the north, which is the direction in which least sunshine is coming from. But there were restrictions from *Vegvesenet* as to where the sensor could be mounted on the mast. The direction it was mounted in is shown in Figure 4.2. The green line shows the south-direction, and the red line and circle show the direction which the sensor actually is mounted in. The sensor and data logger is programmed to measure the global radiation every 10 seconds, and then save an average every hour.

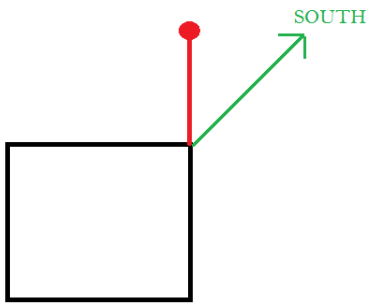

Figure 4.2: The direction of the installed sensor

Figure 4.3 shows a plot of values for the horizontar solar radiation from Galgo in the period January to April 2017 averaged over each 24 hours, and Figure 4.4 shows the daily profile of the solar radiation in the first quarter of 2017 and for the month of April.

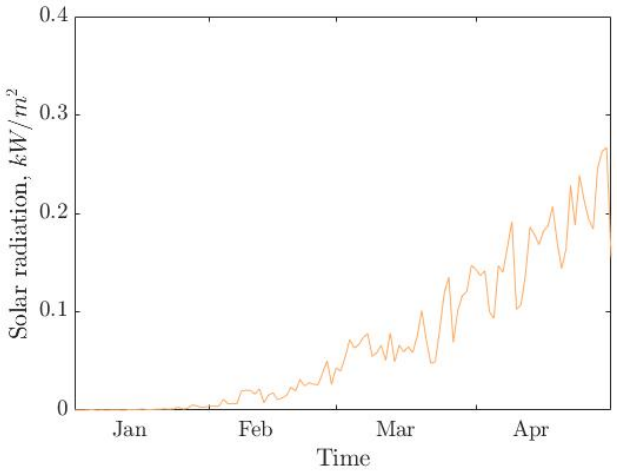

Figure 4.3: 24-hour averaged solar radiation from Galgo for Jan-Apr 2017

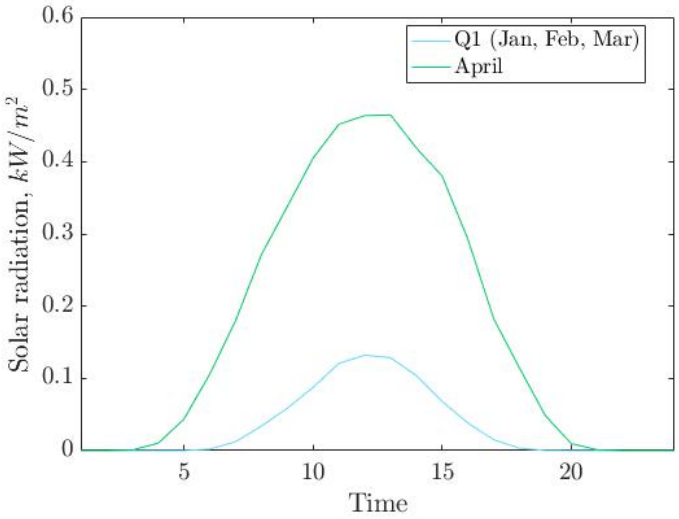

Figure 4.4: Hourly distribution of solar radiation on an average day for the first quarter and April at Galgo in 2017

Holt

The Norwegian Meteorological Institute has a weather station at Holt on the island of Tromsø. Its location as compared to Galgo is shown in Figure 3.1 as a blue circle and its location on the island of Tromsø is shown in Figure 4.5.

Figure 4.5: The location of Holt weather station in Tromsø

Solar data from this station can be obtained from *LandbruksMeteorologisk Tjeneste* [NIBIO,], and data from 2016 will be compared to the simulated WRF solar data from the same location to classify the quality of the simulations. The measured data from Holt is in hourly values, and plots showing 24 hour averages are shown in Figure 4.6. A plot showing the average daily distribution of solar radiation for each quarter year is shown in Figure 4.7. The same plots for solar radiation at Holt in 2017 is shown in Figure 4.8 and Figure 4.9, respectively.

It is found when comparing to solar radiation data from Holt in previous years that the average radiation in 2016 was 6.56 W/m^2, while the average radiation in 2007-2015 was 6.58 W/m^2, thus 2016 seems to be a representative year for the solar radiation.

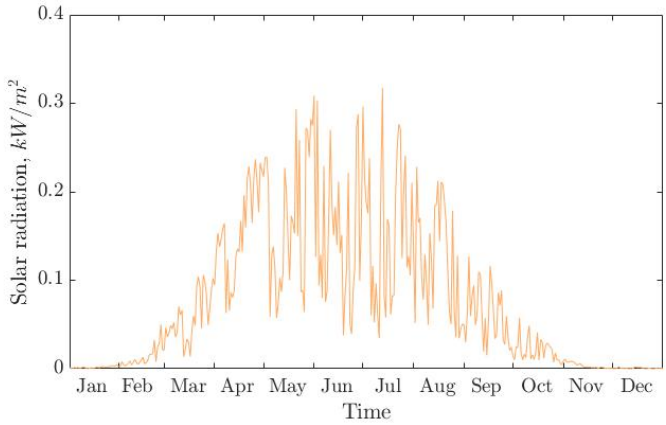

Figure 4.6: 24-hour averaged solar data from Holt in 2016

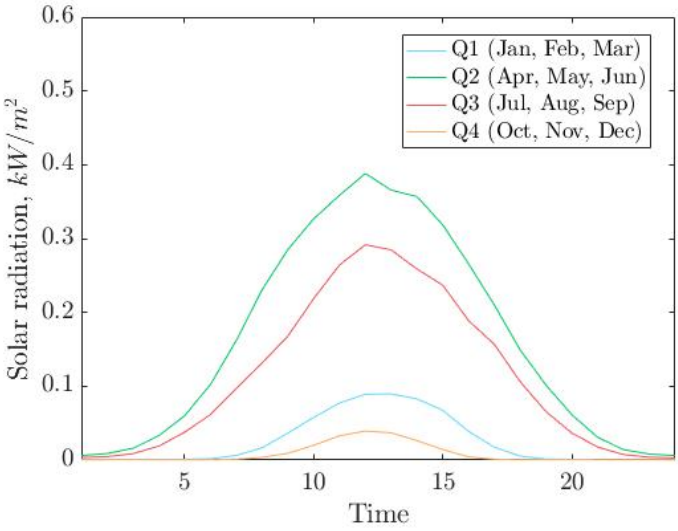

Figure 4.7: Hourly distribution of solar radiation on an average day in each quarter year at Holt in 2016

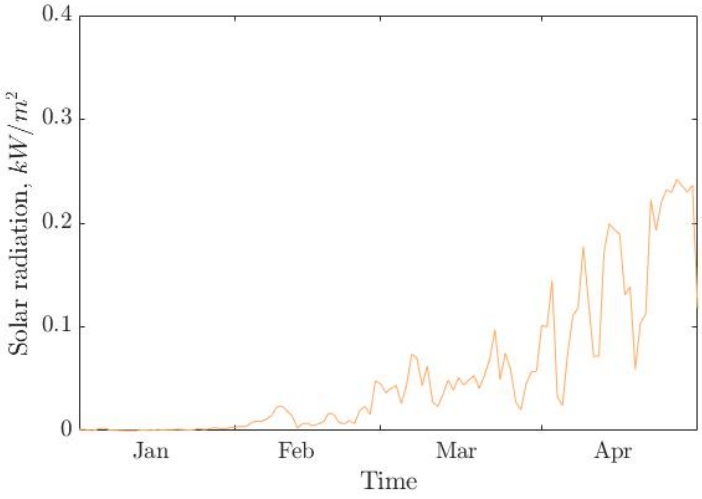

Figure 4.8: 24-hour averaged solar data from Holt in 2017

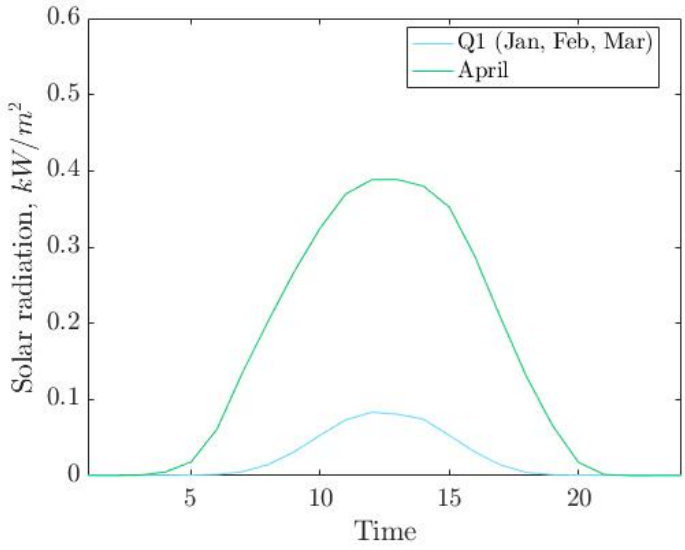

Figure 4.9: Hourly distribution of solar radiation on an average day in each quarter year at Holt in 2017

4.1.2 WRF

Since in situ measurements of solar radiation at Galgo has only been done since December 2016, simulated solar radiation will be used in the simulations of the hybrid system, as it is advantageous that the simulation is done for a

whole year. Solar radiation is simulated for 2016 at two locations; Galgo and Holt. The simulated data for Holt will be compared to in situ measurements at Holt to assess the representativeness of the simulated data, as simulation of solar radiation using WRF is a relatively novel process.

The *namelist* used for the WRF simulations is attached in Appendix C. The dynamic solver used is ARW, and the simulation is done with a 3x3 km resolution. The meteorological input data for the WRF simulation is the ERA-Interim data set from the European Centre for Medium-Range Weather Forecasts (ECMWF).

Galgo

The simulated solar radiation at a horizontal surface at Galgo in 2016 is plotted in Figure 4.10 showing 24-hour averages. Figure 4.11 shows hourly distribution of solar radiation on an average day in each quarter year.

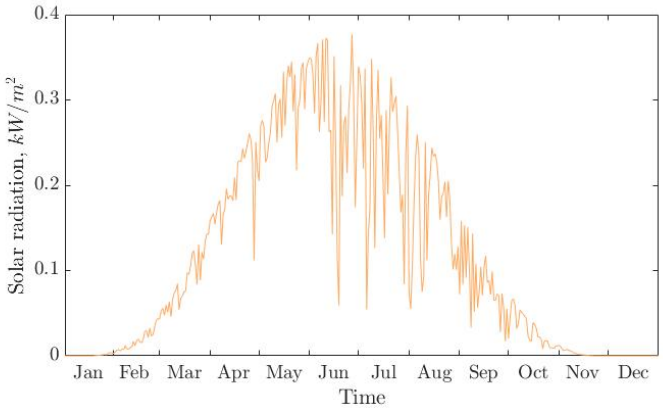

Figure 4.10: 24-hour averaged simulated solar data from Galgo in 2016

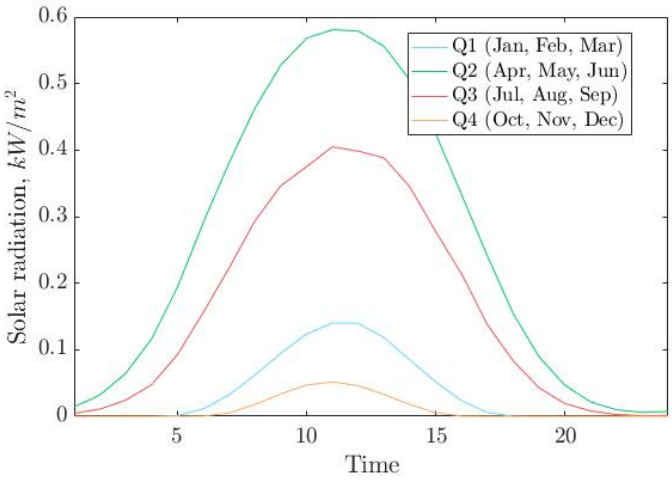

Figure 4.11: Hourly distribution of solar radiation on an average day in each quarter year at Galgo in 2016

Holt

The simulated solar radiation at Holt in 2016 is shown with 24-hour averaged values in Figure 4.12 and hourly distribution of average days in each quarter year in Figure 4.13.

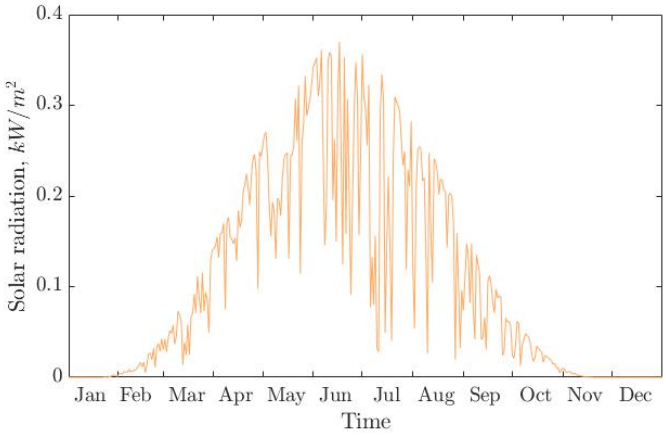

Figure 4.12: 24-hour averaged simulated solar data from Holt in 2016

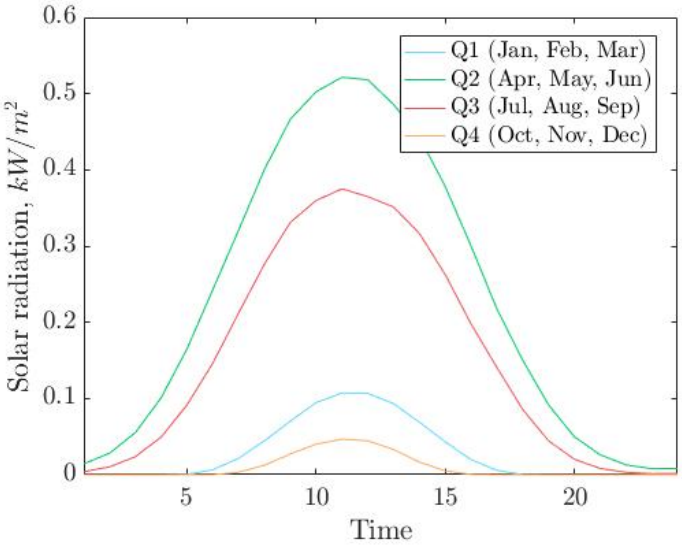

Figure 4.13: Hourly distribution of simulated solar radiation on an average day in each season at Holt in 2016

4.2 Wind resource data

4.2.1 In situ wind measurements

Rieppi

As *Troms Kraft* has already looked into the possibility of installing wind turbines in Skibotn, wind data is received from one of the masts used in this former study. The location of the wind sensor is shown as a red circle in Figure 4.1 and Figure 3.1.

There are two masts by the lake Rihpojavri (hereafter the location is referred to as Rieppi), shown in Figure 4.14. *Troms Kraft* only owns wind data from 2014 measured at the mast called 2503 to the right in the figure. After this, data is only available from the mast called ITAS to the left in the figure, now owned by *The Norwegian Meteorological Institute*.

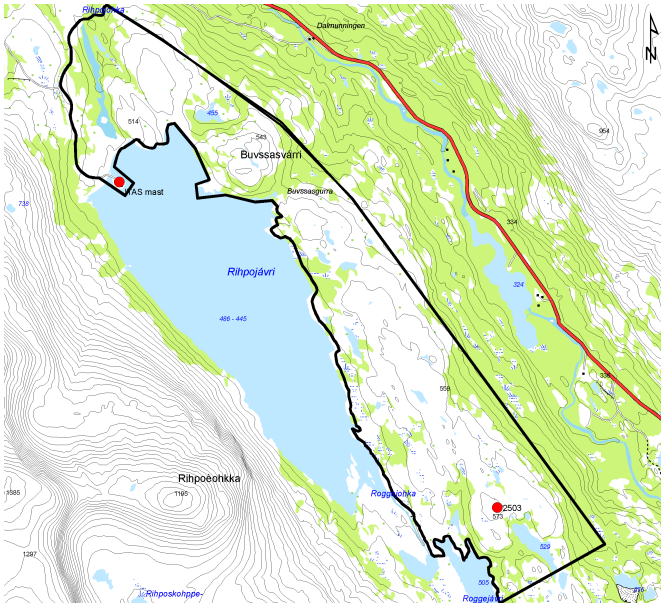

Figure 4.14: The mast with wind and temperature sensors by Rieppi

The wind sensor in the ITAS mast is at a height of 10 meters, and values from this sensor in 2016 and 2017 are used in this thesis. The data is given with hourly intervals, each value being the average from the last ten minutes.

From *The Norwegian Meteorological Institute*, only wind data since 2010 is available, but comparing the average wind speed in 2016 to the average in the period 2010-2015 can be useful to see how the wind characteristics were in 2016. In 2016, the wind speed average was 5.97 $^{m}/_{s}$, while in 2010-2015 the average was 6.22 $^{m}/_{s}$, giving a decrease of 4.2% compared to previous years. In [Weir, 2017], a map of Norway showing the wind conditions in 2016 compared to the average in the period 2000-2015 is included. It shows that in northern Norway, the wind resource was lower than previous years, with a decrease of 4% to 6%.

A wind rose showing wind directions and wind speeds during 2016 is shown in Figure 4.15, and wind roses for each quarter year in 2016 is shown in Figure 4.16. The wind rose shows the direction in which the wind comes *from*.

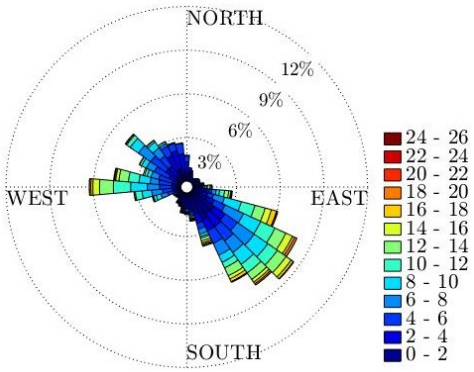

Figure 4.15: Wind rose for Rieppi in 2016

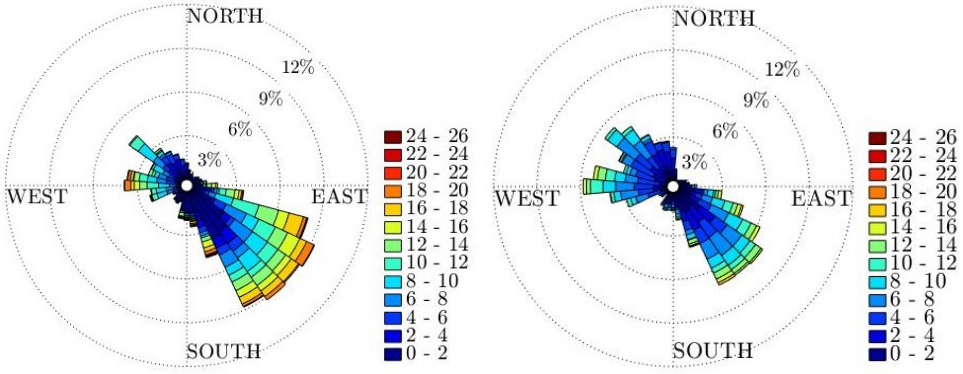

(a) First quarter **(b)** Second quarter

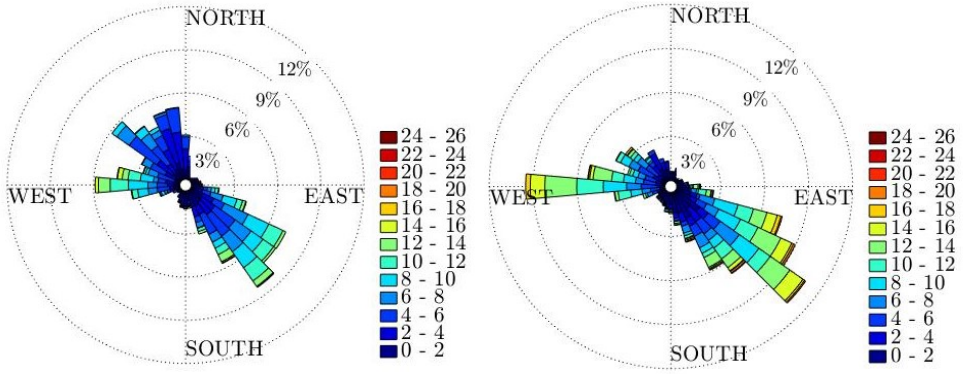

(c) Third quarter **(d)** Fourth quarter

Figure 4.16: Wind roses for Rieppi 2016 showing each quarter year

A wind rose plotted for the period January-April 2017 is shown in Figure 4.17, and wind roses for each month is shown in Figure 4.18.

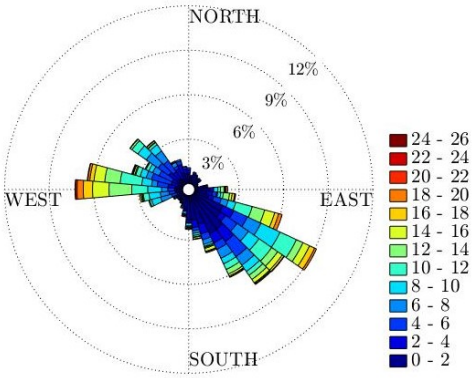

Figure 4.17: Wind rose for Rieppi Jan-Apr 2017

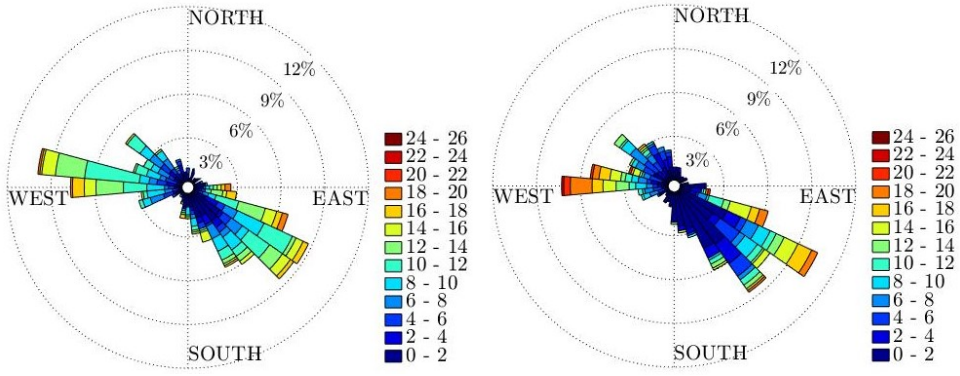

(a) January **(b)** February

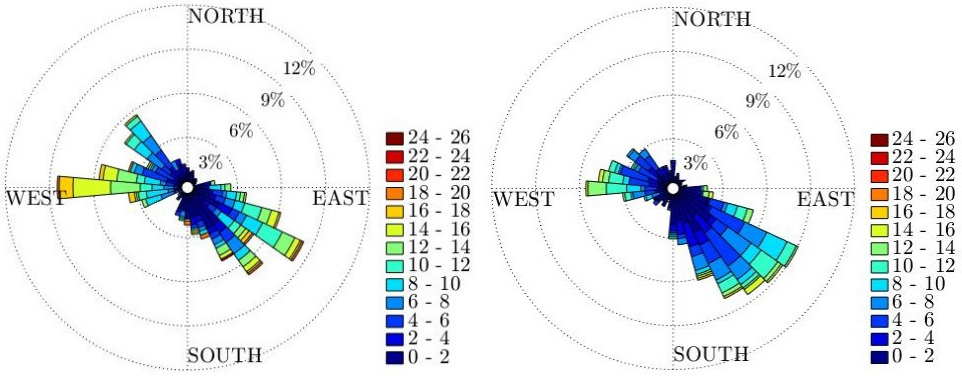

(c) March **(d)** April

Figure 4.18: Wind roses for Rieppi 2017 showing each month

As is evident in both the wind data from 2016 and 2017, the dominating wind directions are from north-west and south-east. This can be explained by the

topography in the area, as the Skibotn valley is oriented from north-west to south-east, which can be clearly seen in Figure 3.2.

4.3 Temperature data

Temperature data from Rieppi in 2016 is received from *The Norwegian Meteorological Institute* as values measured once per hour. A plot of 24-hour averaged temperatures at Rieppi is shown in Figure 4.19. The average temperature in 2016 is calculated to be 0.9 °C.

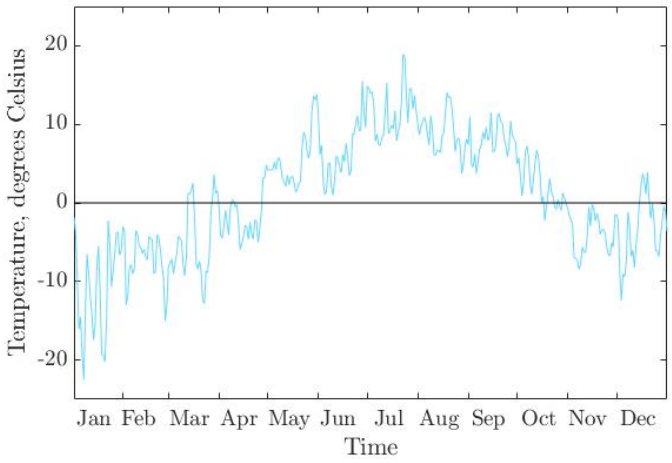

Figure 4.19: Plot of 24-hour averaged temperatures at Rieppi in 2016

4.4 Production data from the hydro power stations

Troms Kraft has provided data for the production of electricity from the Skibotn hydro power station. As already mentionde, the production rate is not dependent on the demand, but rather the electricity price. It has a higher production when the electricity price is high, and if the electricity price decreases, the production also decreases.

A restriction on the production from the power stations is the water level in the reservoirs. The water level must always be kept between specific values, which are set inter alia to preserve the ecology in the area. Thus, the production

may need to be decreased in the summer and autumn, when there may be a naturally lower level in the reservoir lakes.

In 2015 and 2016 the power station was out for revision, and hence the production data from this period is not representative. *Troms Kraft* has provided data from the period 2010-2014. A plot showing daily averages for each of the years 2010 to 2014 is shown in Figure 4.20. From this figure it is apparent that the power output from the hydro power station varies from year to year.

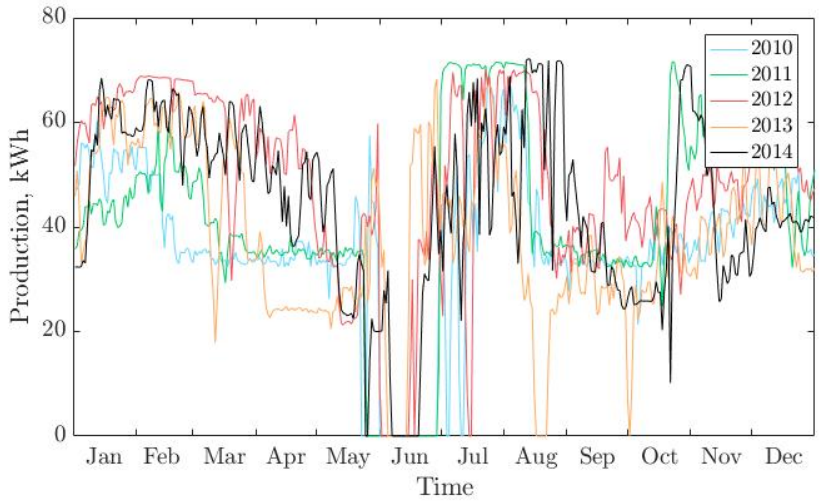

Figure 4.20: Production data averaged every 24 hours for the hydro power stations in each of the years 2010-2014

4.5 Consumption data

Troms Kraft has provided data for the electricity consumption in the concession area of *Troms Kraft* in 2016, which includes 15 municipalities and almost 120 000 inhabitants (a list of the municipalities and their number of inhabitants is included in Appendix B). This will be used to compare the output from the hybrid system to the trends of the consumption. The demand 2016 is plotted in Figure 4.21 and Figure 4.22, showing daily averages and hourly day-profiles in each quarter year, respectively. It is seen that the largest demand for electricity is in January, and the lowest demand in July.

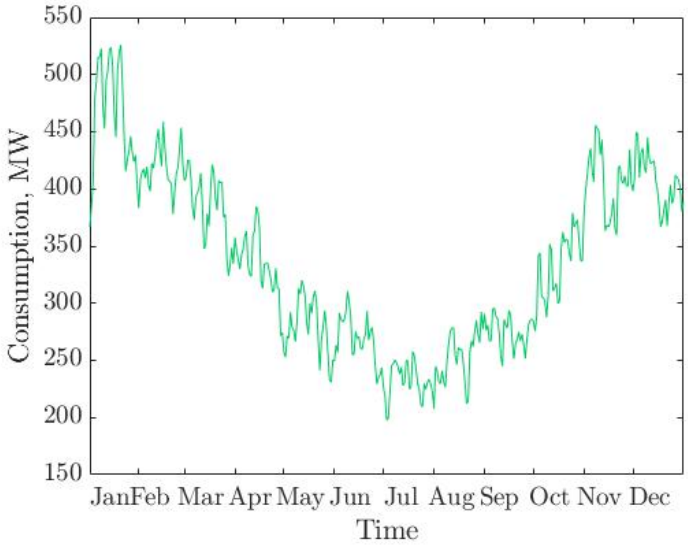

Figure 4.21: Daily averaged consumption data for Troms in 2016

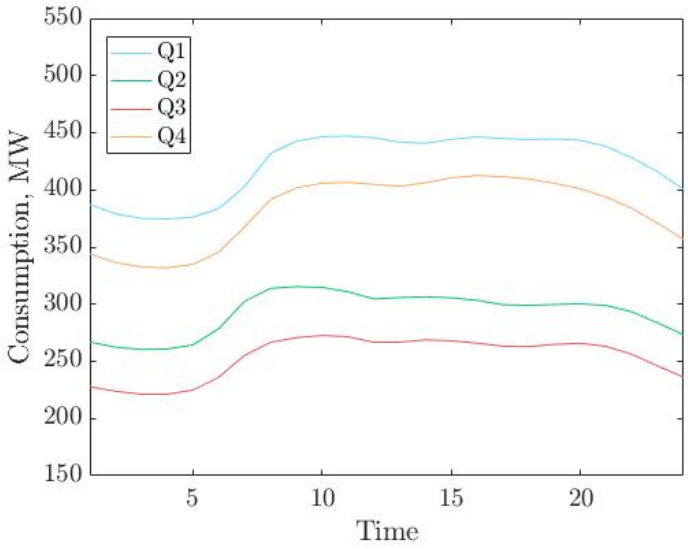

Figure 4.22: Average daily consumption profile in each quarter year in 2016, plotted with hourly values

4.6 Economic data

The price of renewable technologies have been decreasing quite dramatically, much due to an increased focus on greener energy and deployment in this field. As more renewable energy is installed, better technology solutions are developed. It is important to bear in mind that because the amount of installed renewable energy increases and its cost decreases rapidly, cost data used should be up to date. By using outdated estimates the calculations may lead to overestimations, and this may even be the case for one-year old data.

In addition, often average costs from the whole of Europe is provided, leading to uncertainty and errors compared to costs for installing renewable capacity in Norway, especially northern Norway, where shipment, existing infrastructure and other factors may result in different costs than in other parts of Europe. Regional differences will also occur due to the available renewable resource at the site, which as discussed, is very variable. Finally, different manufacturers produce products with different characteristics and costs, which will affect the total cost of the system.

Care must thus be taken when performing a economic analysis of a hybrid system, and the results must only be regarded as indications.

In a project such as a hybrid system, several costs and incomes must be taken into account:

- Capital cost: the investment required to be able to commission the plant
- Operation and maintenance (O& M) cost: variable or fixed costs which is due to operating the plant and other maintenance required during its lifetime
- Replacement costs: The cost of replacing system components
- Salvage cost: If a component has not operated its full lifetime at the end of the lifetime of the whole system, it has a salvage value
- Income due to sale of electricity: as the plant produces electricity, the market electricity price governs the income

When conversions between currencies is done, the average exchange rate in 2014 and 2015 is found at *DNBs* web pages [ASA,], and is shown in Table 4.1.

Table 4.1: Average exchange rates between currencies in 2014 and 2015

Conversion	Multiply by
$USD_{2014} \longrightarrow NOK$	6.3000
$USD_{2015} \longrightarrow NOK$	8.0640

4.6.1 Typical costs of a solar power plant

The capital cost of a PV plant includes the cost of the modules themselves and the cost of balancing the system. The balancing costs comprises basically everything except the module costs, e.g. the inverter and other power electronics, preparation of the site and construction of the framework, system design, labour hours, etc. [IRENA, 2015]. Because the cost of PV modules has decreased very rapidly, the costs of balancing the system have become more important.

The price of PV modules was in 2014 only $\frac{1}{4}$ of its price in 2009, and the cost of PV systems of utility-scale (installed capacity of above 1 MW) have decreased by 29% – 65% from 2010 to 2014 [IRENA, 2015].

In a report from *WWF* and *Accenture* [Zaitsev et al., 2016], the average capital cost of a 10 – 100 kW solar power plant in Norway in 2015 was 14000 NOK/kW, where the modules account for 8900 NOK/kW, inverter 1200 NOK/kW, installation 2800 NOK/kW and other equipment 1100 NOK/kW. Hence, the modules are expected to account for approximately 64% of the total capital cost, the inverter 8.5%, installation 20% and other equipment 7.5%.

There is very little documentation on costs for solar power plants in northern Norway, especially large-scale systems. However, after speaking to the company *Solbes AS* [Øystein Kleven,], a typical capital cost for large-scale solar power plants (power converters excluded) is taken to be 7500 NOK/kW_p, as they stated that it definitely is possible to achieve a cost below 10000 NOK/kW_p for a system, and as a system of the size considered in this thesis will result in lower costs than smaller systems. They also agreed that a price down to 5000 NOK/kW_p could be possible. The costs for tracking systems, however, has not been obtained, but *Solbes AS* would guess that a cost increase between 40% and 80% compared to stationary systems is not unlikely.

The power converters have a shorter lifetime than the solar modules, and hence must be replaced. Their lifetime is 10-15 years, thus they must be replaced at least once during the lifetime of the solar power system, with a cost range of 1200 – 1600 NOK/kW [Zaitsev et al., 2016]. However, as the estimate from *Solbes AS* was drastically lower for a PV power plant than the capital cost given in [Zaitsev et al., 2016], also the capital cost of the inverter is scaled down by the

same fraction, giving an estimate of 700 NOK/kW.

Operation and maintenance costs are generally lower for solar power plants than wind power plants, partly because there are no moving parts. In [Multiconsult, 2013], a ground-mounted solar power plant with installed capacity of 1 MWp in Norway in 2013 had a annual O&M-cost of 2% of the total investment cost. This is the same value as the one given in [Zaitsev et al., 2016].

The lifetime of a solar power plant is in economic calculations usually taken to be 25 years, and most often a warranty of 25 years is given from the PV module producer. But it has been experienced that modules have the capacity to live longer than this, maybe even up to 30-50 years. In [IRENA, 2015] the average capacity factor in Europe in the period 2013-2014 is given as approximately 14%, and in [REN21, 2016], the average capacity factor in 2016 in Europe is given as 12.3%. The capacity factor is defined as how large a proportion the actual power output from the power plant is of the output that would result if the plant was operating at its rated capacity for a full period of time (typically 1 year).

4.6.2 Typical costs of a wind power plant

In [IRENA, 2015], it is stated that because the technology has improved drastically and installed costs have decreased correspondingly, onshore wind power is (on a worldwide basis) one of the most competitive electricity sources, both considering renewable and fossil fuel sources. However, it is projected that the costs of PV electricity will decrease more rapidly in the next years than onshore wind, hence the difference between the two electricity sources will most likely decrease.

The largest part of the capital cost of wind power plants are the turbines themselves, and they are on a worldwide average between 64% and 74% of the total capital cost [IRENA, 2015]. The construction costs are typically 4% – 10% and other costs (e.g. infrastructure and buildings) account for 4% – 10%. The cost of connecting to the grid is typically between 8% and 11% of the capital cost considering projects all over the world. These percentages coincides to some extent with the breakdown of capital cost in a report from *NVE*, where the capital cost of five projects commissioned in the period 2011-2013 in Norway was distributed as follows: turbines 66%, construction of turbine foundations 5%, construction of infrastructure and non-electrical systems 14%, grid connection 8%, costs for use of land area and other one-time costs 1% and project management 6% [Sidelnikova et al., 2015]. However, there is a very low number of projects available for cost estimates in [Sidelnikova et al., 2015], and the projects had a large spread in capital costs.

According to [IRENA, 2015], the average total installed costs of utility scale wind farms in Norway in 2014 was 1978 $\text{USD}_{2014}/\text{kW} \approx 12461\ \text{NOK}/\text{kW}$. In [REN21, 2016], the weighted average capital cost of a wind farm in Europe in 2015 was $1917\ \text{USD}_{2015}/\text{kW} \approx 15459\ \text{NOK}/\text{kW}$. In [Sidelnikova et al., 2015], the capital cost of wind plants commissioned in the period 2011-2013 in Norway was $12005\ \text{NOK}/\text{kW}$. *Troms Kraft* has provided cost data from their wind power plant *Fakken* in Troms, where each turbine of 3 MW had a cost of 23 million NOK, implying a cost of $7667\ \text{NOK}/\text{kW}$. If this is taken as 66% of the total capital cost, the capital cost for the whole wind turbine system is calculated to be approximately $13700\ \text{NOK}/\text{kW}$.

From the costs found here, it is seen that the capital cost of a wind power system in Norway is well represented by a value of $13700\ \text{NOK}/\text{kW}$.

The O&M costs of onshore wind power plants were reported by [IRENA, 2015] to be $0.0211 - 0.0390\ \text{USD}_{2014} \approx 0.13 - 0.25\ \text{NOK}$ per kWh produced in Norway in 2014. In [Sidelnikova et al., 2015], a value of $0.15\ \text{NOK}/\text{kWh}$ is used for O&M costs, which is equivalent with what *Troms Kraft* has provided for their wind power plant at *Fakken*.

The typical lifetime of a wind power plant is taken to be 25 years in economic analyses, but they can operate for longer time spans than this. The average capacity factor in the period 2010-2014 in Europe was approximately 27% [IRENA, 2015]. The capacity factor was on average (in Europe) in 2016 given as 27.7% in [REN21, 2016], and the estimated capacity factor in Norway is calculated by *NVE* to be 33.8% in [Sidelnikova et al., 2015] in the period 2011-2013.

4.6.3 Typical costs for a solar/wind hybrid system

A hybrid system consisting of a solar, wind and hydro power plant will have a higher capital cost than each power plant separately, as inter alia controlling features and regulators are more complex. There is very little documentation on these extra costs, and in this thesis they are not regarded in the NPV analysis, which hence must be kept in mind when discussing the result. Also costs of grid extensions are omitted from this study.

From the discussion in this section, the following economic data is chosen for the simulations:

Table 4.2: Estimates of costs associated with a hybrid system

Cost	Unit	Value
Capital cost PV power plant, including installation	NOK/kW_p	7 500
Capital cost inverter	NOK/kW	700
Capital cost wind power plant, including installation	NOK/kW	13 700
Annual O&M cost solar	percentage of capital cost	2
Annual O&M cost wind	NOK/kWh	0.15

In Norway and Sweden there is an electricity certificate market which exists to promote renewable electricity production. The electricity producers receives one certificate per renewable MWh they produce, and the certificates are sold to power suppliers and electricity customers which are legally required to buy certificates. The supply and demand determines the price of the certificates [NVE, 2017]. It is also possible to apply for funding from *Enova*.

4.6.4 Electricity prices

From the website `nordpoolspot.com`, electricity prices in Tromsø is found for 2016 [Nord Pool,]. The prices are hourly averages, and will be used in the economic analysis. A plot of daily averages of the electricity price throughout the year in Tromsø in 2016 is shown in in each quarter of the year is shown in Figure 4.23. The electricity price had high peaks in January 2016, and the average electricity price in Tromsø in 2016 is calculated to be 0.23 NOK/kWh.

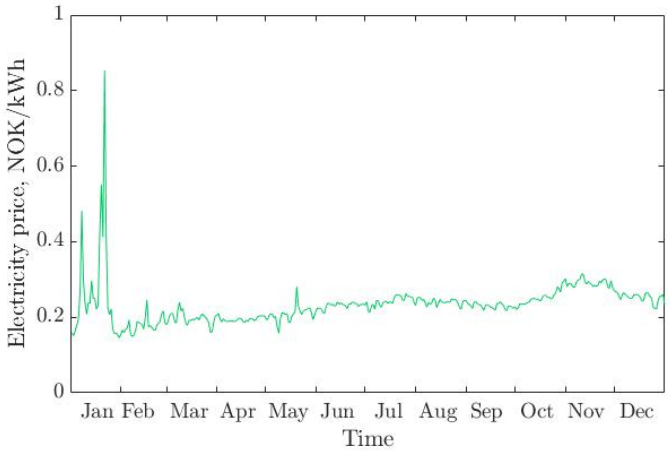

Figure 4.23: Daily averaged electricity prices in Tromsø in 2016

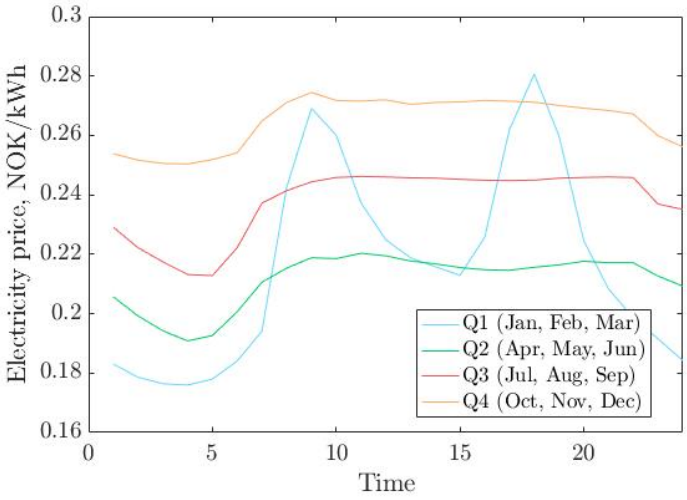

Figure 4.24: Average daily profile of electricity prices in each quarter year, plotted with hourly values

In addition, *Troms Kraft* has provided future projections for electricity prices in Tromsø, with an average for each year in the period 2017-2040, which will be used in the simulations. These projections show that the electricity price tend to increase the next decades. These data are not publicly available, hence their exact values cannot be given in this thesis, but they are overall expected to increase to some degree.

4.7 Statistical analysis of weather data

4.7.1 Representativeness of WRF simulated solar radiation data

As simulations also were done for Holt, the simulated data from Holt in 2016 (described in subsubsection 4.1.2) and the actual measured solar radiation data (described in subsubsection 4.1.1) will be compared by using the Pearson correlation coefficient, the RMSE and the bias, explained in Section 2.7. By analysing the results, a choice is made if the simulated solar radiation data for Galgo should be used as they are or if they should be altered to fit the measured solar conditions better regarding amount of radiation and timing.

4.7.2 Comparison of solar radiation at different locations

For both the measured and simulated solar radiation data at Galgo and Holt, the solar radiation in $^{kWh}/_{m^2}$ (the sum of $^{kW}/_{m^2}$ each hour) in a period of time (2016 and/or Jan-Apr 2017) will be calculated to be able to compare the measured and simulated solar radiation at different locations.

4.7.3 Anti-correlation between solar and wind resources

The Pearson coefficient (Equation 2.11) is calculated for the simulated solar radiation data from Galgo in 2016 (described in subsubsection 4.1.2) and the wind power data from Rieppi in 2016 calculated from the wind speed data described in subsubsection 4.2.1 by using Equation 2.4, using the air density at 0°C; $1.29\ ^{kg}/_{m^3}$. The coefficient is calculated for data series which are hourly averages, 24-hour averages, weekly averages and monthly averages.

An anti-correlation analysis is also done on measured solar radiation at Galgo (see subsubsection 4.1.1) and measured wind speed data at Rieppi in the first four months of 2017 by calculating the Pearson coefficient in the same way as explained for the 2016 data.

4.8 Simulation software: HOMER Pro

There is a large number of software available to simulate hybrid systems, and each has advantages and disadvantages. In this thesis, *HOMER Pro* is used, because of its many options for optimisation, sizing and visualisation and its user-friendliness. It is also one of the most widely used programs worldwide for

hybrid systems. It is mainly designed for small-scale systems and microgrids, but can be used for large-scale systems as well. It is developed by the National Renewable Energy Laboratory (NREL) in USA for on-grid systems and off-grid systems [Sinha and Chandel, 2014]. A disadvantage of the software is its "black box" characteristics; the codes used for programming the software cannot be seen or changed,and not all calculated parameters are given as outputs.

The main focus of the simulation will be to obtain the technological performance of the system with different parameters. For example, PV panels may have tracking systems or not, and different values of the albedo and/or surface roughness can be simulated, in addition to different PV efficiencies, PV slopes, turbine losses, and wind speeds. Another interesting aspect which will be examined is the economics of the system.

To simulate a hybrid system using *HOMER Pro*, inputs regarding the technology options, the costs of the components, the resources available and any electric loads must be provided. It does not output variability at a more detailed level than hourly, but can take inputs of smaller time resolution (down to one-minute intervals). The software simulates a large number of different configurations of the system in each time step during a year, where the energy balance between the possible amount of energy produced and the demand is calculated. *HOMER Pro* then calculates the energy flow to and from the system components [HOMER Energy, 2016]. It can be chosen that HOMER optimises the system regarding system size and other variables.

Simulations are only done for the PV and wind components, as the hydro power stations are already existing. Also, since the hydro power stations have been operated based on electricity price rather than electricity demand, their power output has varied from year to year (as can be seen in Section 4.4). In addition, there is a lack of production data from 2016. To simulate a hydro power station, HOMER takes as input the stram flow to the turbines, which could not be received from *Troms Kraft*. Thus, a simulation of the hydro power stations turned out to be difficult. Instead, a theoretical analysis is done on the interaction between the PV, wind and hydro components. Restrictions in the area on for instance grid capacity should be taken into account, and the correlation between electricity produced and electricity consumption in the region will be studied.

HOMER Pro contains several modules, each representing different components of the system. The modules used for the hybrid system simulations in this thesis are described in the section below. The information about the modules is from HOMER's User Manual ([HOMER Energy, 2016]).

4.8.1 PV module

HOMER calculates the power output from the PV modules by using data series for the global horizontal irradiation (GHI) as input, in addition to parameters defining the characteristics of the PV modules, such as efficiency, temperature coefficient, derating factor etc. The calculations are appended in Appendix D.

4.8.2 Inverter module

HOMER simulates a centralised inverter (see Subsection 2.5.2).

As the lifetime of power converters is shorter than for PV modules and wind turbines, the converters must be replaced during the lifetime of the system, and the new converter still has a value when the lifetime of the other components is over. This value is called salvage value and is calculated by:

$$S = C_{\text{rep}} \cdot \frac{t_{\text{rem}}}{t_{\text{conv}}}$$

Where C_{rep} is the replacement cost of the converters, t_{rem} is the remaining lifetime of the converters and t_{conv} is the lifetime of the converters. The relationship between the replacement cost and salvage value is thus assumed to be linear.

4.8.3 Wind module

In each time step, HOMER uses the logarithmic vertical profile of wind speed (Equation 2.5) to calculate the wind speed at the hub height of the wind turbine(s) from the wind speed data series input at a given height and a given surface roughness. It then uses the power curve given for the wind turbine to estimate the power output.

4.8.4 Electrical load

Represents the local electricity demand that must be met before the remaining electricity produced can be sold to the grid.

4.8.5 Advanced grid module

The advanced grid allows a variation of the electricity price throughout the year to be taken into account for the simulation period. Real time electricity prices can be imported to the program. Also the maximum capacity of the grid can be defined for the simulations.

4.8.6 Multi-year analysis

The multi-year analysis allows changes of certain parameters in the system's lifetime to be accounted for. The parameters that can be included in the multi-year analysis are PV degradation, grid electricity price, etc. The changes can be expressed as a percentage each year or a multiplier for every year of the total lifetime of the system. When using this module HOMER simulates each year separately instead of extrapolating the results from the simulation of one year to the rest of the lifetime of the system. When using the multi-year module, the size of the PV and wind systems must be specified manually, and cannot be optimised by HOMER.

4.9 Inputs to simulations

The simulation of the hybrid system will be performed for 4 scenarios (denoted S1-S4); S1 has standard PV modules, S2 horizontal PV tracking system, S3 vertical axis PV tracking system and S4 two-axis tracking system. The systems are astronomical tracking systems (ref. subsubsection 2.1.6), as HOMER calculates the position of the Sun the system adjusts to. In all these scenarios, the tracking system changes position continuously, and the converter is set to have the same input capacity as the maximum PV power output (rounded up to the nearest 0.5 MW) from the system, thus able to invert all the power produced from the PV modules. Also an attempt of simulating a scenario with bifacial modules (see subsubsection 2.1.6) even though HOMER does not have the ability to do this automatically was done, but it did not give reasonable values, and should instead be performed in later studies with other types of simulation software.

As the PV power potential in northern Norway is not analysed to the same degree as wind power potential, the different scenarios focus on variations in the PV components. In addition, there are less possibilities for varying wind power components in HOMER than varying PV power components.

Table 4.3 shows the PV simulation parameters and settings which differ in

the different scenarios. The azimuth angle was originally chosen to be the conventional value 0°(PV modules facing south). However, it was discovered when there was under 24 hours left to the submission of this thesis that changing the azimuth angle to be more eastward resulted in a higher energy output than when it is kept at 0°, due inter alia to the timing error of the simulated solar radiation data. As there was no time to perform all simulations all over again, one simulation is done for the scenario with stationary modules and one for the scenario with horizontal-axis tracking systems, to see how large the effect of changing the azimuth angle to its optimal value has. These results are shown in Section 5.2, and it is important to remember that the remaining simulation results does not take into account this timing error effect.

The simulated solar radiation data also overestimates the measured values, but this is accounted for by choosing a scaling of 0.7 of the original simulated values (see Subsection 5.1.1).

The optimal slope angle is found by simulating the system with different angles combined with different types radiation levels and observing which slope is optimal. This is done in Subsection 5.3.1.

Table 4.3: Inputs to HOMER that varies with scenario

	Tracking system	Panel slope (degrees)	Panel azimuth (degrees west of south)	Converter size/ maximum output (MW)
S1	No tracking	50.00	0.00	14
S2	Horizontal axis	-	0.00	14.5
S3	Vertical axis	69.00	-	19
S4	Two-axis	-	-	19.5

Table 4.4 shows the simulation parameters and settings for the PV and wind components.

Table 4.4: PV and wind component and resource inputs to HOMER Pro (similar for all scenarios)

PV parameter/setting	**Unit**	**Value**
PV module type		Generic flat plate PV
Lifetime	Years	25 (ref. Subsection 4.6.1)
Derating factor	%	90 (ref. Subsection 2.1.4)
Size	MW	20
Efficiency at STC	%	20
Temperature coefficient	% change in efficiency/°C	-0.5 (ref subsubsection 2.1.4)
NOCT	°C	47.00 (default in HOMER)
Electrical bus	AC or DC	DC
Ground reflectance	%	see description below the table
PV capital cost	NOK/kW	7 500 (ref. Subsection 4.6.1)
PV replacement cost	NOK/kW	7 500 (ref. Subsection 4.6.1)
PV O&M cost	NOK/year	150 (ref. Subsection 4.6.1)
Converter capital cost	NOK/kW	700 (ref. Subsection 4.6.1)
Converter replacement cost	NOK/kW	700 (ref. Subsection 4.6.1)
Converter O&M cost	NOK/year	14 (ref. Subsection 4.6.1)
Converter lifetime	Years	15 (ref. Subsection 4.6.1)
Converter efficiency	%	95
Converter parallel with AC generator		yes
Global horizontal irradiance	kW/m²	Imported data described in subsubsection 4.1.2, scaled by 0.7
Wind parameter/setting	**Unit**	**Value**
Wind turbine type		Generic
Rated capacity of each turbine	MW	3
Lifetime	Years	25 (ref. Subsection 4.6.2)
Hub height	Meters	80
Consider ambient temperature effects		no
Number of turbines		7
Capital cost	NOK/kW	13 700 (ref. Subsection 4.6.2)
Replacement cost	NOK/kW	13 700 (ref. Subsection 4.6.2)
O&M cost	NOK/kWh produced	0.15 (ref. Subsection 4.6.2)
Total turbine losses	%	0.8
Electrical bus	AC or DC	AC
Wind speed	m/s	Imported data described in subsubsection 4.2.1
Altitude above sea level	Meters	492
Anemometer height	Meters	10
Wind speed profile		Logarithmic
Surface roughness length	Meters	see description below the table

The PV component of the hybrid system is chosen to be a 20 MW system, and the wind component a 21 MW system consisting of 7 turbines. The choice of size of PV system is done in collaboration with Charlotte Tiller, as *Fakken* has lower grid capacity, and a similar size of PV system makes a comparison of the feasibility of the locations easier. In addition, a PV system of 20 MW is very large and has not been constructed in northern Norway before, so implementing a larger system is not expedient. The choice of wind power system may seem small, but it makes it easier to compare to the power output from the PV system. In addition, *Troms Kraft* did in 2014 applied for constructing a wind power plant in the area with a capacity of up to 80 MW [Troms Kraft, 2014], but this was rejected, partly because of environmental factors. Therefore, it seems that a very large wind power plant is not expedient to examine.

When importing the simulated solar radiation data, HOMER calculates a clearness index representing the clearness of the atmosphere (normally between 0 and 1 representing cloudy and clear conditions respectively, see Appendix D to see its calculation), and it turns out to be above 1 in July, and zero in June. These are bizarre values, and can be explained by the overestimation of the simulated radiation data compared to measured values. As the clearness index divides the GHI at the surface of the Earth by a calculated extraterrestrial horizontal radiation, very high values of solar radiation at the Earth's surface can cause the clearness index to become above 1. As HOMER expects a clearness index between 0 and 1, a clearness index which is very large may cause a bug in the software, causing the clearness index to be zero in June. Further examination of the calculation of the clearness index in HOMER is not possible, as it does not output the clearness index calculated for any shorter time period than one month. This must be kept in mind when discussing the results.

The efficiency of the PV modules is chosen to be 20% from the information in Subsection 2.1.4. The values given there of best-research cell efficiencies are 22-25%, but HOMER takes as input the module efficiency, which is found in subsubsection 2.1.5 to be lower than the cell efficiency. In addition, the efficiency should be for commercial modules, hence the efficiency is chosen to be a bit lower, namely 20%. In Subsection 2.5.2, inverter efficiencies of 97-98% are found, and 99% is found to be the efficiency in the latest age of inverters, hence an efficiency of 95% is thought to be reasonable to use. The inverter in HOMER is a central inverter (see Subsection 2.5.2).

The wind turbines used in the simulation resembles V90 3 MW turbines from *Vestas*, which is the type of turbine installed in another wind farm owned by *Troms Kraft*, namely *Fakken* wind power plant in Troms. The power curve of the turbines is given by *Troms Kraft* and is shown in Figure 4.25. The power curve should ideally be given for an air density of 1.29 kg/m^3, but *Troms Kraft* only had information for air densities up to 1.27 kg/m^3, and hence this power

curve is used. In the simulations, ambient temperature effects are chosen to not be included as this caused the power output from the wind turbines to exceed 3 MW at high wind speeds. Because the power curve is given from *Troms Kraft*, this is the power output at different wind speeds that should be simulated.

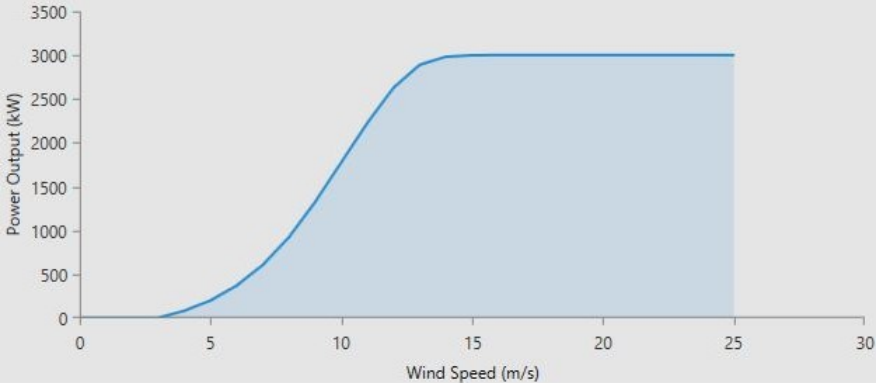

Figure 4.25: Power curve of a V90 3 MW wind turbine. Snapshot from HOMER

The hub height of the turbines are 80 meters, and the electrical losses from the wind turbines to the transformer station are received from *Troms Kraft* to be 0.8%, and this is used as input to the simulations. However, this does not take into account turbulence/wake losses and other losses. HOMER does not calculate any turbulence parameters. Therefore, in this thesis, such losses are omitted, and must be taken into account when discussing the results. For a representative loss value, a turbulence and wake loss analysis should be done on the terrain and the eventual distance between turbines in the power plant, hence it is agreed in collaboration with *Troms Kraft* that the exact examination of these effects are outside the scope of this thesis.

At *Fakken*, the wind turbines have asynchronous induction generators, causing the grid connection to consist of a power converter connected to the rotor of the generator, converting approximately 30% of the total power from the wind turbine (see Subsection 2.5.3).

Regarding the albedo and surface roughness values chosen for the simulations, different approaches are done for the technical and economic analysis. HOMER does not have the ability to change the albedo through the year of simulation. Therefore, in the technical analysis, the simulations are done for the following three combinations of albedos and surface roughnesses (the values are from Table 2.1 and Table 2.2):

- **Fresh snow**: albedo 90% and surface roughness 0.003 m

- **Old snow**: albedo 60% and surface roughness 0.003 m
- **Heathland**: albedo 20% and surface roughness 0.01 m

The results from each of the simulations in HOMER then have to be manually merged together so that the simulation results represent a year when there is fresh snow in the period 1 Oct-31 Mar, old snow 1 Apr-15 Jun, and heathland 16 Jun-31 Sep. This corresponds well with Figure 3.4 showing the number of days with snow cover in the Skibotn area, as this approach gives results representing a year with 258 days of snow cover.

In the economic analysis, an average albedo and surface roughness is found for use in the simulations by using a trial-and-error approach until values for albedo and surface roughness are found so that the energy output is equal to the corresponding scenario in the technical analysis. This is chosen as the approach because implementing different albedos and surface roughnesses manually when the revenue from grid sales is different from year to year (due to changing electricity prices, ref Subsection 4.6.4) will be extremely time-consuming. In addition, HOMER does not output grid sales revenue from the PV and wind component separately, which complicates the process of finding economic parameters for each component.

Table 4.5 shows the simulation parameters and settings for other inputs to HOMER that does not change with different scenarios. The load of the system is the amount of electricity the wind turbines consumes while operating (e.g. during start-up), and data is provided by *Troms Kraft* for the electricity consumed by the turbines at *Fakken*. The average electricity consumed by 7 such turbines are set as input to the load in HOMER, and to resemble that the consumption is not constant, a random variability is set.

The discount rate is by recommendations from *Troms Kraft* set to 5%, and the simulations and calculations in this thesis do not consider inflation rate.

Table 4.5: Other inputs to HOMER Pro (similar for all four scenarios)

Parameter	Unit	Value
Advanced grid inputs		
Type of electricity rates		Real time rates
Sale capacity	MW	100
Purchase capacity	MW	100
Load inputs		
Load average	kW	26.928
Load peak month		None
Load profile		Blank
Day-to-day variability	%	100.00
Timestep	%	1
Multi-year inputs		
Grid electricity price	$^{\text{multiplier}}/_{\text{year}}$	Values described in Subsection 4.6.4
Degradation of PV panels	$^{\%}/_{\text{year}}$	0.5 (ref. Subsection 2.1.4)
Economics and system settings		
Discount rate	%	5.00
Inflation rate	%	0.00
Annual capacity shortage	%	100.00
Project lifetime	Years	25 (ref. Subsection 4.6.1 and Subsection 4.6.2)

4.10 Simulation outputs

Firstly, the effect of choosing an optimal azimuth angle to account for timing errors in the simulated solar radiation data is examined, and the reader is reminded that in the remaining results, this effect is not included.

Then, the combined effect of radiation level and PV slope is examined to be able to decide an optimal slope angle at the location, which will be the slope angle used in the simulations.

The results are divided in a technical part and a economic part, and in addition a future scenario is simulated.

4.10.1 Technical part

In the technical part, the PV and wind turbine power outputs will be examined in the different scenarios. Also values for capacity factors and amount of electricity produced and electricity purchased and sold will be given and discussed.

A sensitivity analysis will be performed for chosen variables. The following list shows which variables will be varied one by one, keeping the other parameters as shown in the tables in the previous section (shown in bold in the list below). The percentages for radiation and wind speed represents percentages of the simulated solar radiation data and measured wind speed data. HOMER calculates the annual average of the solar radiation input and wind speed input, and this annual average is scaled up or down according to the percentages given in the list below.

- PV module efficiency: 17%, **20%**, 23% and 30%
- Inverter efficiency: **95%** and 99%
- Slope of PV modules: 40°, 50°, 60°, 69°, 80°and 90°
- Solar radiation: **70% (annual average**1.967 kWh/m^2 **per day)**, 80% (2.248 kWh/m^2 per day), 90% (2.529 kWh/m^2 per day), 100% (2.81 kWh/m^2 per day)
- Wind turbine losses: **0.8%**, 5%, 10%, 15%, 20% and 30%
- Wind speed: 80% (4.776 m/s per day), 90% (5.373 m/s per day), 95% (5.672 m/s per day), **100% (**5.97 m/s **per day)**, 105% (6.269 m/s per day), 110% (6.567 m/s per day) and 120% (7.164 m/s per day)

For the tracking scenarios, the above parameters will be varied when applicable. In Scenario 2 and 4, for example, changing the slope of the panels is not possible. A slope of 69°instead of 70°is chosen because HOMER sets the latitude of the location as the default angle, and therefore it is interesting to examine this value.

When varying the PV efficiency in HOMER, also the size of the PV system must be changed manually, as the multi-year module is used which causes size optimisation to be unavailable. Thus, when the efficiency is changed from 20% to 23%, also the system size must be changed by the same relative amount, hence from 20 MW to 23 MW. Even though a PV efficiency of silicon PV modules of 30% has not been accomplished yet, it is included in the sensitivity analysis to observe the effect of increasing the efficiency to the extreme, and in the future an efficiency of 30% can be achievable, as work is performed continuously to increase the efficiency of PV cells. The inverter efficiency sensitivity is chosen to be at 99% because this is found to be a possible value to achieve for commercial inverters today.

As mentioned in Subsection 2.2.5, wake losses can account for a power loss of up to 25%, and therefore the effect of choosing different loss values is examined.

The sensitivity values for wind speed is chosen based on the values found in [Weir, 2017], where wind conditions in 2016 was seen to be approximately 5% lower than the period 2000-2015. ±10% and ±20% are chosen because later years will show other deviations.

As part of the technical analysis, also the power output from the PV and wind components throughout one year will be examined, and compared to the electricity demand in the area and the maximum grid capacity. As the demand is given for 15 municipalities in Troms, this demand is larger than the grid capacity in Skibotn. To solve this, the hourly values for the demand is scaled by a factor such that its maximum value is just below 100 MW. In this way, the electricity produced from the hybrid system can be compared to the trends of the demand in the area. Also the interaction with the existing hydro power stations will be examined, and includes combining the power output from the PV and wind components with the power output from the hydro power stations in 2014 (as there is no available data from 2016).

Finally, solutions for connecting the hybrid system to the grid will also be discussed, and advantages and disadvantages with how HOMER connects the system to the grid are examined. Also economic aspects of connecting the system to the grid will be discussed.

4.10.2 Economic part

In the economic part, NPV and LCOE values will be calculated for Scenario 1, and values needed for their calculations are specified. The NPV is calculated by Equation 2.12, and the LCOE from Equation 2.13. In the formula for LCOE, the electricity generated is taken to be the sum of wind power output and the converter power output achieved from HOMER simulations, and these includes the effect of degradation of the PV modules. The NPV and LCOE of only the solar or wind component is given, and this is estimated from individual simulations of systems consisting of only solar components or only wind components, as HOMER does not give the grid sales separately for the solar and wind components.

The economic results are shown for the costs found in Subsection 4.6.3, in addition to a case with low costs and one with high costs (approximately ±30%). The reason for the choice of low and high costs range is the information from *Solbes* in Subsection 4.6.1 that the variation in PV systems can be from 5000 NOK/kW to 10000 NOK/kW. Although it is found in Subsection 4.6.2 that in the future PV system costs are expected to decrease more than wind power systems, the relative change in costs is taken to be the same for both systems. This is both for simplicity and due to lack of information on wind system costs.

The costs used in the low and high cost cases are shown in Table 4.6.

Table 4.6: Estimates of low and high costs associated with a hybrid system

Cost	Unit	Low value	High value
Capital cost PV power plant, including installation	NOK/kW_p	5 000	10 000
Capital cost inverter	NOK/kW	467	933
Capital cost wind power plant, including installation	NOK/kW	9 133	18 267
Annual O&M cost solar	percentage of capital cost	2	2
Annual O&M cost wind	NOK/kWh	0.10	0.20

In addition, a sensitivity analysis is done on the NPV and LCOE found using the costs values from Subsection 4.6.3. The following variables will be varied one by one, keeping the other parameters as explained previously (shown in bold).

- PV slope: 40°, 50°, 60°, 69°, 80°and 90°
- Solar radiation level: **70% (annual average** 1.967 kWh/m^2 **per day)**, 80% (2.248 kWh/m^2 per day), 90% (2.529 kWh/m^2 per day), 100% (2.81 kWh/m^2 per day)
- Wind turbine losses: **0.8%**, 5%, 10%, 15%, 20% and 30%
- Wind speed: 60% (annual average 3.582 m/s per day), 80% (4.776 m/s per day), **100% (**5.97 m/s **per day)** 120% (7.164 m/s per day) and 140% (8.358 m/s per day)
- Discount rate: 2%, **5%** and 8%
- Electricity price (only applicable for the NPV): 50%, 100%, 150% and 200% of the original price

The choices of sensitivity variables are the same as in the technical analysis, in addition to variation of the economic variables discount rate and electricity price. The choice of discount rate is done because the discount rate is very uncertain, and in addition it is very probable that it will vary during the lifetime of the system. The electricity price is essential for the profitability (at least the NPV value) of the system, and is therefore included in the sensitivity analysis. As it is difficult to predict the electricity prices in the future, simple values are

chosen, up to a doubling in price.

It is important to keep in mind that as the PV energy output changes, the inverter size is changed so that it always has the capacity to convert all electricity output from the PV modules, hence better PV performance increases the costs of the inverter. However, the inverter costs comprise a relatively small share of the total costs, and the effect is not drastic. A sensitivity analysis is not performed on PV and inverter efficiency as it is not known how a change in these efficiencies influence the costs of the components.

As representative cost information for tracking systems are not available, the focus is on which costs the tracking systems must be purchased for to be economically equal (equal NPV or LCOE) to the scenario with stationary modules (S1).

4.10.3 Future scenario

Finally, a system with stationary PV modules which can represent a future situation is simulated and analysed both technically and economically. The parameters changed compared to Scenario 1 are:

- Costs: all costs (capital and O&M costs both for PV and wind components) are taken to be approximately 30% lower than the costs in S1
- PV efficiency: the efficiency of the PV modules is set to 30%, and hence the size of the PV system increases to 30 MW
- Inverter efficiency: chosen to be 99%
- Inverter size: due to a higher PV power output, the inverter size is increased. To be able to convert all output from the PV modules, the size is set to 22 MW

Also in this case, the assumption that both PV systems and wind turbine systems decrease with the same amount is not completely correct compared to what is expected in the future, but it is chosen in this analysis because of simplicity. Cost projections for the future are in any case very uncertain, and the economic aspect is not the most important part of the thesis. It is done for estimating indications on the system's profitability.

The electricity prices are kept as in Scenario 1, as it is difficult to predict their development in the far future.

4.11 Sources of error

A summary of the most important sources of errors are included in the end of the chapter.

4.12 Comparison with *Fakken*

A master's thesis is written by Charlotte Tiller concerning a hybrid system at another location in Northern Norway called *Fakken*, where the feasibility of adding a solar power plant to an already existing wind power plant at the location is examined. Therefore, a comparison of the potential solar resource in Skibotndalen and Fakken will be performed.

5

Results and discussion

5.1 Statistical analysis of weather data

5.1.1 Representativeness of WRF simulated solar radiation data

The Pearson coefficients (Equation 2.11), RMSE (Equation 2.9) and the bias (Equation 2.10) calculated for the simulated solar radiation data from Holt in 2016 (described in subsubsection 4.1.2) and the measured solar radiation data from Holt in 2016 (described in subsubsection 4.1.1) are shown in Table 5.1. The parameters are calculated using values averaged every 60 minutes, 24 hours, weekly and monthly, and the calculation is done for the whole year and for each month separately. For weekly and monthly data resolution the parameters are only calculated for the whole year. The coefficient is non-applicable for December, as the simulated data contains only values of 0 W/m^2. Table 5.2 shows the calculated mean for the simulated and measured solar radiation data for 2016 and each month separately.

Table 5.1: Statistical parameters for the simulated solar radiation data and measured solar radiation data at Holt in 2016

Time period	Parameter	Data resolution			
		60 min	daily	weekly	monthly
2016	Pearson	0.8459	0.9004	0.9678	0.9784
	RMSE	97.86	58.15	46.13	44.99
	Bias	28.93	28.85	28.93	28.75
January	Pearson	0.6834	0.7485		
	RMSE	2.413	1.477		
	Bias	-1.292	-1.292		
February	Pearson	0.7597	0.7881		
	RMSE	22.96	7.758		
	Bias	2.92	2.92		
March	Pearson	0.8256	0.8284		
	RMSE	59.41	20.56		
	Bias	9.125	9.051		
April	Pearson	0.8894	0.7448		
	RMSE	91.82	40.63		
	Bias	21.74	21.39		
May	Pearson	0.8233	0.8076		
	RMSE	142.9	83.49		
	Bias	69.92	69.33		
June	Pearson	0.7108	0.5723		
	RMSE	196.4	136.6		
	Bias	114.2	114.2		
July	Pearson	0.7893	0.7941		
	RMSE	140.0	79.79		
	Bias	53.26	53.26		
August	Pearson	0.7946	0.7376		
	RMSE	129.1	70.09		
	Bias	50.22	50.22		
September	Pearson	0.7935	0.6623		
	RMSE	74.36	35.64		
	Bias	21.88	21.88		
October	Pearson	0.7416	0.6011		
	RMSE	34.84	13.78		
	Bias	6.306	6.306		
November	Pearson	0.7525	0.9544		
	RMSE	6.644	1.938		
	Bias	-1.641	-1.641		
December	Pearson	-	-		
	RMSE	1.024	0.8694		
	Bias	-0.65	-0.65		

Table 5.2: Calculated mean of the simulated solar radiation data and measured solar radiation data at Holt in 2016, given in W/m^2

Time period	Holt	WRF Holt
2016	76.41	105.31
January	1.61	0.32
February	12.76	15.69
March	59.10	68.13
April	159.20	180.69
May	171.09	240.63
June	152.87	267.11
July	152.08	205.34
August	120.30	170.51
September	59.90	81.77
October	20.40	26.71
November	3.35	1.71
December	0.65	0.00

A plot showing the daily averaged values of simulated solar radiation and measured solar radiation for Holt in 2016 is included in Figure 5.1.

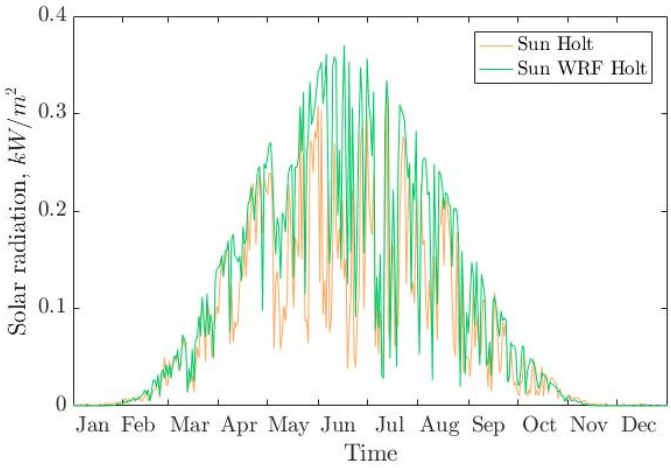

Figure 5.1: Daily averages of simulated and measured solar radiation data at Holt in 2016

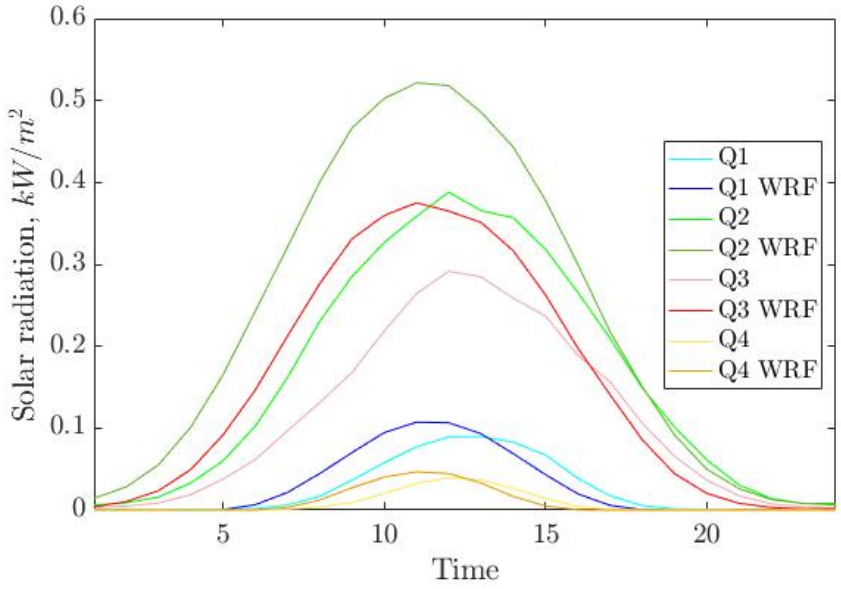

Figure 5.2: Daily profile of simulated and measured solar radiation data at Holt in 2016

From Table 5.1 it can be seen that the majority of calculations of the Pearson coefficient between the two data sets is above 0.75, implying high positive correlation according to Figure 2.15. For the whole year, the positive correlation on a monthly basis is very high with a value of approximately 0.98. Among the months, January, June and October inherits slightly weaker positive correlation between simulated and measured data on an hourly basis, while on a daily basis June, August, September and October are the months with weakest correlation. Regarding the RMSE, it increases with increasing solar radiation, and is largest in the summer months.

The bias calculated for the two data sets shows a slight underestimation in the winter months January, November and December when the solar radiation is low. In the rest of the months however, the bias shows an overestimation, increasing with increasing solar radiation levels. The bias for the whole year also shows an overestimation of the measured values, regardless of the data resolution. It is evident that when the bias has its largest absolute value, the radiation level is also at its highest during the year. From Table 5.2, it is seen that over the span of 2016, the WRF simulations overestimate the solar radiation by approximately 38%, which is a high overestimation.

Also in Figure 5.1 and Figure 5.2 this overestimation is evident. It can be seen from Figure 5.2 that the overestimation is largest in the second quarter when

the solar radiation is at its strongest.

The WRF simulated data thus overestimate the measured solar radiation to a quite large degree from May to August, and it also shifts the solar noon with 1-2 hours on average. Nevertheless, they seem to show a good positive correlation with the measured radiation. As this is the only option to achieve solar radiation data for one whole year, the simulated data is used in the anti-correlation analysis with the wind resource and in the simulation of the hybrid system. In the simulations, however, the radiation data is scaled by a factor of 0.7 to better resemble the solar conditions at the location. It must be kept in mind that the overestimation examined here is at Holt in Tromsø, and that the overestimation may be different in Skibotn. Skibotn is as mentioned known to be a dry area, and there is a higher number of days with clear weather there compared to Tromsø. Therefore, the overestimation may not be as high in Skibotn as in Tromsø, but as an overestimation of 38% is the best estimate available, this is used when deciding the scaling of the simulated solar radiation data. In the anti-correlation analysis, only the relationship between the solar radiation data and the wind resource data is examined, and hence the results are the same independent of the scaling of the solar radiation data.

The solar noon in the simulated radiation seems to be shifted so that it occurs approximately 2 hours earlier in the day compared to the measured values. This may raise suspicion that there is a timing error between the two data sets, but after examining them thoroughly, no simple relation is found. Some days the simulated solar sunrise occurs 1-3 hours earlier than the measured radiation, but this is not the case for all days. In addition, the time sunset occurs in the two data sets does not have any clear relationship. This is also evident from figure Figure 5.2, where in the first and fourth quarter (when the solar resource is low), there seems to be a simple shift in the daily profile. But, in the second and third quarter, there seems to be good correlation in the evening as the radiation is decreasing, while the radiation in the morning is seen to appear earlier than in the measured values.

This shift of solar noon will affect the correlation coefficient, and the correlation could have been even better if this shift was not present. As there seems to be no simple correction to perform on the simulated data, it is used as is. However, as mentioned in Section 4.9, to account for this effect in the simulations, the azimuth angle of the PV modules could have been changed. As there was not enough time to change all simulation results, one simulation is done for stationary and one for horizontal-axis tracking using the azimuth angle which gives the highest output. It is then important to bear in mind that the remaining simulation results will underestimate the solar potential in Skibotndalen.

5.1.2 Comparison of solar radiation at different locations

Table 5.3 shows the solar radiation at different locations for different time periods.

Table 5.3: Solar radiation at different locations for different time periods

Location	kWh/m^2 **in 2016**	kWh/m^2 **in Jan-Apr 2016**	kWh/m^2 **in Jan-Apr 2017**
Holt	669	168	156
Holt WRF	923	192	-
Galgo	-	-	198
Galgo WRF	1027	224	-

It can be seen that in 2017, the measured solar radiation data at Galgo is actually 27% higher than at Holt, confirming that Skibotn is an area with a large solar resource.

The data from 2016 confirms that the simulated data at Holt is approximately 70% of the measured data at Holt in 2016, while the simulated data at Galgo in January-April 2016 is 17% higher than the simulated data at Holt, confirming that the simulated data at Galgo may not overestimate as much as the simulated Holt data.

It can be seen that the simulated values at Galgo in the first four months of 2016 overestimates the measured values at Galgo in the first four months of 2017 by 13%, and that the overestimation at Holt in the first four months in 2016 was 14%, which seem to indicate that the overestimation is quite similar at Holt and at Galgo, and as expected somewhat larger at Holt. Comparing with the overestimation of the 2017 data at Holt by the 2016 WRF data at Holt shows an overestimation of 23%, implying that there may be a 10% less overestimation at Galgo. However, as measured values at Galgo are only available for January to April in 2017 and simulated data is only available from 2016, a comparison is difficult to perform because the solar radiation changes from year to year. It can for instance be seen that the solar resource at Holt has decreased by 7% from the first four months of 2016 to the first four months of 2017, and as the change between 2016 and 2017 at Galgo is not known, there is an uncertainty in these estimates.

As it is the best estimate available a scaling of 70% of the simulated solar radiation seems to be quite reasonable. It must be kept in mind that this may underestimate the solar resource to some degree, and therefore a sensitivity analysis is done on several radiation levels. Also the fact that the measured data contains a few missing values while the simulated data has no missing

values will affect the comparison, as this may underestimate the $^{kWh}/_{m^2}$ for the measured values.

5.1.3 Anti-correlation between solar and wind resources

Galgo and Rieppi 2016

The resulting Pearson coefficients are shown in Table 5.4. It shows the coefficient when calculated using values averaged every 60 minutes, daily, weekly and monthly, and the calculation is done for the whole year and for each month separately. For weekly and monthly data resolution only the coefficient for the whole year is calculated. The coefficient is non-applicable for December, as the simulated data contains only values of 0 $^{W}/_{m^2}$.

It is important to keep in mind that the simulated solar data shifts the solar noon to be earlier than it actually is, and thus the anti-correlation analysis will be affected. If there is negative correlation, this may be underestimated. In addition, since the simulation of solar radiation data is not able to simulate small and rapid weather phenomena, the hourly and daily correlation may give other results than they would if measured solar radiation at Galgo were used. However, as the correlation analysis between the simulated data at Holt and measured data at Holt shows good positive correlation, the anti-correlation analysis on an hourly an daily basis for 2016 are included.

Table 5.4: Pearson coefficient for the simulated solar radiation data at Galgo and measured wind speed data at Rieppi in 2016

	Data resolution			
Time period	60 min	daily	weekly	monthly
2016	-0.0921	-0.2594	-0.4762	-0.6891
January	-0.0094	-0.0899		
February	0.0535	-0.0315		
March	-0.0073	-0.2777		
April	0.0701	-0.2294		
May	0.0386	-0.1593		
June	0.1001	0.2088		
July	0.0061	-0.0463		
August	0.0016	-0.3321		
September	0.0373	-0.1888		
October	-0.0417	-0.2607		
November	-0.0443	-0.2664		
December	-	-		

A plot showing the daily averaged values of solar radiation and wind power per square meter for 2016 is included in Figure 5.3, and a plot of the average dailt profile in each quarter year is shown in Figure 5.4. Note that the solar radiation plotted is on a horizontal surface, and that PV modules tilted at an optimum angle will receive more radiation.

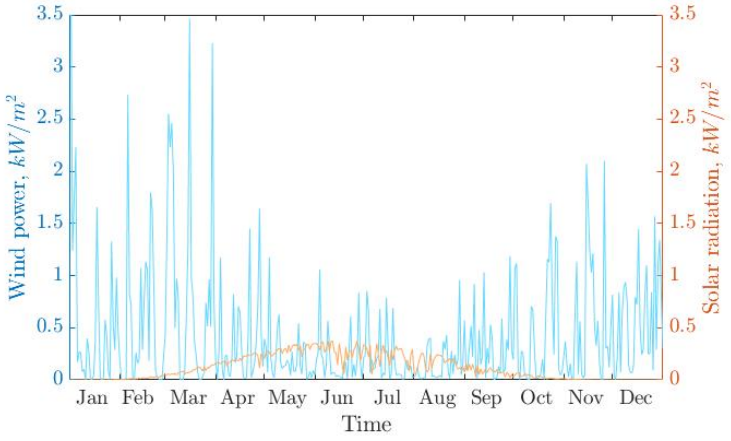

Figure 5.3: Daily averages of available solar and wind power per unit area in 2016

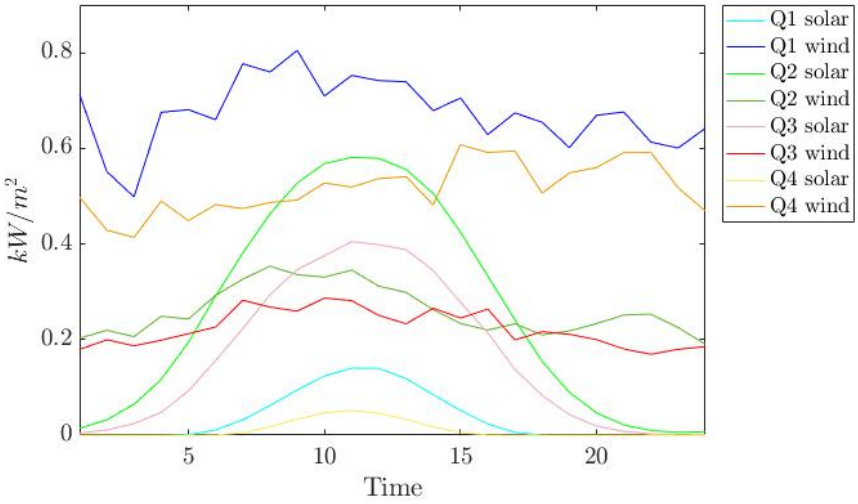

Figure 5.4: Daily profile of available solar and wind power in each quarter year in 2016

From Table 5.4, it can be seen that there is little correlation between the solar and wind resource, at least on smaller time scales. On an hourly basis, there are no signs of anti-correlation, as the Pearson coefficient is below -0.25 for all

time periods. On a daily basis, all months have a negative Pearson coefficient, but the coefficients are too small to assume negative correlation except for the months March, October and November, which shows low negative corerlation (ref. Figure 2.15). The coefficient increases in absolute value when using daily averages instead of hourly averages. During the whole year of 2016, there is a no obvious negative correlation on an hourly basis, and a low negative correlation on a daily basis. Weekly there is a moderate anti-correlation, and monthly there is actually high negative correlation.

In Figure 5.3 and Figure 5.4, it seems to be the case that in the months January-March and October-December, there is higher wind than in the rest of the year, and that these are also the months with least solar radiation. This confirms the findings from the Pearson coefficient that there is a high negative correlation on a monthly basis.

From this discussion, it can be concluded that there is an anti-correlation between the wind resource and simulated solar resource at Rieppi and Galgo, respectively, on a weekly and monthly basis in 2016, but that on shorter time scales, there is low to none anti-correlation.

Galgo and Rieppi 2017

The Pearson coefficient is calculated for the measured solar radiation data from Galgo in 2017 (described in subsubsection 4.1.1) and the measured wind speed data from Rieppi in 2017 (described in subsubsection 4.2.1) and the results are shown in Table 5.5. It shows the coefficient when calculated using values averaged every hour, 24 hour and week, and calculations are done for the whole period January-April 2017 and for each of the months separately. For weekly and monthly data resolution only the coefficient for the whole period is calculated.

Table 5.5: Pearson coefficient for measured solar radiation data at Galgo and measured wind speed data at Rieppi in 2017

	Data resolution			
Time period	60 min	daily	weekly	monthly
Jan-Apr 2017	-0.1191	-0.2989	-0.4912	-0.9805
January	-0.0612	0.0904		
February	-0.0239	-0.2634		
March	-0.0270	-0.2265		
April	-0.1130	-0.5336		

A plot with the daily averaged values of solar radiation and wind power at Rieppi per square meter for 2017 is shown in Figure 5.5, and a plot showing the average daily profile in each month of both the wind power and solar radiation is shown in Figure 5.6. The figures show the solar radiation at a horizontal surface, and it should be noted that a tilted PV module will receive more radiation.

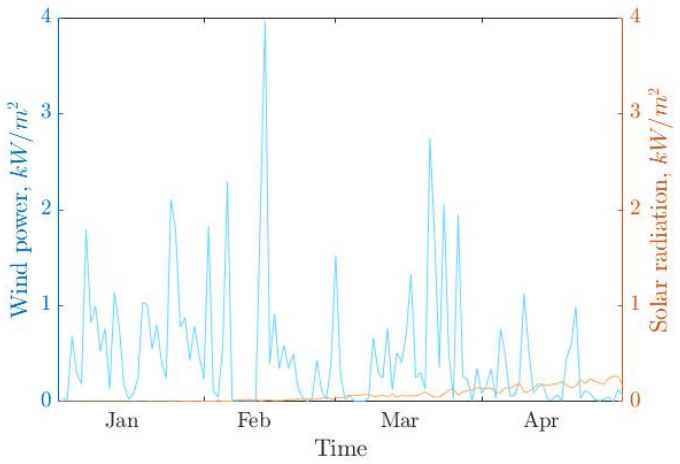

Figure 5.5: Daily averages of available solar power per unit area at Galgo and wind power per unit area at Rieppi in 2017

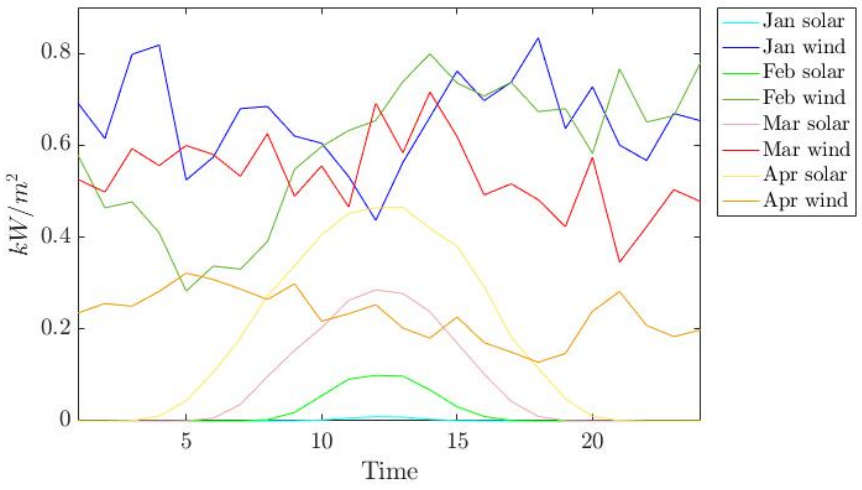

Figure 5.6: Daily profile of available solar and wind power showing each month January to April 2017 separately

For the measured solar and wind resource in 2017 at Galgo and Rieppi, re-

spectively, the Pearson coefficient turns out to be negative for all time periods considered when using hourly averaged data series, as can be seen in Table 5.5. However, the absolute values are small, and any anti-correlation cannot be concluded. The daily coefficient values implies no correlation in January and March, low anti-correlation in February, and moderate anti-correlation in April (ref. Figure 2.15). For the whole period, there is a low negative correlation on a daily basis. Weekly averages for the whole period leads to a low to moderate negative correlation and monthly averages actually leads to very high anti-correlation.

Also in the first four months of 2016 (where simulated solar radiation data is used), the Pearson coefficient using daily averaged data series shows negative correlation in March and April. However, the Pearson coefficients for 2017 actually implies slightly higher negative correlation than in the same months in 2016. One of the reasons for this can be that solar noon difference in simulated solar data and measured solar data, which could be avoided if using only measured data.

In Figure 5.5 and Figure 5.6 there is little obvious anti-correlation present, and the wind resource seems to be quite random. February has two days with very high winds, but January and March seem to be on the same level. What can indicate negative correlation is that in April, the wind power resource per unit area is lower than in the other months, and then also the solar resource has increased a substantial amount compared to the previous months. This can explain the large negative Pearson coefficient calculated for monthly values.

5.2 Analysing the effect of the timing error of WRF-simulated solar radiation data on the simulation results

5.2.1 Effect on technical results

In Subsection 5.1.1 the simulated solar radiation data was found to overestimate the measured solar radiation, and this was accounted for. The time shift of the simulated data did not seem to have a simple relationship during the day, even if the average values showed a time shift of the solar noon by approximately 2 hours (see Subsection 5.1.1). Therefore, the simulated solar radiation was not corrected for this error. As written in the Methodology chapter (see Section 4.9), the effect of the timing error could have been minimised by changing the azimuth error to a value which gave a higher PV energy output. Because there

was no time to re-do all simulations, the effect of this change in azimuth is analysed here. Table 5.6 shows the simulation results for the PV energy output when using an azimuth angle that gives the maximum energy output.

Table 5.6: PV energy output when the azimuth angle is changed to the value which gives the highest energy output. When two values are given they are for year 1 and year 25 of the lifetime of the system (year 1/year 25)

	Azimuth angle giving the highest PV energy output (degrees west of south)	PV energy output in year 1 (MWh)	Total electricity production (MWh)	Inverter size
S1	310°	18 677/16 560	84 736/82 619	18 MW
S2	290°	20 349/18 042	86 407/84 101	20 MW

The yield in Scenario 1 and 2 is calculated to be 933 $^{MWh}/_{MW_p}$ and 1017 $^{MWh}/_{MW_p}$, respectively. The PV energy output and yield values are increased by 13% and 8.3% compared to when employing an azimuth angle of 0°(modules facing southwards) (see below in Table 5.11).

These results show that it seems to be a higher energy output from the PV modules when they are facing more eastwards than southwards. The angle which gives the highest PV output is unexpectedly small, considering that the WRF data seem to shift the measured data by only approximately 2 hours. 2 hours should according to Equation 2.1 account for a 30°change, which should mean that the azimuth angle which gives the maximum output is expected to be approximately 330°. It is difficult to examine why there is such a substantial effect on the optimal azimuth compared to what is conventional, but the fact that the timing offset is different for different times of the year can be one explanation. In the second quarter for instance, the timing offset is very large before solar noon (see Figure 5.2), which can affect the result drastically.

What can be concluded is at least that the time shift in the simulated values have a substantial effect, and that if measured solar radiation values were to be used, the energy output could have turned out to be larger than what is found in Table 5.11. It must be kept in mind that the results in Section 5.3 does not take into account this effect. It is expected, however, that the sensitivity analysis done with an optimal azimuth angle gives similar changes as the ones done with 0°azimuth angle, hence the sensitivity results are still representative.

5.2.2 Effect on economic results

Table 5.7 shows the NPV and LCOE in Scenario 1 if the azimuth angle is taken to be the one found as optimal above, namely 310°west of south.

Table 5.7: NPV and LCOE in Scenario 1 if the PV azimuth angle found as optimal; 310°

	NPV solar (NOK)	NPV wind (NOK)	NPV (NOK)	LCOE ($^{NOK}/_{kWh}$) solar/wind/total
Azimuth 310°	-159 860 565	-215 491 100	-374 483 950	0.8890/0.4590/0.5467

The total NPV is found to decrease in absolute value from approximately -377 million NOK to -374 million NOK. This is a small decrease, and is only 0.8%. The change in total LCOE is from 0.56 $^{NOK}/_{kWh}$ to 0.55 $^{NOK}/_{kWh}$, a decrease of 1.8%.. The solar NPV changes from -162 million NOK to -159 million NOK, which implies a change of 1.3%. These are small changes, and does not have a substantial effect on the profitability of the hybrid system. The solar LCOE changes by 10% where the absolute change in solar LCOE is 0.10 $^{NOK}/_{kWh}$, thus the LCOE is more sensitive to the azimuth angle than the NPV.

Also in the economic analysis, the sensitivity analysis done with an optimal azimuth angle is expected to give similar relative changes as the ones done with 0°azimuth angle, and therefore the sensitivity results are still representative.

5.3 Technical analysis

5.3.1 Analysing the effects of radiation level on optimal PV slope angle and terrain on energy output

Because there is uncertainty in the simulated solar radiation resource, the effect on optimal slope of the radiation level is examined. Table 5.8 and Table 5.9 shows resulting PV energy output when the solar radiation is changed in combination with the PV slope in Scenario 1 and 3, respectively. In the tables, the terrain is changed throughout the year in the way explained in Section 4.9.

Table 5.8: Power output in Scenario 1 (in MWh in year 1) from the PV modules with different combinations of solar radiation and PV slope

		Solar radiation level			
		70% radiation	80% radiation	90% radiation	100% radiation
PV slope	40°	16 358	19 679	22 849	25 749
	50°	16 511	19 982	23 287	26 297
	60°	16 424	19 946	23 294	26 333
	69°	16 173	19 669	22 984	25 991
	80°	15 639	19 012	22 206	25 103
	90°	14 908	18 075	21 075	23 801

Table 5.9: Power output in Scenario 3 (in MWh in year 1) from the PV modules with different combinations of solar radiation and PV slope

		Solar radiation level			
		70% radiation	80% radiation	90% radiation	100% radiation
PV slope	40°	21 615	26 637	31 275	35 394
	50°	22 366	27 753	32 717	37 106
	60°	22 731	28 334	33 488	38 034
	69°	22 748	28 426	33 644	38 241
	80°	22 383	28 009	33 174	37 723
	90°	21 688	27 131	32 124	36 526

From Table 5.8 it is seen that at a lower solar radiation level, the optimal slope changes. This is mainly because a lower radiation level leads to more cloudy weather, which in turn causes a higher fraction of diffuse radiation (coming from all directions), making a lower tilt angle the optimal one. In Scenario 1 for 70% and 80% radiation, it is seen to be 50°, while it for 90% and 100% radiation is 69°. The optimal PV slope is 69°under all radiation levels in Scenario 3. The optimal slope angle is not 69°in Scenario 1 because Scenario 3 employs a tracking system and will receive more direct radiation than the stationary modules.

As mentioned, HOMER calculates unrealistic values for the clearness index when importing the simulated solar radiation data. In this thesis however, the main results are found when using a radiation level of 70%, which although cannot be examined due to the black box feature of the HOMER software, seems to change the clearness index, as HOMER shows that lower slope angles of the modules are better at lower radiation levels. This is at least a sign that the software includes the effect of a change in clearness index at lower radiation levels.

As a radiation level of 70% is used in the simulations, the slope in each scenario is therefore chosen to be **50°in Scenario 1** and **69°in Scenario 3**, but the fact that a higher slope may be optimal if the radiation turns out to be higher that the 70% level must be kept in mind.

Table 5.10 shows outputs from the simulations for a hybrid system with 20 MW PV modules and 21 MW wind turbines in Scenario 1 to Scenario 4 when using different terrain types (keeping the terrain constant for the whole year of simulation).

Table 5.10: Energy output in the different scenarios (in MWh in year 1) from the PV modules and wind turbines with different combinations of terrain types. For S1 and S3 the optimal slopes 50°and 69°are used, respectively

	Terrain type		
	Heathland Albedo 20% Roughness 0.01 m	**Old snow** Albedo 60% Roughness 0.003 m	**Fresh snow** Albedo 90% Roughness 0.003
S1	PV: 15 924 WT: 67 581	PV: 16 837 WT: 65 191	PV: 17 519 WT: 65 191
S2	PV: 18 072 WT: 67 581	PV: 19 004 WT: 65 191	PV: 19 700 WT: 65 191
S3	PV: 21 726 WT: 67 581	PV: 23 318 WT: 65 191	PV: 24 501 WT: 65 191
S4	PV: 22 016 WT: 67 581	PV: 23 389 WT: 65 191	PV: 24 576 WT: 65 191

It can actually be seen that the wind energy output is smaller at smaller roughness lengths. Intuitively, this seems strange, but it is evident in Figure 2.6 that this is true. The reason is that the measurements at 10 meters are constant while only the roughness length changes. Then, at smaller roughness lengths, the wind speed increases more rapidly from 0 to 10 meters above the ground, but it also means that at 80 meters height (the hub height), the speed is lower. The energy output with snow covered ground is approximately 3.5% lower than the energy output with heathland.

The PV energy output is larger with snow, especially fresh snow, and the quantitative value of energy increase differs between different scenarios, but the energy output is approximately 6% higher with old snow and around 11% higher with fresh snow (compared to heathland) The technical analysis will as mentioned be done with fresh snow 1 October- 31 March, old snow 1 April-15 June, and heathland in the period 16 June-31 September. The financial analysis will be done using the average albedo and surface roughness which

best resembles the electricity output found in the technical analysis. Using a trial-and-error method by changing the albedo and surface roughness in the simulations, the albedo **45.70%** is found to give an equal PV energy output to the nearest MWh for Scenario 1 as in the technical analysis (see Table 5.11), and a surface roughness of **0.004835 m** is found to give an equal wind energy output to the nearest MWh for Scenario 1 in the technical analysis. For Scenario 3, an albedo of **45.61%** and the same average surface roughness as used for S1 is found to give the same energy output as the technical analysis for S3.

The fact that an average albedo is used in the economic analysis is a source of error. The average albedo causes the electricity production to not include that there is a large effect of the snow albedo in May and 1-15 June, when there also is a large amount of solar radiation, and thus underestimates the production in this period of time. In October to February, there will still be an underestimation of the output as the average albedo is lower than the snow albedo, but in these months, the solar radiation is quite low, hence the effect is not as dominant as in May and the first half of June. In the period 15 June to 30 September, however, the production is overestimated, as the average albedo is higher than the albedo for heathland.

This will affect the grid sales revenue, as the electricity price changes throughout the year. As can be seen in Figure 4.23, the variation in electricity price is very large in January, but in this month the solar radiation is low and the effect is not as substantial. In the rest of the year, the electricity price does not have any large peaks or very high variations, but what can be observed from Figure 4.24 is that the electricity price in general is higher in the fourth quarter, second highest in the third quarter and third highest in the second quarter. The peaks in January affects the daily profile in the first quarter, giving two peaks during the day which are as high as the average in the fourth quarter year. This variation in electricity price from quarter to quarter together with an average albedo cause an effect on the grid sales revenue compared to using different albedos in different months. The resulting effect will be similar to the effect on the electricity production; an underestimation in the period 1 October to 15 June and an overestimation in the period 16 June to 30 September.

5.3.2 Simulation results

The results from the simulations of the hybrid system where the change in terrain throughout the year is taken into account is displayed in Table 5.11. The slope angles in Scenario 1 and Scenario 3 are chosen to be the ones found as optimal in Subsection 5.3.1, and the solar radiation level is as mentioned taken to be 70% of the simulated data series.

Table 5.11: Technical output parameters from HOMER simulations of the different scenarios under 70% solar radiation when different terrains throughout the year is taken into account. The two values in each cell represent the first and last year of the system's lifetime, respectively (year 1/year 25). If only one value is given, it represents year 1

	PV production ($^{MWh}/_{year}$)	PV production (% of total production)	PV mean output (MW)	PV capacity factor (%)
S1	16 511/14 640	20.00/18.14	1.885/1.671	9.42/8.36
S2	18 788/16 659	22.14/20.14	2.145/1.902	10.72/9.51
S3	22 748/20 169	25.62/23.39	2.597/2.302	12.98/11.51
S4	22 972/20 369	25.80/23.57	2.622/2.325	13.11/11.63

	WT production ($^{MWh}/_{year}$)	WT production (% of total production)	WT mean output (MW)	WT capacity factor (%)
S1	66 059/66 059	80.00/81.86	7.541/7.541	35.91/35.91
S2	66 059/66 059	77.86/79.86	7.541/7.541	35.91/35.91
S3	66 059/66 059	74.38/76.61	7.541/7.541	35.91/35.91
S4	66 059/66 059	74.20/76.43	7.541/7.541	35.91/35.91

	Converter output ($^{MWh}/_{year}$)	Total electricity production ($^{MWh}/_{year}$)	Electricity purchased ($^{MWh}/_{year}$)	Electricity sold ($^{MWh}/_{year}$)
S1	15 686/13 908	82 570/80 698	44.58	81 553
S2	17 849/15 826	84 847/82 717	44.50	83 716
S3	21 610/19 161	88 806/86 228	44.47	87 477
S4	21 824/19 350	89 031/86 427	44.46	87 691

For Scenario 1 in year 1, the energy output divided by the rated power of the PV system (referred to as the yield) is found to be $\frac{16511\text{MWh}}{20\text{MW}_\text{p}} = 826\,^{\text{MWh}}/_{\text{MW}_\text{p}}$. In Scandinavia, a yield of $1000\,^{\text{MWh}}/_{\text{MW}_\text{p}}$ is sought for a PV system to be good, and a value of $800\,^{\text{MWh}}/_{\text{MW}}$ is common to refer to as suitable. Thus, the power output from a PV system in the Galgo-area shows a good energy output.

To compare, the corresponding value for Scenario 2, 3 and 4 are: $\frac{18788\text{MWh}}{20\text{MW}_\text{p}} = 939\,^{\text{MWh}}/_{\text{MW}_\text{p}}$, $\frac{22748\text{MWh}}{20\text{MW}_\text{p}} = 1137\,^{\text{MWh}}/_{\text{MW}_\text{p}}$ and $\frac{22972\text{MWh}}{20\text{MW}_\text{p}} = 1149\,^{\text{MWh}}/_{\text{MW}_\text{p}}$. These values show a good potential for PV power in Skibotn when employing tracking. The capacity factors for the PV system implies a PV power potential that is

slightly below the average for Europe, found Subsection 4.6.1 to be 14% and 12.3% for 2013-2014 and 2016, respectively.

The above table clearly shows that the PV power output increases with tracking. However, there is actually little difference between the vertical axis and two-axis tracking. In subsubsection 2.1.6, it was found that in many cases, one-axis tracking often turn out to be the best overall solution, as it gives a decent power output increase while not being as expensive and complicated to implement as two-axis tracking, and in this case, it seems that vertical axis tracking can turn out to be a better solution than two-axis tracking. For horizontal axis tracking, there is an increase of 14% compared to stationary modules, and for vertical axis and two-axis tracking the increase is 38% and 39%, respectively. These results implies that vertical-axis is the best choice for a tracking system in this location.

The wind power output comprises a larger fraction of the total power output than the PV power output. This is expected, as the capacity factor of wind power plants usually are larger than that for PV power plants. Compared to the capacity factors found in Subsection 4.6.2 (27-28% in Europe and approximately 34% in Norway), the value of 36% achieved at the Rieppi site is a high value, and indicates that there is a good wind resource at the site. However, this is as mentioned without any turbulence and wake losses, and thus overestimate the amount of electricity available for sale. Another way of classifying the wind resource at a location was found in subsubsection 2.2.1 to be that the average wind speed is above 6.5 $^{m}/_{s}$ at hub height. It is found in subsubsection 4.2.1 that the average wind speed was 5.97 $^{m}/_{s}$ in 2016 at 10 meters height, which implies a wind speed of 8.67 $^{m}/_{s}$ (using Equation 2.5) at hub height (80 meter) using a surface roughness of 0.1 meters, hence the wind resource is well above the thumb of rule for feasibility of wind power plants. In addition, it was also found in subsubsection 4.2.1 that the average in 2016 was 4-6% below the average in the period 2000-2015, hence the wind potential may reach even higher.

Other sources of error in this case is firstly that HOMER does not take into account the wind direction. It only considers the wind speed and the power curve of the turbine. Although the wind turbines can be controlled so that they always face the wind, there is a delay in this operation, and not all wind gusts will be able to be captured by the turbine. In addition, measurements of weather conditions can contain errors, and maintenance of the sensors are important. In addition, solar and wind resources are very local, and measured wind speed and direction or solar radiation at one location may be very different from a location only a short distance away.

The column in Table 5.11 named *Electricity purchased* is due to the load defined in the hybrid system resulting from the power demand of the wind turbines

inter alia under start-up. HOMER calculates the energy balance in each hour, and in some hours the electricity generated from the wind and PV components will not be enough to supply this load. In these cases, electricity must be purchased from the grid. However, this is a small value compared to the electricity sold.

Figure 5.7 and Figure 5.8 shows the power output from the solar and wind components as 24 hour averages and weekly averages, respectively. Figure 5.7 only shows the PV output for Scenario 1, while Figure 5.8 shows PV outputs for all four scenarios. The wind output is equal for all scenarios.

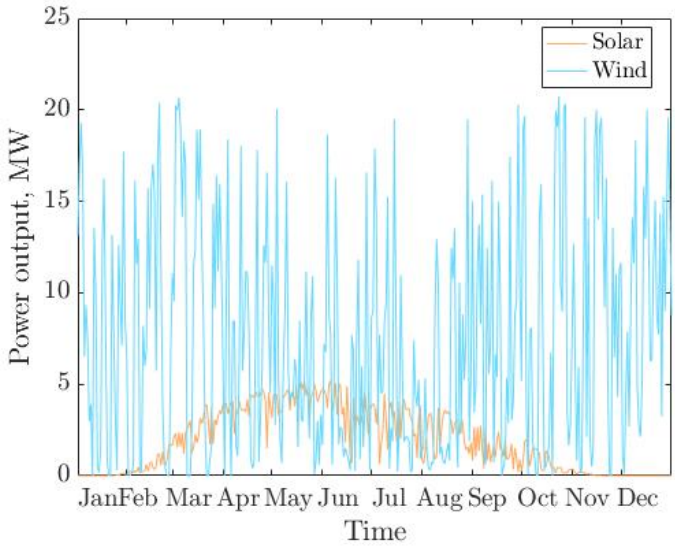

Figure 5.7: 24 hour averages of the solar and wind power output in Scenario 1

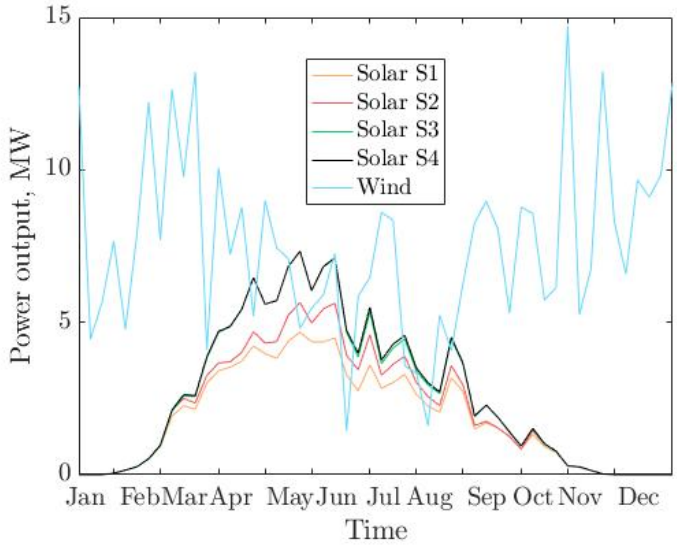

Figure 5.8: Weekly averages of the solar and wind power output in all scenarios

In Figure 5.8, the power output from Scenario 3 is almost not showing, which shows its closeness to the PV power output in Scenario 4. From Figure 5.7, it is confirmed that the wind power output accounts for a larger share of the total electricity production, but it is also evident that the wind resource has a larger variance than the solar resource.

In Figure 5.8, which shows weekly averages, the monthly anti-correlation between the wind and solar resource is evident, as the power output from the wind turbines is smaller in the summer months, when the power output from the PV modules are largest. The two renewable power plants does, however, give a very variable output, which means that operating them in combination with the existing hydro power stations will be advantageous to obtain a less variable electricity production.

5.3.3 Sensitivity analysis

Because there are uncertainties and natural variations in both the solar and wind resource, a sensitivity analysis is done on these parameters. In addition, the effects of changing the PV efficiency, PV slope and wind turbine losses are included in the figures below.

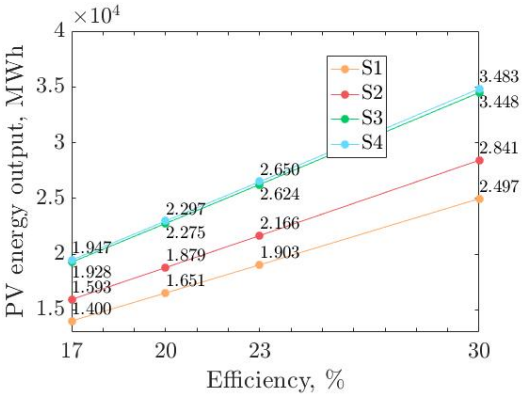

(a) PV efficiency sensitivity

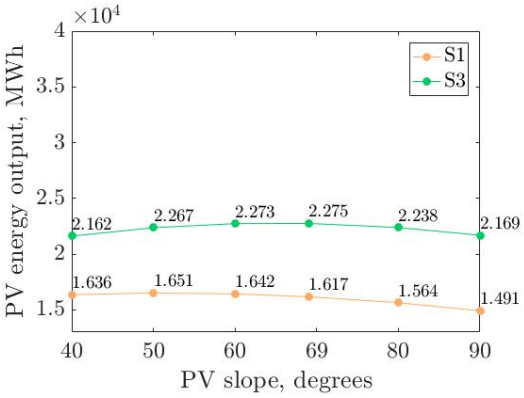

(b) PV slope sensitivity

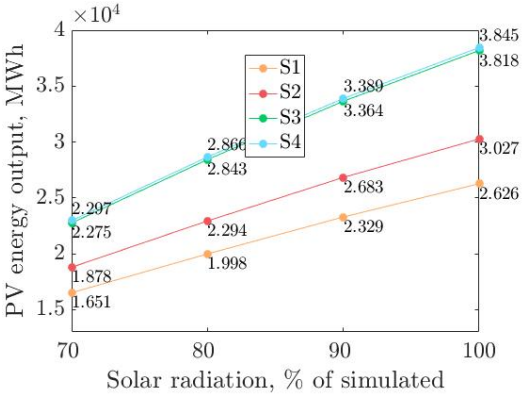

(c) Solar radiation sensitivity

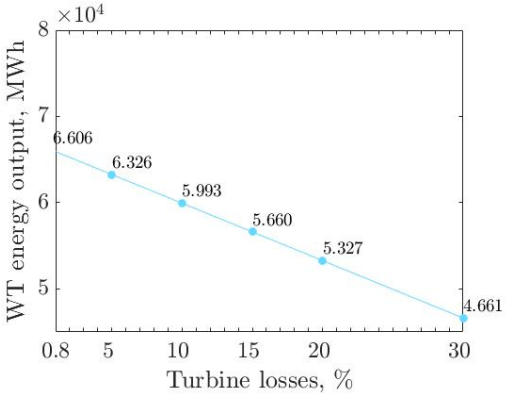

(d) WT losses sensitivity

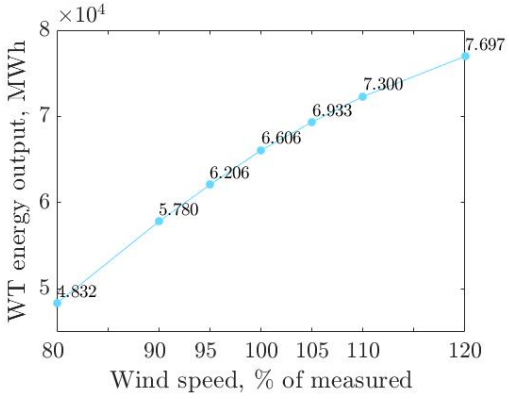

(e) Wind speed sensitivity

Figure 5.9: Sensitivity analysis of the PV power output (in year 1) when varying different parameters

Changing the efficiency has a high impact on the energy output from the PV modules, as expected. When changing the efficiency from 20% to 17%, the

decrease in energy output is approximately 15% in all scenarios. Changing the efficiency from 20% to 23% causes an increase of 15%, which implies a nearly linear relationship between PV efficiency and electricity produced. The change in electricity produced from the modules when increasing the PV efficiency from 20% to 30% is approximately 50%. This leads to the conclusion that increasing the efficiency of PV modules is a major contributor to achieve better PV penetration in the energy market.

Table 5.12 shows the effect when changing the inverter and PV efficiency simultaneously. Note that the values represents the *inverter* outputs in year 1 under different efficiencies, and not the PV output.

Table 5.12: *Inverter* energy output at different PV efficiencies and inverter efficiencies. Values are for year 1 and in MWh

S1	17%	20%	23%	30%
95%	13 301	15 686	18 082	23 719
99%	13 861	16 346	18 843	24 717

S2	17%	20%	23%	30%
95%	15 135	17 849	20 576	26 992
99%	15 772	18 600	21 443	28 129

S3	17%	20%	23%	30%
95%	18 311	21 610	24 930	32 758
99%	19 082	22 520	25 980	34 138

S4	17%	20%	23%	30%
95%	18 492	21 824	25 177	33 085
99%	19 270	22 743	26 237	34 478

From the above table, it is seen that changing the inverter efficiency has a quite small impact on the inverter energy output . An absolute change of 4% from 95% to 99% efficiency causes a change in energy output of approximately 4%, while it is already been discussed that an absolute change in PV efficiency of 3% from 20% to either 17% or 23% causes a change in energy output of ±15%. Thus, the effect of changing the PV efficiency is substantially larger than changing the inverter efficiency. However, as the inverter comprises a smaller share of the costs than the PV modules, an increase in inverter efficiency may be less expensive to achieve than an increase in PV efficiency.

Even though the change of PV slope is already discussed in Subsection 5.3.1, the results are here presented in a plot to compare the effect of slope with the effect of varying other variables. Noting that Figure 5.9a, Figure 5.9b and Figure 5.9c have the same limits on the y-axis, it is evident that the solar radiation level is the variable which affects the PV power output most.

From Figure 5.9b, it can be seen that there is little difference in Scenario 1 between 50°and 60°; only a marginal decreased power output of approximately 0.55%. Even though 50°gives a higher power output, an advantage of having a slope of 60°instead is that less snow will gather on the modules, and that rain

can more easily wash off dust from the modules. For Scenario 3, there is little difference from 69°to 60°(approximately 0.088% decrease).

It is interesting to examine the effect the solar radiation level has on the PV power output, especially because the solar radiation data used in the simulations are simulated data and not measured. From Table 5.2, it is found that for the whole of 2016, the mean measured radiation at Holt is approximately 70% of the simulated radiation at Holt. Because the solar conditions and number of days with clear weather are different at Galgo, the effect of scaling the simulated solar radiation with 0.8 and 0.9 in addition to using the original simulated data is also examined. The change in power output is quite drastic with change in solar radiation levels (see Figure 5.9c), and the yield under different radiation levels in different scenarios are shown in Table 5.13.

Table 5.13: Yield of PV component under different radiation levels, given in $^{MWh}/_{MW_p}$

	70% radiation	80% radiation	90% radiation	100% radiation
S1	826	999	1164	1313
S2	939	1147	1341	1513
S3	1137	1421	1682	1909
S4	1149	1433	1695	1922

If the radiation turns out to be 80% of the simulated data, the stationary modules is seen to give a good electricity output of 999 $^{MWh}/_{MW_p}$, and a radiation level of 90% gives a yield above 1000 $^{MWh}/_{MW_p}$. It is not completely unrealistic that the solar radiation is 80% of the simulated data, hence the yield may be greater than 826 $^{MWh}/_{MW_p}$. taking into account the the timing error of the simulated solar radiation data can increase this yield by approximately 13%, causing a yield of 1129 $^{MWh}/_{MW_p}$, being an even better value for the feasibility of the PV system.

Regarding the change in wind energy output due to wind turbine losses, the effect of increasing the losses from 0.8 to 20% accounts for a decrease in power output of 19%, a very large amount. Thus, it must be kept in mind that the energy output from the wind turbine overestimates the actual energy output to some degree. The capacity factor for different amounts of losses is shown in Table 5.14, and shows that at 10% losses the wind power plant has the same capacity factor as the average capacity factor in Norway in 2011-2013.

Table 5.14: Capacity factor of WT component with varying values of turbine losses

0.8% losses	5% losses	10% losses	15% losses	20% losses	30% losses
35.91%	34.39%	32.58%	30.77%	28.96%	25.34%

The effect of changing the wind speed is large. This is expected because the power output from a wind turbine is a function of the wind speed cubed, making it a large contributor to the power output from a wind turbine. Decreasing the wind speed by 20% causes a decreased power output by 27% and an increase in wind speed by 20% causes an increased power output by 24%. The power output is hence more sensitive to lower wind speeds than higher wind speeds compared to the measured values. This is due to the power curve of the wind turbines. At a higher wind speed, the wind turbines operate for a larger amount of time at their rated power, but will never exceed a production of 3 MW each. At low wind speeds, however, they will be producing below their rated power for a larger amount of time, down to no power production.

It is expected that the *The Norwegian Meteorological Institute* does perform maintenance of the wind sensors at Rieppi, but the wind speed sensitivity is an interesting factor, as the wind resource can change from year to year. As was found in subsubsection 4.2.1, the wind resource in 2016 was weaker than the average in the period 2000-2015 by 4% to 6%. Thus, the wind energy output at 105% wind speed may better represent the production data at Rieppi, which gives a capacity factor of 38%. However, it is still important to remember that this is without wake and turbulence losses, and the wind power potential at Rieppi is in any case lower than this value.

5.3.4 Interaction with existing power plants

In Figure 5.10 the solar and wind power output is plotted together with the electricity consumption in the area, which is scaled down to never exceed 100 MW, and the power output in 2014 from the hydro power stations already existing in Skibotn. The values are weekly averages.

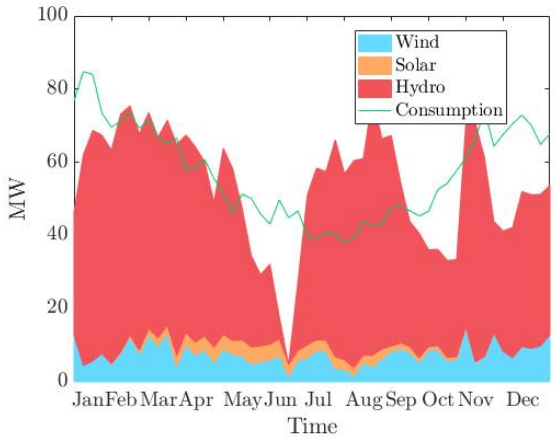

Figure 5.10: Weekly averages of power output from the PV and wind components together with the electricity consumption (scaled down to not exceed the grid constraints in the area) and the hydro power output in 2014

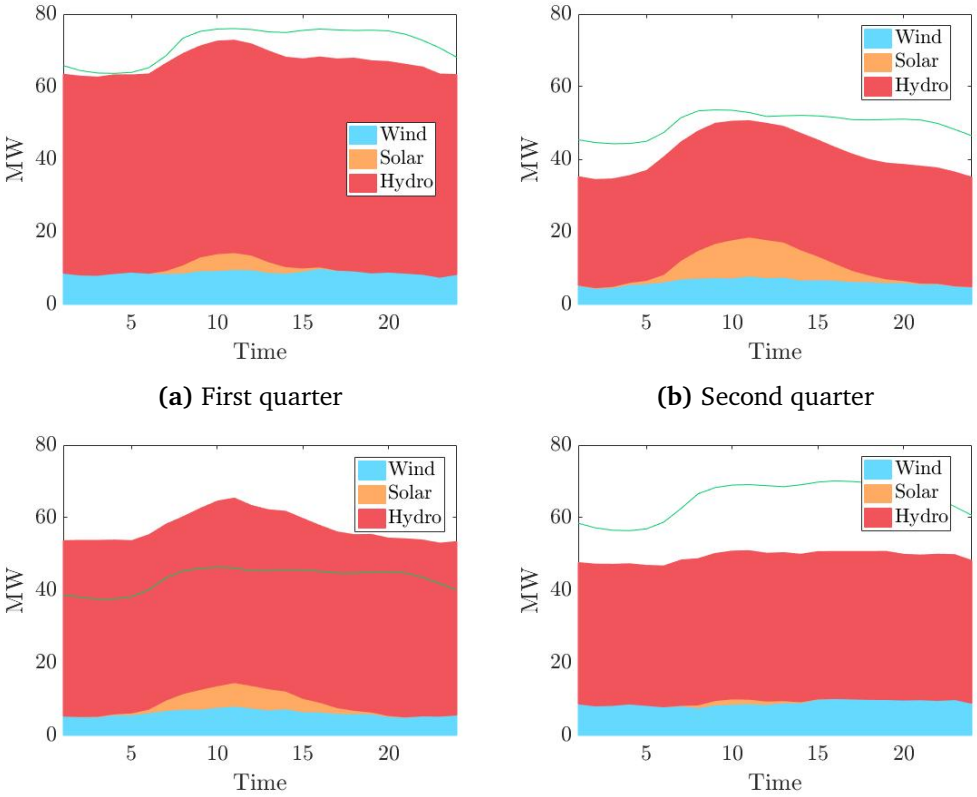

(a) First quarter

(b) Second quarter

(c) Third quarter

(d) Fourth quarter

Figure 5.11: Average daily profile in each quarter year of power output from the PV, wind and hydro (in 2014) components together with the electricity consumption scaled to fit the grid constraint

What can be seen from the figures above is that the power output from the solar and wind components never exceeds the grid capacity of 100 MW. In the spring, both the solar and wind power output are large, while in June there seems to be a dip in the wind power output while the PV component produces a high amount of power in the summer months.

During the day, the wind power produced is quite constant, seeming to decrease to a small degree in the morning and evening in the second and third quarter, which corresponds with the wind speed plotted in Figure 5.4. In the fourth quarter, the wind power increases slightly in the evening. The solar power output is as expected; high in the middle of the day and low to none in the evening and night. It has its highest output in the second quarter, as the solar radiation is highest in May, except for a short peak in the end of June (ref. Figure 4.10).

The two renewable technologies in combination gives a very variable output, and connecting a hybrid system consisting of PV and wind turbines directly to the grid can cause controlling problems if the electricity network is not designed for handling such variations. Connecting the solar and wind hybrid system together with the existing hydro power stations can therefore be very advantageous, as hydro power is easy to control and can respond quickly to changes in demand or changes in the PV and WT output.

The way the hydro power stations were operated in 2014 is not necessarily representative for the operation in 2016 or in the future, but it is the best data available. In June, there was a rapid drop in hydro power output, implying that the electricity prices were low in this period. It can be seen that the maximum grid capacity is never reached, implying that larger wind and/or PV components can be employed, which may be examined in the future. It can also be seen that there is very little correlation between the hybrid system power output and the trends of the demand in the area.

From Figure 5.11 it is seen that the combination of the three renewable sources causes the power output from the hybrid system to pertain a shape quite similar to the shape of the demand during the day. The solar power output causes it to be a peak in the middle of the day, and also the demand is high at this time. However, the demand continues to be high until the evening, and this does not the hybrid system fulfil. If the hydro power stations are operated according to the output of the solar and wind components of the hybrid system, a smoother output from the total system can be achieved. As mentioned, the water in the reservoirs can be stored, while the solar radiation and wind resource not exploited in the instance they occur are lost. Hence, the solar and wind power output should be prioritised, and the hydro power station operated according to this.

Figure 5.12 shows the combined power output if the hydro power stations are operated at their maximum capacity continuously. It can be seen that the combined output almost reaches the maximum grid capacity in the area. This is not a realistic case at all, but it is interesting to see if the grid capacity will ever be exceeded by the hybrid system electricity production if the hydro power plants are operated differently than in 2014.

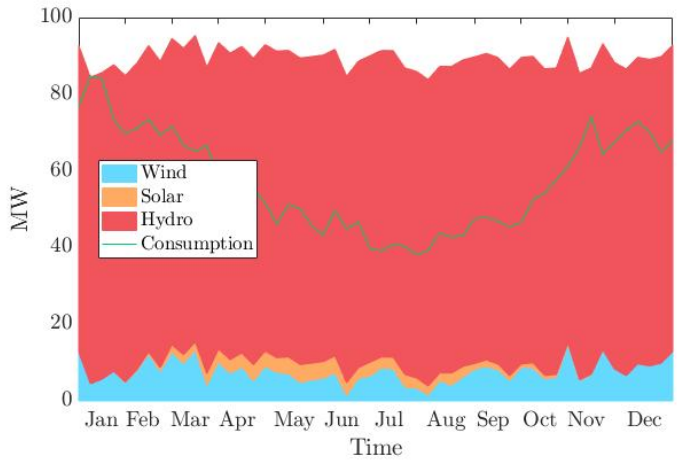

Figure 5.12: Electricity generated from the PV and wind components together with the electricity consumption (scaled down to not exceed the grid constraints in the area) and the hydro power output if the hydro power station is operated at its maximum capacity during the whole year

5.3.5 Connecting the hybrid system to the grid

As mentioned in Section 4.9, the PV inverter in HOMER is a central inverter (see Subsection 2.5.2). It converts all the power output from the PV modules simultaneously, and each module cannot be controlled individually. Higher yields can be achieved if other inverter configurations are employed, but these configurations in turn are most likely more expensive, as a higher number of inverters are needed, each with a control regime.

The central inverter configuration in addition is affected to a larger degree by mismatch between the modules, as all modules are connected in series. This can be avoided by employing one of the other configurations described in Subsection 2.5.2. The lowest effect of mismatch is achieved by using the individual configuration, but this requires both DC-DC and DC-AC converters, causing a more expensive system.

As mentioned in Section 4.9, the wind turbines resembled in these simulations are of the type used at another wind farm owned by *Troms Kraft*, which has asynchronous induction generators, employing a power converter which converts approximately 30% of the power output from the wind turbine (see Subsection 2.5.3). This configuration causes the wind turbines to have semi-variable speed, but the configuration has as mentioned shown to have good control of the power output. Using a full capacity power converter will increase the costs of the systems, and may not be feasible even if the power output

is controlled to a higher degree, and as mentioned in Subsection 2.5.3, the setup with a full capacity converter has in some cases been seen to have a lower efficiency than the 30% converter configuration. As HOMER only takes the power curve of the wind turbines as input, the converter configuration is chosen when choosing which power curve to use.

HOMER does not need to curtail any of the renewable components simulated, as the hybrid system never exceeds the maximum grid capacity. However, if the power output from the hybrid system exceeds either the demand in the area or the maximum power capacity, it should be regulated in the way described in Subsection 2.5.4.

5.4 Economic analysis

5.4.1 Scenario 1

Table 5.15 shows the economic data for the hybrid system. The NPV is calculated by Equation 2.12 and the LCOE is calculated by using Equation 2.13. All values in the table represent the whole lifetime of the system, where future costs and revenues are discounted to present value by the discount factor using a discount rate of 5.00%. The rows in the table represents results when the costs are as the ones found in Subsection 4.6.3 for Scenario 1, and approximately ±30% of these costs (defined in Subsection 4.10.2). In Table 5.15, the sum of electricity from the wind turbines and the inverter is shown for the whole lifetime of the system in the column *Electricity available for sale*, where the electricity generated in each year is multiplied by the discount factor, as in the denominator in Equation 2.13.

The four last rows represents the NPV and LCOE if only the costs of the solar component change, or only the costs of the wind components change. The inverter costs and revenues are included in the calculation of the solar NPV and solar LCOE.

Table 5.15: Economic parameters where the values represent the whole lifetime of the system. The NPV and LCOE are calculated by using Equation 2.12 and Equation 2.13, respectively. Low and high costs refers to approximately ±30 of the costs originally assumed in Scenario 1. The revenue from electricity sold is equal for all cost cases. The four last rows represents the NPV and LCOE if only the costs of the solar component change, or only the costs of the wind components change

	PV capital cost (NOK)	PV O&M costs (NOK)	WT capital cost (NOK)	WT O&M costs (NOK)
S1	150 000 000	42 281 834	287 700 000	139 654 248
Low costs	100 000 000	28 187 889	191 800 000	93 102 832
High costs	200 000 000	56 375 778	383 600 000	186 205 664

	Inverter capital cost (NOK)	Inverter replacement cost (NOK)	Inverter O&M cost	Inverter salvage value (NOK)
S1	9 800 000	4 713 968	2 762 413	964 656
Low costs	6 533 333	3 142 645	1 841 609	643 104
High costs	13 066 667	6 285 290	3 683 218	1 286 208

	Electricity available for sale (MWh)	Grid sales revenue solar (NOK)	Grid sales revenue wind (NOK)	Grid sales revenue (NOK)
All cases	1 141 922	46 625 641	211 863 148	259 356 493

	NPV solar (NOK)	NPV wind (NOK)	NPV (NOK)	LCOE ($^{NOK}/_{kWh}$) solar/wind/total
S1	-161 967 918	-215 491 100	-376 591 313	0.9891/0.4590/0.5569
Low costs	-92 436 732	-73 039 684	-164 608 711	0.6593/0.3060/0.3713
High costs	-231 499 104	-357 942 515	-588 573 915	1.3188/0.6120/0.7425
Low solar costs	-92 436 732	-215 491 100	-307 060 127	0.6593/0.4590/0.4960
High solar costs	-231 499 104	-215 491 100	-446 122 500	1.3188/0.4590/0.6478
Low wind costs	-161 967 918	-73 039 684	-234 139 898	0.9891/0.3060/0.4322
High wind costs	-161 967 918	-357 942 515	-519 042 729	0.9891/0.6120/0.6817

The total NPV of the system is approximately -368 million NOK, and the solar and wind NPV are -162 and -215 million NOK, respectively, implying little profitability of the system. If the costs are decreased to 70% of those originally

assumed, the total NPV decreases (in aboslute value) by 51%, and if the costs are increased by 30%, the NPV increases by 51%. The solar NPV changes by ±39% and the wind NPV by ±59%. If only the PV costs are changed by ±30%, the change in total NPV is ±17%, and if only the wind costs are changed by ±30%, the total NPV changes by ±34%. The NPV is hence more sensitive to changes in wind costs, which is expected because the wind components has higher costs than the PV components. The NPV showed only a negligible change when the azimuth angle was changed to its optimal angle.

The LCOE calculated for the system shows more positive results. The total LCOE is 0.56 NOK/kWh. For only the wind power plant it is slightly lower; 0.46 NOK/kWh, and for only a PV plant, the LCOE is 0.99 NOK/kWh, which is desirable. When the capital and O&M costs are changed by ±30%, all three LCOE values changes by ±30%. When only the PV costs are changed by ±30% the total LCOE changes by ±10%, and if only the wind costs are changed by ±30% the total LCOE changes by ±20%. Thus, also the LCOE is more sensitive to wind costs, due to the higher costs of the wind components compared to the PV components. Taking into account the timing error of the simulated solar data, the total LCOE is expected to change only a negligible amount, but the solar LCOE may decrease by 10%, to 0.89 NOK/kWh.

The wind NPV is more negative than the solar NPV. This is due to the higher capital and O&M costs for wind. However, the grid sales revenue from the wind turbine plant alone is larger than that from the PV plant, as wind turbines produce more power than PV modules per MW installed. The wind LCOE is lower than the solar LCOE. This is because of the same reason; a higher power yield from a similar rated power from wind turbines than PV modules. Therefore, the cost of producing one kWh is lower for wind than for PV, and the wind power plant can tolerate a higher electricity price to be profitable.

In Norway, the electricity price is low compared to many other countries. The LCOE represents the minimum electricity price required for the power plants to be profitable. As the average electricity price in Tromsø in 2016 was 0.23 NOK/kWh, none of the LCOE values implies profitability of the hybrid system or separate PV and wind power plants. The most optimal case, when there is a decrease in all costs by 30% the LCOE turns out to be 0.39 NOK/kWh, which is a quite satisfactory value, especially if the electricity prices increases in Norway in the future. It is also worth noting that the electricity certificate market in Norway and Sweden (see Subsection 4.6.3) will cause the actual received price for the electricity sold to the grid to be somewhat higher than the average electricity price.

5.4.2 Sensitivity analysis

NPV sensitivity

Figure 5.13 shows the NPV values when changing the PV slope, the solar radiation level, wind turbine losses, wind speed, discount rate and electricity prices.

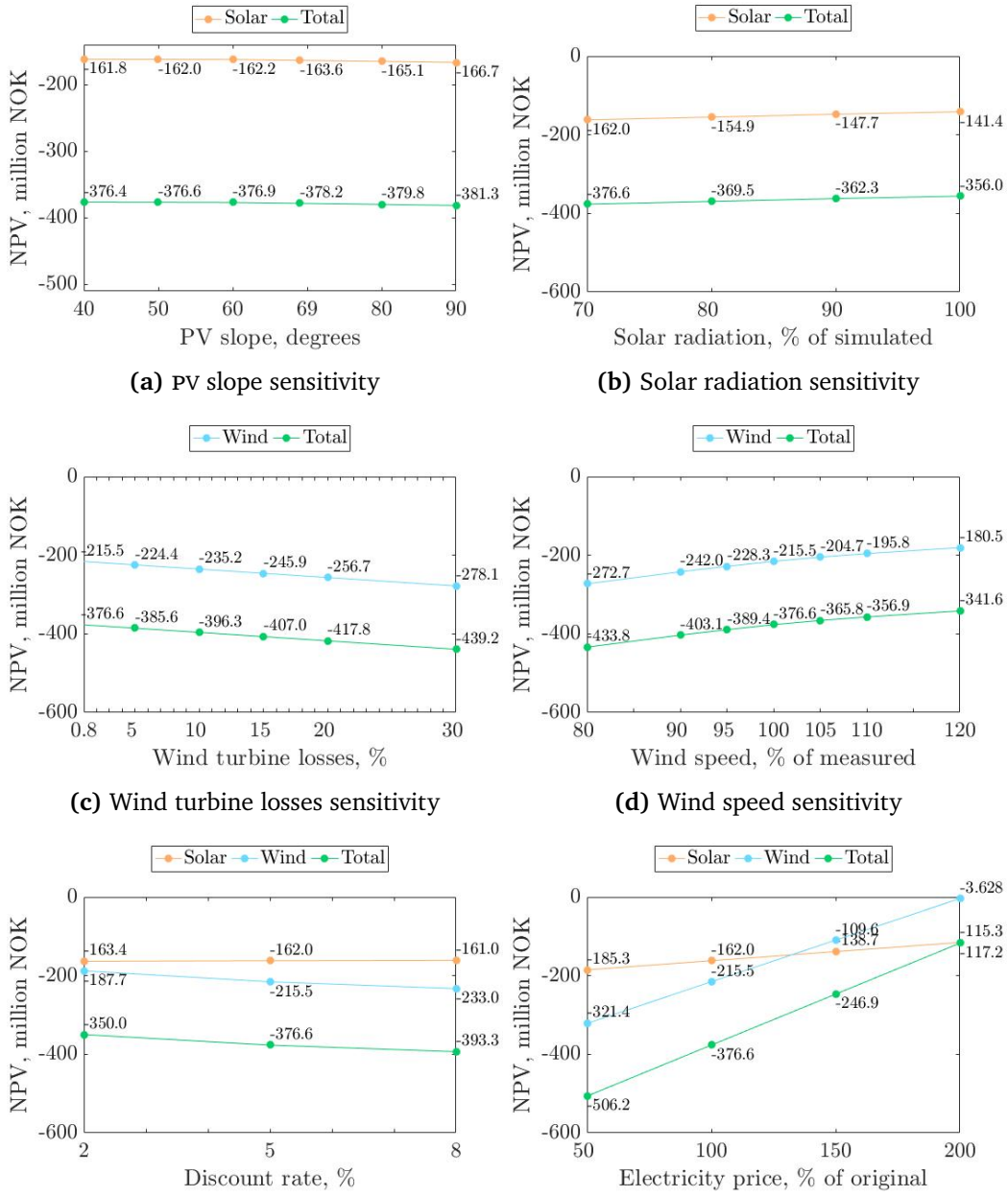

(a) PV slope sensitivity

(b) Solar radiation sensitivity

(c) Wind turbine losses sensitivity

(d) Wind speed sensitivity

(e) Discount rate sensitivity

(f) Electricity price sensitivity

Figure 5.13: Sensitivity analysis of the NPV when varying different parameters

When changing the slope angle of the PV modules, the change in total NPV is not drastic. It increases (in absolute value) by only 0.3 million NOK by a change from 50°to 60°. The solar radiation level does on the other hand have a larger effect on the NPV. From 70% to 80% radiation, the total NPV decreases

by approximately 7 million NOK, and to 90% and 100% it decreases by 14 and 20.5 million NOK. The solar NPV changes by the same values.

The NPV is sensitive to turbine losses. Including 10% losses makes the total NPV more negative by 20 million NOK. 20% losses causes a change of 41 million NOK and 30% losses a change of 63 million NOK. Turbulence losses, wake losses and other losses should therefore be examined if an eventual wind power plant is to be installed in the area.

The wind speed have large effects on the NPV. A wind speed increased by 20% gives an absolute decrease in total NPV by 35 million NOK, while a 20% decrease causes an increase of 57 million NOK. Also here it is seen that lower wind speeds causes a larger change in NPV than higher wind speeds. An increase in wind speed of ±5% causes a change in the total NPV of approximately 13 million NOK.

Changing the discount rate has a larger effect on the wind NPV than the solar NPV. This is due to the fact that the wind component has much higher O&M costs than the PV component, and thus these future costs are more sensitive to a change in discount rate. Even though the wind component also has higher grid sales revenue than the PV component, they are not large enough to compensate for the effect of the high O&M costs.

The changes in total NPV when changing the revenue from grid sales to 1.5 and 2 times its original value are decreases (in absolute value) of 130 million NOK (69% decrease) and 259 million NOK (34% decrease) to -247 and -117 million NOK, respectively. An electricity price half of the original value causes an increase of 130 million NOK (34% increase). Figure 5.13f shows that the wind NPV is much more sensitive to electricity price than the solar NPV. This is because the wind turbine plant produces a larger amount of power than the PV power plant, and hence the revenue from grid sales is larger for the wind power plant. When changing the electricity price, the grid sales revenue is changed by the same factor, and hence the change is larger for a larger revenue. It can actually be seen that with a doubling of the electricity prices, the NPV of the wind power plant decreases to only -3.6 million NOK (a 98% decrease). A doubling of the electricity price changes the solar NPV to -115 million NOK (29% decrease).

LCOE sensitivity

Figure 5.14 shows the LCOE values when changing the PV slope, the solar radiation level, wind turbine losses, wind speed and discount rate.

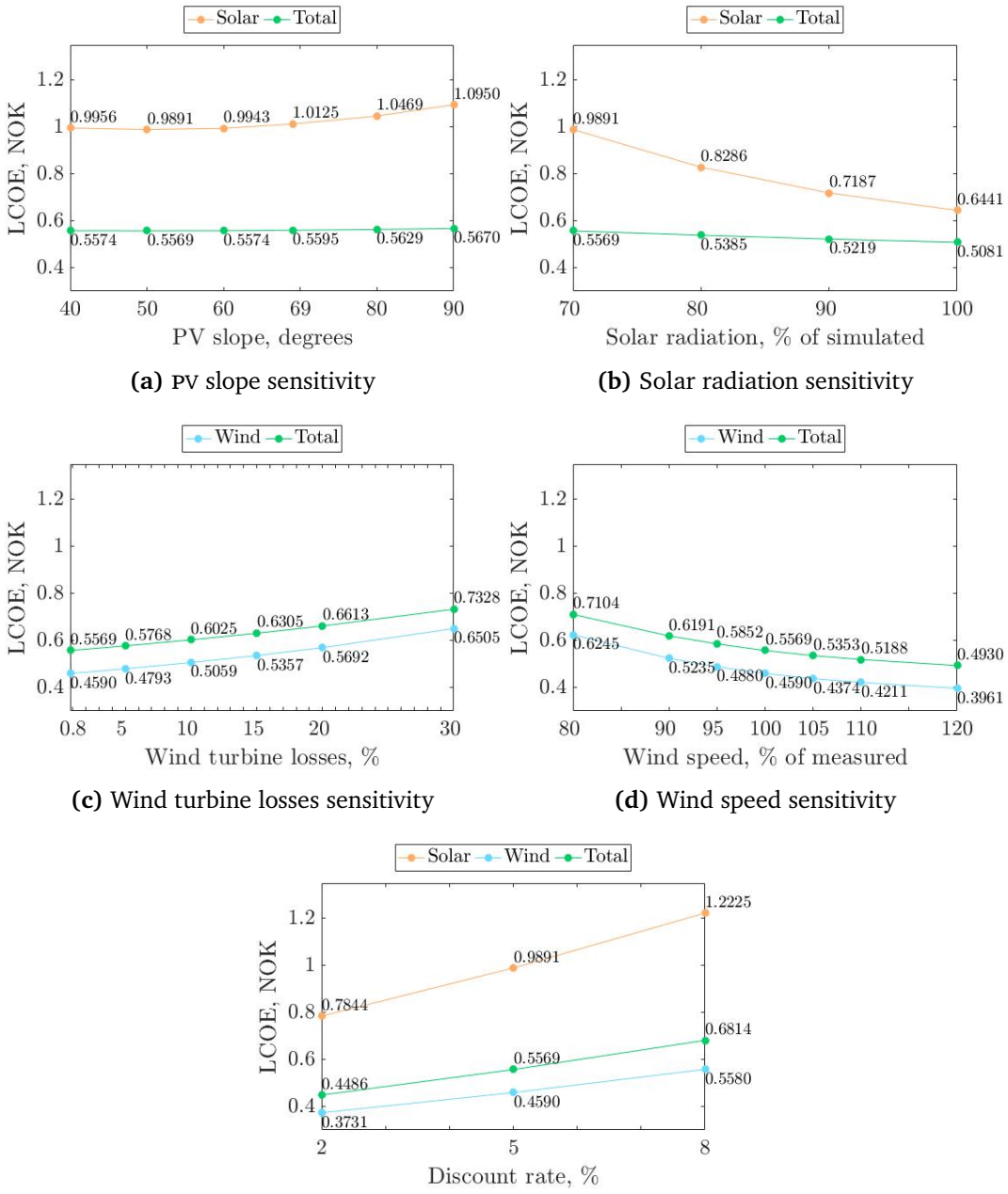

(a) PV slope sensitivity

(b) Solar radiation sensitivity

(c) Wind turbine losses sensitivity

(d) Wind speed sensitivity

(e) Discount rate sensitivity

Figure 5.14: Sensitivity analysis of the NPV and LCOE when varying different parameters

The LCOE is not very sensitive to changes in PV slope, but the change in the solar LCOE is larger for higher slope angles. A slope angle of 90°gives a high LCOE

of 1.10 NOK/kWh. The sensitivity to changes in solar radiation level, however, is larger. The change in solar LCOE is with a change in solar radiation level to 80%, 90% and 100% 0.15 NOK/kWh, 0.27 NOK/kWh and 0.35 NOK/kWh, respectively, giving solar LCOE values of 0.83 NOK/kWh, 0.72 NOK/kWh and 0.64 NOK/kWh. All these values are below 1 NOK/kWh, which is favourable.

Regarding turbine losses, the total LCOE increases with 4% when including wind turbine losses of 5%, and 8% when increasing wind turbine losses from 0.8% to 10%. As it is found in Subsection 2.2.5 that wake losses can account for up to 25% turbine losses, the LCOE at 20% and 30% losses are interesting to examine further. At 20% losses the total and wind LCOE are 0.66 NOK/kWh and 0.57 NOK/kWh, respectively, which are substantially larger than the average electricity price in Tromsø in 2016 (0.23 NOK/kWh). At 30% losses the total and wind LCOE are 0.73 NOK/kWh and 0.65 NOK/kWh, respectively, and these are high LCOE values.

For a decrease in wind speed of 20%, the total LCOE increases by 28%, and for a 20% increase in wind speed, the total LCOE decreases by 11%. The same changes causes an increase of 36% and a decrease of 14% in the wind LCOE. As the wind resource in 2016 was found to be 4-6% lower than in the period 2000-2015 in subsubsection 4.2.1, the effect of increasing the wind speed by 5% is interesting to examine. It can be seen in Figure 5.14d that this causes a 4% decrease in the total LCOE (to 0.44 NOK/kWh), and a 5% decrease in the wind LCOE (to 0.54 NOK/kWh).

For a discount rate of 2%, the total LCOE decreases to 0.45 NOK/kWh (a decrease by 19%). A discount rate of 8% leads to a total LCOE of 0.68 NOK/kWh (an increase of 22%). The solar LCOE is more sensitive to changed discount rate than the wind LCOE because the PV available electricity changes more with discount rate than the O&M does, while for the wind component, the available electricity is not affected as much as the O&M costs. This corresponds well with the effect of discount rate on NPV as it there was found that the O&M costs of the wind component changes more than the wind grid sales. At a discount rate of 8% it can be seen that the total LCOE actually is 0.68 NOK/kWh, which is high compared to the average electricity price in tromsø in 2016. At 2% discount rate, the total LCOE is as low as 0.45 NOK/kWh, hence discount rate is an important factor.

As a final remark, it can be seen that in none of the sensitivity cases does the LCOE turn out to be lower than the average electricity price in Tromsø in 2016; 0.23 NOK/kWh, but again electricity certificates will contribute to a higher effective price received for the sold electricity, the exact value depending on the certificate market (see Subsection 4.6.3).

5.4.3 Tracking scenarios

Because Scenario 2 with horizontal axis tracking turned out to have a much smaller increase in power output compared to stationary modules than the vertical tracking, and it is reasonable to assume that the costs for horizontal axis tracking are quite similar to the vertical axis tracking costs, Scenario 2 is omitted from the financial analysis. In addition, two-axis tracking only has marginal power output increase compared to Scenario 3, and it has a higher installation cost and higher complexity than one-axis tracking systems, hence also this scenario is omitted from the economic analysis.

Table 5.16 shows how high costs PV systems with vertical-axis tracking can have to have the same NPV or LCOE as Scenario 1 with stationary modules. Only the change in costs of the PV modules is changed, as the inverter size is always 19 MW in Scenario 3, and its costs depends on its size.

Table 5.16: Costs for PV modules with vertical-axis tracking systems in Scenario 3 if they are to have the same NPV or LCOE as stationary modules in Scenario 1

	Percentage of S1 costs	NPV solar
S1	1	-161 967 918
S3	105.69	-161 967 112

	Percentage of S1 costs	LCOE solar
S1	1	0.9891
S3	137.95	0.9891

	Percentage of S1 costs	NPV total
S1	1	-376 591 313
S3	105.69	-376 590 470

	Percentage of S1 costs	LCOE total
S1	1	0.5569
S3	120.04	0.5569

To obtain similar NPV values, the costs of vertical axis tracking can be almost 6% higher. For the LCOE values to be similar, the costs can be higher. For an equal solar LCOE as with stationary modules, the costs can be 38% higher, and for an equal total LCOE they can be 20% higher. It is seen that the NPV is more sensitive to cost variations than the LCOE, which lies in the nature of their calculations. These results show that if the tracking system is 40-80% more expensive than stationary PV systems, as found in Subsection 4.6.1, tracking systems are non-profitable to an even higher degree than stationary modules even if they produce a larger amount of electricity.

5.5 Future scenario

A future case as described in the methodology chapter (Subsection 4.10.3) is simulated for the scenario with stationary PV modules. The simulation results are shown in Table 5.17.

Table 5.17: Technical output parameters from HOMER simulations of a future scenario with stationary PV modules when different terrains throughout the year is taken into account. The two values in each cell represent the first and last year of the system's lifetime, respectively (year 1/year 25). If only one value is given, it represents year 1

PV production ($^{MWh}/_{year}$)	PV production (% of total production)	PV mean output (MW)	PV capacity factor (%)
24 967/22 137	27.43/25.10	2.850/2.527	14.25/12.64

WT production ($^{MWh}/_{year}$)	WT production (% of total production)	WT mean output (MW)	WT capacity factor (%)
66 059/66 059	72.57/74.90	7.541/7.541	35.91/35.91

Converter output ($^{MWh}/_{year}$)	Total electricity production ($^{MWh}/_{year}$)	Electricity purchased ($^{MWh}/_{year}$)	Electricity sold ($^{MWh}/_{year}$)
24 717/21 916	91 025/88 195	44.34	90 584

The yield in this future scenario in year 1 is calculated to be 1248 $^{MWh}/_{MW_p}$, which is an excellent value. Compared to the regular scenario with stationary modules (in Table 5.13), the yield value is increased with approximately 51%. If one compares the inverter output values, the effect is seen to be even larger, because both the efficiency of the PV modules and the inverter is increased in this future scenario. The increase in inverter output is from 15 686 MWh to 24 717 MWh in year 1, giving an increase of approximately 58%.

An increase of 11% is seen in the amount of electricity sold compared to Scenario 1, and this will affect the economic aspects. Table 5.18 shows economic parameters for the future scenario. The economic analysis is as mentioned done with an average albedo and surface roughness length, and in this future scenario an albedo of 45.74% and surface roughness of 0.004835 meter was found to

give an energy output similar to the technical results shown in Table 5.17.

Table 5.18: Economic parameters where the values represent the total value in the whole lifetime of the system, and future costs and revenues are discounted to present value. The NPV and LCOE are calculated by using Equation 2.12 and Equation 2.13, respectively

PV capital cost (NOK)	PV O&M costs (NOK)	WT capital cost (NOK)	WT O&M costs (NOK)
150 000 000	42 281 834	191 800 000	93 102 832

Inverter capital cost (NOK)	Inverter replacement cost (NOK)	Inverter O&M cost	Inverter salvage value (NOK)
10 266 667	4 938 442	2 893 957	1 010 592

Electricity available for sale (MWh)	Grid sales revenue solar (NOK)	Grid sales revenue wind (NOK)	Grid sales revenue (NOK)
1 263 353 439	73 958 542	211 863 148	286 689 131

NPV solar (NOK)	NPV wind (NOK)	NPV (NOK)	LCOE (NOK/kWh) solar/wind/total
-73 039 684	-135 411 766	-207 584 008	0.6300/0.3060/0.3912

The PV capital and O&M costs are higher than in the low cost case in the economic analysis because in this future scenario, the efficiency is increased to 30%, increasing the size of the system to 30 MW, again increasing the costs of the system. Also the inverter had to be increased, and hence its costs and salvage value are increased.

Compared to the regular Scenario 1, the total NPV of the future scenario has decreased (in absolute value) by 45% to -208 million NOK, and the solar and wind NPV has decreased by 55% and 37%, respectively, to -73 and -135 million NOK. For LCOE, the decreases in total, solar and wind LCOE are 28%, 36% and 33%, respectively. The total LCOE turns out to be only 0.39 NOK/kWh, which is not very large compared to the average electricity price in Norway in 2016; 0.23 NOK/kWh., and including the effect of electricity certificates will contribute to making the price received for the electricity sold even higher. If the costs of PV and wind components decrease by the amount assumed here, this hybrid system can turn out to be less non-profitable. If in addition the electricity prices increase in the future, there may even be a profitability.

5.6 Sources of error

A summary of the most important sources of errors is given here.

The fact that simulated solar radiation data is used in this thesis, and not measured data, is already discussed, but cannot be stressed enough. There is a large uncertainty in the solar resource at the area. The timing error is as mentioned not taken into account in the simulation results, which will underestimate the solar potential in Skibotndalen. The overestimation of the simulated solar radiation is accounted for, but there is still uncertainty in how much the overestimation is at Galgo compared to at Holt, hence the effect of changing the radiation level has been examined.

HOMER calculates values of the clearness index in May-July that are not correct, which due to the black-box nature of the software cannot be corrected. HOMER also does not explicitly simulate shading (by objects or other PV modules), mismatch between modules or dust at the modules, but takes as input one derating factor which includes all these effects. In reality these effects are much more complicated.

The fact that HOMER does not take into account the wind direction and turbulence effects from the terrain and wake effects causes the wind energy output to be overestimated. HOMER does not take into account any variation of the weather resources from year to year in the multi-year analysis.

Because an average albedo and surface roughness is used in the economic analysis, there will be some error prone to this, because the variation in power output and electricity prices is not correct during the year. The cost of grid extension is not considered in this thesis. When constructing power plants, the grid lines must be extended to the location of the power plant, which is expensive. Depending on the exact location of the wind and PV power plant, this cost will contribute to an even lower profitability of the system. In addition, the cost of controlling several renewable power plants simultaneously may be more expensive than controlling each separately, as a more complicated regulator may be needed, and this is not included in this thesis.

5.7 Comparison with *Fakken*

As mentioned, a master's thesis is being written on the feasibility of a large-scale hybrid system at Fakken, where there already exists a wind power plant owned by *Troms Kraft* [Tiller, 2017]. A PV power system of 20 MW is simulated at location together with the existing wind power plant of 54 MW. Therefore, a

short comparison is done on the two locations Fakken and Skibotndalen.

The Pearson correlation coefficients at Fakken is using daily (24 hour) averaged values slightly less than the corresponding coefficients in Skibotndalen. The values for February, March and April at Fakken are -0.95, -0.12 and -0.36, while the values in Skibotndalen are -0.26, -0.23 and -0.53. However, the values are still small negative values, and it is difficult to conclude that there is any anti-correlation in any of the locations at a daily basis.

The solar radiation at Fakken in the period February to April 2017 was measured to be 151 MWh/m^2. The solar radiation for Galgo is calculated in Subsection 5.1.2 only for the period January to April 2017, but calculating it for February-April 2017 gives a value of 197 MWh/m^2, which shows that the solar radiation at Galgo is 30% higher than at Fakken. This is due to the dry weather in Skibotndalen, the colder temperature because it is at a higher elevation and not by the coast such as Fakken, and the higher albedo due to a higher number of snow days during the year.

The yield for stationary modules when not optimizing for timing error of simulated solar radiation at Fakken is 660 MWh/MW_p, which for Skibotndalen was 826 MWh/MW_p, giving an increase of 25% in the yield in Skibotndalen compared to Fakken. When optimising for the timing error of the simulated data the values are 736 MWh/MW_p and 933 MWh/MW_p, respectively, giving an increase of 27% in Skibotndalen.

To compare the wind resource at Fakken and at Rieppi, the capacity factor of the existing wind power plant at Fakken and the capacity factor of the simulated system in this thesis can be compared. At Fakken, the capacity factor is 29.4%, which means that if turbine losses are approximately 20% (see Table 5.14, the performance of the two power plants are similar.

6

Conclusion and further study

6.1 Summary

The comparison of WRF-simulated solar radiation data at Holt in Tromsø showed good correlation between the two data sets. However, an overestimation and shift of the solar noon by approximately 2 hours compared to measured values at the same location. Because of the overestimation, the data set is scaled to 70% of its original values before used in the hybrid system simulations. There was found no simple relationship for the shift in the solar noon, hence the timing of the data series was kept as is. However, the timing error could have been minimised by using a different azimuth angle, but it was discovered when there was under 24 hours to the deadline of this thesis. The simulation results does not include this optimising, which implies that they underestimate the solar potential in Skibotndalen, but an analysis is done on the effect of changing the azimuth angle.

The measured solar radiation values at Galgo this far in 2017 showed that Galgo in Skibotndalen has an exceptional solar resource compared to Holt. The simulated data for Galgo is seen to not overestimate the solar radiation as much as it does at Holt, but as this is obtained by comparing 2016 data with 2017 data, it is very uncertain. The scaling of 70% is therefore chosen to be kept.

Regarding the anti-correlation of the wind and simulated solar resource at Galgo in 2016, there is found to be moderate on a weekly and monthly basis. If the simulated solar radiation data did not have a timing error, the anti-correlation could have turned out to be even higher. In the first four months of 2017, when measured solar radiation data from Galgo is used, the anti-correlation is on a weekly basis moderate, and actually very high on a monthly basis.

The effect of changing the azimuth angle to an optimal angle (the one which gives highest PV output; 310°west of south for stationary modules and 290°for horizontal-axis tracking) causes the PV power production with stationary modules to be approximately 13% higher than with an azimuth angle of 0°. For the horizontal-axis tracking, the increase was found to be 8.3%. The NPV values and the total LCOE showed negligible change when the optimal azimuth angle was used, while the solar LCOE decreased by 10%. The sensitivity analyses done with 0°azimuth angle are still regarded to be representative, as the relative change with changing parameters is expected to be quite similar.

From the simulations done in HOMER, the optimal slope for stationary PV modules was found to be 50°, and for vertical-axis tracking it was 69°. The effect of albedo and surface roughness on both PV and wind energy output is significant, and for the technical analysis the albedo and surface roughness is changed throughout the year, with snow cover 258 days of the year and heathland in the rest of the year, as Skibotndalen is an area with many snow days. The economic analysis would be extremely time consuming to perform in HOMER if the terrain is changed during the year, and hence it is simplified by using average albedos and surface roughnesses which are seen to give similar outputs as the systems with changing albedo.

The technical feasibility of the PV component of the hybrid system is shown to be good, with a PV yield of 826 $^{MWh}/_{MW_p}$ for stationary modules. Taking into account the timing error of the simulated solar radiation data, the yield for stationary modules may be up to 13% higher, giving a potential yield of 933 $^{MWh}/_{MW_p}$, being an excellent value for Scandinavia. Out of the three different astronomical tracking systems simulated (horizontal-axis, vertical-axis and two-axis tracking), the vertical-axis tracking system turned out to give the best energy output enhancement compared to its cost and complexity, and its yield was calculated to be 1137 $^{MWh}/_{MW_p}$, also an excellent value.

As there is an uncertainty in the simulated solar radiation data used for simulations, a sensitivity analysis is done on different radiation levels. For instance, a radiation level of 80% of the simulated values gives a yield of 999 $^{MWh}/_{MW_p}$ for stationary PV modules, which implies that there might be a substantial PV electricity potential in the area if the overestimation by the

simulated solar radiation data is lower at Galgo than at Holt. Including the effect of timing error, this yield can turn out to be 13% higher, thus 1129 $^{MWh}/_{MW_p}$. Sensitivity analyses are also done for the PV efficiency, inverter efficiency and slope angle.

The energy output from the wind power plant is seen to be large, resulting in a capacity factor of 36%. However, this is when turbulence and wake effects are not taken into account. A sensitivity analysis is done on turbine losses and wind speed, as especially the turbine losses are uncertain. If 20% losses are included, the capacity factor turns out to be 29%, which still is a decent value compared to average capacity factors in Europe and Norway. The wind speed average in 2016 was found to be 8.67 $^{m}/_{s}$ at hub height, which is well above the thumb of rule which classifies a location as feasible for wind power plants (6.5 $^{m}/_{s}$).

The power output from the hybrid system, including the hydro power station production data from 2014 (as this is the best available data) is plotted for one year and for average days in each quarter year. This shows that the power output from the hybrid system does not exceed 100 MW, which is the maximum grid capacity in the area, and the PV and wind components can be even larger. The variation in the hydro power output is large as it is operated depending on the electricity price, and not the demand. The power output from the PV and wind components is very variable, but does to some degree follow the tendency of the demand in the area on a daily profile, because there is a peak in the PV output in the middle of the day. However, the demand is usually high in the evening as well, which the hybrid system does not fulfil. To achieve a smoother power output from the hybrid system, the hydro power stations can instead be operated according to the output of the solar and wind components, as the water in the reservoir can be saved if it is not used, while unused solar radiation and wind is lost if not exploited at the instant they occur. It is also seen that even if the hydro power stations are operated at full capacity for the whole year, the total power output from the hybrid system does not exceed the maximum grid capacity.

In the economic analysis, an NPV value of approximately -380 million NOK of the hybrid system implies that the hybrid system is not profitable at all. The NPV for only the PV component is around -162 million NOK, and the NPV for the wind component is in the range of -215 million NOK. The wind NPV has the largest negative values even though the electricity produced by the wind system is larger than the electricity produced by the PV system, because the capital and O&M costs are much larger than for the PV system. Regarding the LCOE value calculated for the hybrid system, it has a value of 0.56 $^{NOK}/_{kWh}$, while the LCOE for the PV system alone is 0.99 $^{NOK}/_{kWh}$ and the LCOE for the wind system alone is 0.46 $^{NOK}/_{kWh}$. taking into account the timing error of the

simulated solar radiation values, the LCOE may decrease by 10%, giving a value of 0.89 NOK/kWh. The LCOE is in any case higher for the PV system than the wind component, which is due to the lower energy production of the PV system compared to the wind system. The LCOE values are higher than the average electricity price in Tromsø (0.23 NOK/kWh), but subsidies from the renewable electricity certificate market in Norway and Sweden and financial support from *Enova* can contribute in making the system more profitable.

The NPV is shown to be very sensitive to the electricity price. The discount rate, wind turbine losses, wind speed and solar radiation affects the economic parameters to a quite large degree, but changing these parameters did not result in positive NPV values. For instance, a solar radiation level of 80% causes a NPV of -370 million NOK and a LCOE of 0.83 NOK/kWh, while wind turbine losses of 20% causes an NPV of -418 million NOK and a LCOE of 0.57 NOK/kWh. PV systems are found to have give an equal total NPV as the hybrid system with stationary PV modules when the solar costs (excluding inverter costs) are 6% higher than the stationary PV system costs. They achieve an equal LCOE when the PV system costs are 20% higher than for the stationary PV system.

A future scenario with lower costs, higher PV efficiency and higher inverter efficiency is simulated, giving the supreme PV yield of 1248 MWh/MW_p. Taking the timing error of the simulated solar radiation data into account, this may even turn out to be 13% higher, thus 1248 MWh/MW_p. The wind energy output is not changed in this scenario, but the economic parameters are changed substantially; the total NPV for the hybrid system is -208 million NOK, while the PV and wind NPV values are -135 million NOK and -73 million NOK, respectively. The total, PV and wind LCOE values are 0.39 NOK/kWh, 0.63 NOK/kWh (approximately 0.57 NOK/kWh if including timing error) and 0.31 NOK/kWh, showing that if costs and efficiencies in the future becomes as assumed, the hybrid system can turn out to be less non-profitable. If electricity prices increase, the system can even turn out to be profitable in the future.

6.2 Concluding remarks

Simulations are always uncertain, and this study contains many of these uncertainties. As a concluding remark, however, it has been found that a large-scale hybrid system consisting of solar, wind and hydro power components is seen to be feasible in the technical aspect. Both the wind and solar resource potential is found to be large at the location. Economically, on the other hand, the system has shown to be non-profitable, but if the costs of PV and wind components decreases, the electricity price increases, and/or subsidies are received, it can turn out to be profitable.

6.3 Further work

To improve and extend the study performed in this thesis, the following examples of further work are given:

- In the future, measured values for one whole year at Galgo can be used to better assess the anti-correlation between the solar and wind resource and the feasibility of a large-scale hybrid system in Skibotndalen

- It has been shown that the size of the components can be increased, as the total power output from the PV, wind and hydro component does not exceed the maximum grid capacity, and this may be assessed in the future

- If later studies concludes with feasibility of a large-scale hybrid system in Skibotndalen, an analysis should be performed on the location, assessing the best sites for the PV component and wind component of the system. The PV power output inter alia depends on the shadowing from the surrounding topography, and the wind power output depends on inter alia the topography and turbulence at different sites

- A wake effect analysis should be performed at the location if a wind power plant is to be constructed, so that the real power output from the wind power component can be estimated

- As simulations of bifacial PV modules was not possible in the simulation software used in this thesis, it can be interesting to see if the potential yield of bifacial modules is different from the one for stationary modules and tracking systems

Appendices

A

Hybrid systems literature review

This section is written in collaboration with Charlotte Tiller, and is therefore identical in our theses. It includes a litterature review of existing and simulated large-scale hybrid systems.

The number of large-scale hybrid systems is limited, thus this is also the case for the available documentation on the state-of the-art of such systems. This literature review considers both case studies on and planned and existing large-scale hybrid systems. Many systems in the literature are combinations of both renewable and conventional power sources to ensure that the power demand is met in periods when the renewable source is not sufficient and in addition, some systems also have an energy storage option. Finally, some systems are located on smaller islands and/or only connected to a low or medium voltage grid. In lack of literature on identical hybrid systems to the ones considered in this thesis, such systems are still included in the literature review, as there are some similarities between them.

Kythnos island, Greece

One of the first large-scale hybrid systems was commissioned at the Greek island Kythnos. It is a decentralised system and is not connected to the grid

on the mainland, but supplies the medium voltage grid on the island. Before the hybrid system, diesel generators supplied the island with electricity. In 1982, five 20 kW wind turbines were installed at the island, comprising the first wind park in Europe [ISET and SMA,]. These were replaced with five 33 kW turbines from *Aeroman* in 1989. In 1998, a 500 kW *Vestas* turbine was installed. In 1983 a 100 kW Siemens PV system with battery storage was added to the system, and at this time it was the largest hybrid system in the world [Strauss and Kleinkauf, 2002].

In year 2000, a new, fully automatic, control system was installed which controls the power supply according to available renewable energy and electricity demand, in addition to a 500 kW battery storage [Strauss and Kleinkauf, 2002]. This led to a renewable contribution of 50% in off-peak periods and the possibility of 100% renewable penetration in periods of low demand. The battery storage can provide high power with short response time for short time intervals if needed. Connected to the system is also a load control, which consists of a power inverter that ensures voltage and frequency stability by cutting off peaks from the wind power inverters that are unwanted, as wind gusts is a challenge in the area [Strauss and Kleinkauf, 2002]. The control system consists of an intelligent power system delivered by *SMA*. It is a computer which monitor every component of the system. [Strauss and Kleinkauf, 2002] reports that the system has operated satisfactory and contributed to large fuel savings. A schematic of the system is shown in Figure A.1.

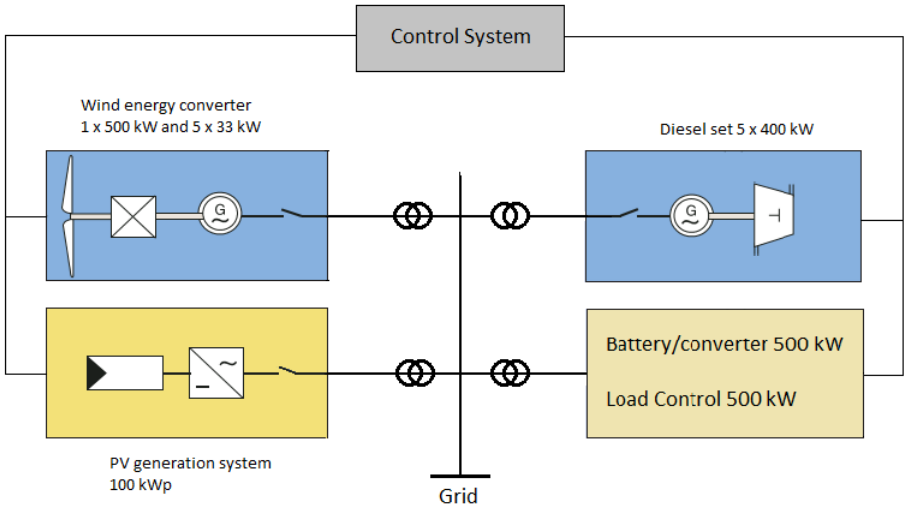

Figure A.1: The arrangement of the hybrid system at Kythnos. Simplified from [ISET and SMA,]

Longyangxia hydro and PV hybrid system, China

Today, the world's largest hybrid system is located in China, by the Longyangxia Dam. It consists of PV and hydro power, and is the first commercial large-scale hybrid system with these two power sources. The 1280 MW hydro power plant was commissioned in 1992 and consists of four 320 MW turbines. In December 2013, a 320 MW PV power plant was commissioned in the same area, and it is connected to the grid through the hydropower plant, via a 330 kV transmission line to one of the hydro power turbines [(IHA), 2015]. The PV plant has undergone almost constant expansion, and today, the PV plant has a capacity of 850 MW and covers 27 km^2 [Philips, 2017].

The PV system is one of the world's largest, and on its own it would cause substantial instabilities on the grid due to large variations in the solar resource. The way it is connected via one of the turbines in the hydro power plant, causes it to function as a fifth turbine. The PV output is tracked and the hydro power turbines can compensate for variations with a very short response time as the control system is simultanously controlling the PV and hydro power plant. In addition, the connection between the power plants has enabled a higher capacity factor of the hydro power station in dry periods [(IHA), 2015].

In [Fang et al., 2017], a method for finding the optimum size of a hybrid system between PV and hydro power is formulated and applied to the Longyangxia hybrid system. The article focuses on the flexibility of the system in the short-term, and therefore three daily schemes for operation of the PV and hydro power plants depending on the type of load demand is used in calculations. The method then optimises the size of the system by maximising the net income during the lifetime of the system for each operation scheme while taking into account two factors; the gross output from the hybrid plant should never be larger than the total installed capacity of the hydropower plant and the solar curtailment should be as small as possible to avoid the solar curtailment fee.

The three operating schemes are:

- **All-day lifting scheme**: the daily curve of the gross output from the combined PV and hydro power is the sum of the output of the hydro power during the day (variable) and the mean daily output from the PV plant (constant). This scheme is suitable for areas where the PV output never exceeds the demand and grid constraints.

- **Daytime lifting scheme**: during the day (08:00-19:00) the curve of the gross output from the hybrid system is the sum of the output of the hydro power during the day (variable) and the mean daily output from the PV plant during daytime (constant). At night time the gross output is equal to the hydro power output. Suitable if the load demand is higher during daytime than during night time

- **Peak-load period lifting scheme**: during two time periods each day, the gross output from the PV+hydro power is the sum of the hydro power output and a portion of the daily mean PV output dependent on how large a percentage the load in the respective time period is of the total load in the two peaks. Outside these two periods, the gross output is equal to the hydropower output. Suitable for regions with two peaks in the electricity demand

It is found for the case of Lonyangxia hybrid system that the net revenue increases with PV system size for all schemes, but in the daytime and peak-load period lifting schemes, the gross output constraint limits the size. In the daytime lifting scenario, there is no solar curtailment. Optimum sizes for different hydropower capacities when also considering an expansion of hydropower is 1030 MW (with 90% hydropower capacity), 2040 MW (with 160% hydropower capacity) and 690 MW (with 105% hydropower capacity), respectively for the three schemes. The article also considers the effect that integrating PV into a hydro power plant has on the water resource allocation

of the reservoir used for the Longyangxia system, and concludes that there is a very low degree of adverse effects.

[Li and Qiu, 2016] proposes a model that optimises a hybrid system between PV and hydro power. It aims at maximising the amount of generated power and minimising the power output fluctuations by varying the reservoir release. Constraints are the water level in the reservoir, the maximum reservoir release and the maximum capacity of the electricity grid. The model is long-term and results are given for time periods of one year, classified into different categories depending on amount of inflow into the Longyangxia reservoir; extremely wet years, wet years, normal years, dry years and extremely dry years. The model results when applied to Longyangxia showed that the model is adequate and that hydropower and PV power are complementary, with the highest anti-correlation in wet years, when a larger amount of precipitation leads to less solar radiation and more hydro power output.

El Hierro island, Spain

El Hierro is a Canary island with 10,000 inhabitants and with its own isolated grid system [Plitt, 2015], [Godina et al., 2015]. Remote and isolated energy systems depending on fossil fuels are vulnerable to prices and has a high transportation cost of fuels. To mitigate this issue a hybrid system construction consisting of wind power and pumped hydroelectric storage was finalized in 2015 [Plitt, 2015]. Five wind turbines with a total capacity of 11.5 MW and a storage capacity of $380,000 m^3$ of water in its upper dam reservoir now provides the island reliable power[Godina et al., 2015] [Plitt, 2015]. Wind power will supply the island with energy directly, and any excess energy will be fed into the hydroelectric facility and pump water from the bottom reservoir to the top reservoir. The top reservoir is in fact a volcanic crater [Godina et al., 2015]. During times at low wind speed or during peak demand, water from the top reservoir is released and runs a set of Pelton turbines for electricity generation [Godina et al., 2015]. The hydroelectric plant can respond to the wind production within milliseconds to even out the total power production [Plitt, 2015]. The diesel power plant will operate only if the cumulative power from both the wind and hydro systems are insufficient in meeting the demand. By October 2015, the renewable penetration was roughly 50% of the total production, and the goal is for the island to be 100% self supplied with renewable energy. The renewable penetration is assumed to increase when those operating the energy system have gained more experience with the new system [Plitt, 2015].

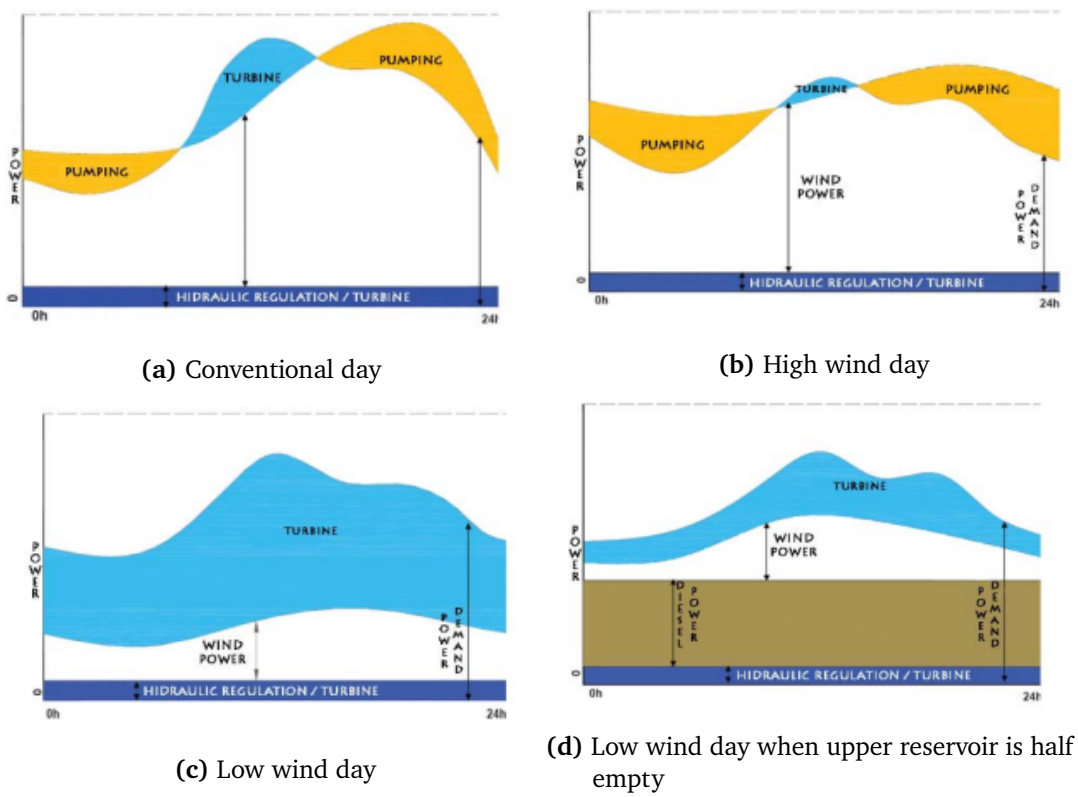

(a) Conventional day

(b) High wind day

(c) Low wind day

(d) Low wind day when upper reservoir is half empty

Figure A.2: Operating scenarios for different wind and reservoir conditions. From [Hallam et al., 2012]

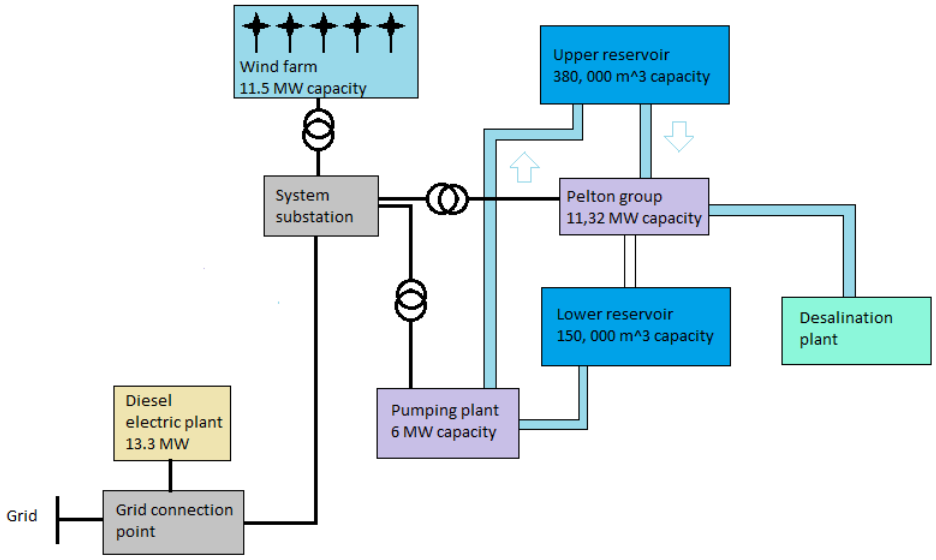

Figure A.3: A diagram showing the hybrid system at El Hierro. Created with information from [Godina et al., 2015] and [Hallam et al., 2012]

Pellworm island, Germany

Pellworm is an island outside the west coast of northern Germany. The island had 1100 inhabitants in 2013 [Gildemeister, 2013] and its annual electricity consumption is approximately 8 GWh, while the total amount of electricity produced on the island is about 25 GWh. The electricity production at the island comes exclusively from renewable sources; PV, wind and biogas plants. The system on the island also uses batteries as a storage solution [Koopmann et al., 2014].

The first PV plant was installed at the island in 1983 and had a capacity of 300 kW. The capacity has since then been increased by another PV plant and wind turbines. The PV modules from 1983 were replaced in 1995 because the inverters had been destructed by lightning [Peschel, 2015].

As seen in Figure A.4, the power plants are located quite long distanced between them. There is a hybrid system consisting of a PV power plant (PVP) and a wind power plant (WPP) to the left in the picture, and this has a capacity of 1072 kW (772 kW PV and a 300 kW wind turbine). In 2013, batteries with a storage capacity of 2160 kWh was installed in conjunction with the system

[Peschel, 2015].

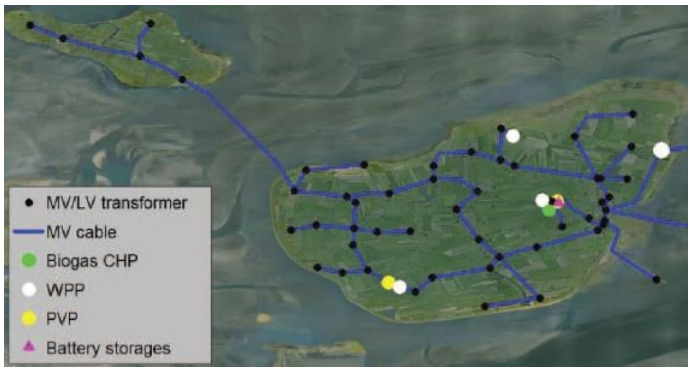

Figure A.4: A map of the power plants and medium voltage grid at Pellworm and its neighboring island. From [Koopmann et al., 2014]

The power plants are connected to the island's electricity grid in the medium voltage range and a large number of small-scale PV modules are connected to the grid via a low voltage grid. The grid on Pellworm is connected to the mainland grid to both export and import electricity. [Koopmann et al., 2014]. It also covers a small neighbouring island to Pellworm.

Because power losses are large when transmitting electricity over long distances, a smart grid in planned on the island, so that the production and demand can be better correlated. In addition, large storage systems are planned to be installed so that electricity can be stored in periods of high production and hence self-sufficiency of the island can be achieved also in periods of low local electricity production [Gildemeister, 2013].

Linha Sete, Brazil

This section is based on a feasibility study of a grid connected hybrid system consisting of PV, wind and a pumped hydroelectric storage facility together with a diesel generator as a back up source, found in [Risso et al., 2017]. The hydroelectric plant has a total head of 655 m and a storage volume capacity of $1,510,000 m^3$. The system was simulated using Homer. The PV panels are planned to be installed as a floating structure on the dams in order to reduce evaporation of the water but also to avoid shading of the land area and hence reduce the environmental impacts of the construction. This will increase the PV system costs by 30% compared to conventional solutions. The wind turbines have a capacity of 1 MW each. Two systems are simulated, one without PV and one containing 10 MW installed capacity.

The hydroelectric plant is simulated as a *Run of the river* connected to a DC bus together with a battery to simulate the pumped storage facility. In order to find the most optimal system size, Homer was asked to simulate a high number of component sizes by implementing different numbers of wind turbines, different capacity sizes of the diesel generator, different inverter capacities and different number of batteries. Sensitivity analysis were conduced on the diesel price, the AC load and the wind speed. At least 95% of the load must be provided by renewable sources.

Because of high PV installation costs, the optimal solution was one without PV. However, some of the systems that included PV was not far from the optimal system solution. The study recommends a system consisting of 100 kW in PV, 20 wind turbines, a diesel generator with a capacity of 19,200 kW and the pumped storage unit which gives an energy cost of USD$ 0.408 per kWh. Alternatively, a system excluding the wind turbines but consisting of 10 MW of PV, a diesel generator with a capacity of 30 MW and the pumped storage gives an energy cost of USD $0.609. The first alternative is considered the most stable one, because it has the same amount of energy available in the reservoir at the end of the year as it contained in the beginning.

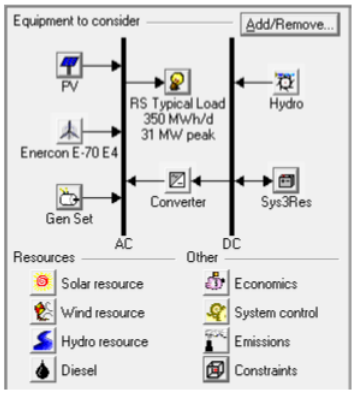

Figure A.5: A diagram showing the hybrid system at in Linha Sete. From [Hallam et al., 2012]

B

Inhabitants in the concession area of *Troms Kraft*

Figure B.1 shows the number of inhabitants in each of the municipalities in the concession area of *Troms Kraft* 1 January 2016.

	2016
	Personer
1902 Tromsø	73 480
1920 Loabák - Lavangen	1 051
1922 Bardu	4 019
1923 Salangen	2 230
1924 Målselv	6 741
1925 Sørreisa	3 452
1926 Dyrøy	1 158
1927 Tranøy	1 543
1928 Torsken	913
1929 Berg	915
1931 Lenvik	11 618
1933 Balsfjord	5 701
1936 Karlsøy	2 282
1938 Lyngen	2 861
1939 Storfjord - Omasvuotna - Omasvuono	1 865

Figure B.1: The number of inhabitants in the municipalities of the concession area of *Troms Kraft* 1 January 2016

C

Namelists

The namelists used for the WRF simulations are appended. The first is the namelist for the WPS, and the second for the actual simulation.

Namelist WPS

```
&share
wrf_core = 'ARW',
max_dom = 2,
start_date = '2016-09-07_12:00:00', '2016-09-07_12:00:00',
end_date   = '2016-10-01_00:00:00', '2016-10-01_00:00:00',
interval_seconds = 21600,
io_form_geogrid = 2,
opt_output_from_geogrid_path = '/home/ynb022/WRF/WRFportal/Domains/Solar2016/',
debug_level = 0,
/
```

```
&geogrid
parent_id         = 1,1,
parent_grid_ratio = 1,3,
i_parent_start    = 1,33,
j_parent_start    = 1,33,
e_we          = 97,97,
e_sn          = 97,97,
geog_data_res = '2m','30s',
dx = 9000,
dy = 9000,
map_proj =  'polar',
ref_lat   = 69.5,
ref_lon   = 20,
truelat1  = 69.5,
truelat2  = 90,
stand_lon = 20,
geog_data_path = '/home/WRF/WPS_GEOG',
opt_geogrid_tbl_path = '/home/ynb022/WRF/WRFportal/Domains/Solar2016/',
ref_x = 48.5,
ref_y = 48.5,
/
```

```
&ungrib
out_format = 'WPS',
prefix = 'FILE',
/
```

```
&metgrid
fg_name = 'FILE',
io_form_metgrid = 2,
opt_output_from_metgrid_path = '/home/ynb022/WRF/WRFportal/Domains/Solar2016/',
opt_metgrid_tbl_path = '/home/ynb022/WRF/WRFportal/Domains/Solar2016/',
/
```

```
&mod_levs
press_pa = 201300 , 200100 , 100000 ,
            95000 ,  90000 ,
            85000 ,  80000 ,
            75000 ,  70000 ,
            65000 ,  60000 ,
            55000 ,  50000 ,
            45000 ,  40000 ,
            35000 ,  30000 ,
            25000 ,  20000 ,
            15000 ,  10000 ,
             5000 ,   1000
/
```

```
&domain_wizard
grib_data_path = '/home/ynb022/WRF/GRIBdata',
grib_vtable = 'Vtable.ERA-interim.pl',
dwiz_name    =Solar2016
dwiz_desc    =To run simulations for two master students
dwiz_user_rect_x1 =59
dwiz_user_rect_y1 =75
dwiz_user_rect_x2 =168
dwiz_user_rect_y2 =155
dwiz_show_political =true
dwiz_center_over_gmt =false
dwiz_latlon_space_in_deg =10
dwiz_latlon_linecolor =-8355712
```

Namelist actual simulation

```
&time_control
run_days                  = 92,
run_hours                 = 11,
run_minutes               = 50,
run_seconds               = 0,
start_year                = 2016,     2016,
start_month               = 06,       06,
start_day                 = 06,       06,
start_hour                = 12,       12,
start_minute              = 00,       00,
start_second              = 00,       00,
end_year                  = 2016,     2016,
end_month                 = 07,       07,
end_day                   = 01,       01,
end_hour                  = 00,       00,
end_minute                = 00,       00,
end_second                = 00,       00,
interval_seconds          = 21600,
input_from_file           = .true.,   .true.,
history_interval          = 10,       10,
frames_per_outfile        = 500000,    500000,
restart                   = .false.,
restart_interval          = 100000,
io_form_history           = 2,
io_form_restart           = 2,
io_form_input             = 2,
io_form_boundary          = 2,
debug_level               = 0,
/
```

```
&domains
time_step                = 54,
time_step_fract_num      = 0,
time_step_fract_den      = 1,
max_dom                  = 2,
e_we                     = 97,       97,
e_sn                     = 97,       97,
e_vert                   = 51,       51,
p_top_requested          = 1000,
num_metgrid_levels       = 38,
num_metgrid_soil_levels  = 4,
dx                       = 9000,     3000,
dy                       = 9000,     3000,
grid_id                  = 1,        2,
parent_id                = 1,        1,
i_parent_start           = 1,       33,
j_parent_start           = 1,       33,
parent_grid_ratio        = 1,        3,
parent_time_step_ratio   = 1,        3,
feedback                 = 0,
smooth_option            = 0,
eta_levels               = 1.0000, 0.9980, 0.9955, 0.9925,
                           0.9890, 0.9850, 0.9805, 0.9755,
                           0.9700, 0.9640, 0.9575, 0.9505,
                           0.9430, 0.9350, 0.9265, 0.9170,
                           0.9060, 0.8930, 0.8775, 0.8590,
                           0.8363, 0.8104, 0.7803, 0.7456,
                           0.7059, 0.6615, 0.6126, 0.5594,
                           0.5041, 0.4479, 0.3919, 0.3384,
                           0.2897, 0.2474, 0.2107, 0.1792,
                           0.1523, 0.1293, 0.1093, 0.0917,
                           0.0763, 0.0629, 0.0513, 0.0413,
                           0.0328, 0.0255, 0.0194, 0.0144,
                           0.0104, 0.0071, 0.0000,
/
```

```
&physics
mp_physics               = 4,        4,
ra_lw_physics            = 5,        5,
ra_sw_physics            = 5,        5,
radt                     = 9,        3,
sf_sfclay_physics        = 2,        2,
sf_surface_physics       = 2,        2,
bl_pbl_physics           = 2,        2,
bldt                     = 0,        0,
cu_physics               = 2,        2,
cudt                     = 5,        5,
isfflx                   = 1,
ifsnow                   = 1,
icloud                   = 1,
surface_input_source     = 1,
num_soil_layers          = 4,
sf_urban_physics         = 2,        2,
/
```

```
&fdda
/

&dynamics
w_damping                = 0,
diff_opt                 = 1,
km_opt                   = 4,
diff_6th_opt             = 0,        0,
diff_6th_factor          = 0.12,     0.12,
base_temp                = 290.,
damp_opt                 = 0,
zdamp                    = 5000.,    5000.,
dampcoef                 = 0.2,      0.2,
khdif                    = 0,        0,
kvdif                    = 0,        0,
non_hydrostatic          = .true.,   .true.,
moist_adv_opt            = 1,        1,
scalar_adv_opt           = 1,        1,
/


&bdy_control
spec_bdy_width           = 5,
spec_zone                = 1,
relax_zone               = 4,
specified                = .true.,  .false.,
nested                   = .false.,   .true.,
/


&grib2
/

&namelist_quilt
nio_tasks_per_group      = 0,
nio_groups               = 1,
/
```

D

HOMER calculations

The following information is from [HOMER Energy, 2016].

D.0.1 PV module

Calculating power output

To calculate the power output from the PV modules in each time step including temperature effects, HOMER uses the following model:

$$P_{\text{PV}} = Y_{\text{PV}} f_{\text{PV}} \frac{G}{G_{STC}} [1 + \alpha_P (T - T_{STC})]$$

where Y_{PV} is the rated capacity of the PV module in kW, f_{PV} is the derating factor of the module in percent, G is the incident solar radiation (in $^{\text{kW}}/_{\text{m}^2}$) on the PV array in the respective time step the calculation is done for, G_{STC} is the incident radiation at STC ($1\,^{\text{kW}}/_{\text{m}^2}$), α_P is the temperature coefficient ($^{\%\text{ efficiency}}/_{^\circ\text{C}}$), T is the temperature of the cell in $^\circ C$, and $T_{STC} = 25^\circ C$ is the temperature of the cell under standard test conditions.

Calculating temperature of PV modules

HOMER can include temperature effects on the PV modules, and then calculates the temperature of the modules in each time step. When there is no solar radiation, the temperature is the same as the ambient temperature. It starts the calculation by defining an energy balance between the radiation energy absorbed by the modules and the sum of the power output and the heat transmitted to the surrounding environment:

$$\tau\gamma G = \eta G + U_L(T - T_a)$$

Where τ is the solar transmittance of the PV module, γ is the solar absorptance of the modules in percentage, η is the electrical conversion efficiency, U_L is a coefficient for the heat transmitted to the surrounding environment ($kW/m^2 \cdot °C$) and T_a is the ambient temperature ($°C$). Solved for T this becomes:

$$T = T_a + G\left(\frac{\tau\gamma}{U_L}\right)\left(1 - \frac{\eta}{\tau\gamma}\right)$$

Because $\frac{\tau\gamma}{U_L}$ is difficult to measure, the NOCT is used instead. Substituting parameters in the equation by the values the NOCT is defined by (see Subsection 2.1.4) and solve it for $\frac{\tau\gamma}{U_L}$ gives:

$$\frac{\tau\gamma}{U_L} = \frac{T_{NOCT} - T_{a,NOCT}}{G_{NOCT}}$$

This can be substituted into the equation for cell temperature if $\frac{\tau\gamma}{U_L}$ is assumed to be constant:

$$T = T_a + G\left(\frac{T_{NOCT} - T_{a,NOCT}}{G_{NOCT}}\right)\left(1 - \frac{\eta}{\tau\gamma}\right)$$

For $\tau\gamma$, HOMER uses the value 0.9. For the temperature dependency of the module efficiency on the cell temperature, HOMER uses the following linear relation:

$$\eta = \eta_{STC}(1 + \alpha_P(T - T_{STC}))$$

Where η_{STC} is the efficiency under STC and maximum power point operation. Substituting this into the equation for T gives:

$$T = \frac{T_a + (T_{NOCT} - T_{a,NOCT})\left(\frac{G}{G_{NOCT}}\right)\left(1 - \frac{\eta_{STC}(1-\alpha_P T_{STC})}{\tau\gamma}\right)}{1 + (T_{NOCT} - T_{a,NOCT})\left(\frac{G}{G_{NOCT}}\right)\left(\frac{\alpha_P \eta_{STC}}{\tau\gamma}\right)}$$

Calculating the radiation incident on PV modules

To calculate the amount of radiation incident on the PV modules, HOMER uses the input data series for the GHI. It assumes that the GHI series is given in LT, and hence uses the procedure described in Subsection 2.1.2 to find the LST. HOMER uses the following EOT (in hours):

$$EoT = 3.82\Bigg(0.000075 + 0.001868\cos\left(\frac{360^\circ}{365}(d-1)\right) - 0.032077\sin\left(\frac{360^\circ}{365}(d-1)\right) - 0.014615\cos\left(2\frac{360^\circ}{365}(d-1)\right) - 0.04089\sin\left(2\frac{360^\circ}{365}(d-1)\right)\Bigg) \quad \text{(D.1)}$$

To calculate the global radiation incident on the PV modules, HOMER uses a model called HDKR. This model divides the diffuse solar radiation into three components; one isotropic component that is equally distributed from all directions, one component that originates from the direction of the Sun (the circumsolar component), and one that originates from the horizon. The global radiation on the PV module averaged over one time step is calculated by:

$$\overline{G} = (\overline{G_{dir}} + \overline{G_d}A_i)R_b + \overline{G_{diff}}(1 - A_i)\left(\frac{1+\cos(\beta)}{2}\right)\left(1 + f\sin^3\left(\frac{\beta}{2}\right)\right) + \overline{G_E}\rho_g\left(\frac{1-\cos(\beta)}{2}\right) \quad \text{(D.2)}$$

- β denotes the angle between the surface and the horizontal, and ρ_g is the albedo of the ground.
- $R_b = \frac{\cos(\theta)}{\cos(\theta_z)}$ is the ratio of direct radiation on the module to the direct radiation on an horizontal surface, θ_z being the azimuth angle given by:

$$\cos(\theta_z) = \cos(\phi)\cos(\delta)\cos(HRA) + \sin(\phi)\sin(\delta).$$

- $\overline{G_E} = \overline{G_{dir}} + \overline{G_{diff}}$ is the GHI on the surface of the Earth, and is the sum of direct and diffuse solar radiation on the Earth's surface, respectively. The calculation of the fraction of direct and diffuse radiation of the GHI is shown below this list.
- $A_i = \frac{\overline{G_{dir}}}{\overline{G_o}}$ is the anisotropy index, which quantifies the transmittance of the direct radiation in the atmosphere, and is used to find the amount of circumsolar diffuse radiation. $\overline{G_o}$ is the radiation on a horizontal surface at the top of the

atmosphere averaged over one time step, and its calculation is shown below this list.

- $f = \sqrt{\frac{\overline{G_{dir}}}{\overline{G_E}}}$ is used to include the fact that there is a larger amount of diffuse radiation coming from the horizon than the rest of the sky.

Fraction of diffuse and direct radiation to GHI HOMER calculates the fraction of diffuse radiation to the global radiation by the following equation, and can from this also estimate the amount of direct radiation:

$$\frac{\overline{G_{diff}}}{\overline{G_E}} = \begin{cases} 1.0 - 0.09k_T & \text{if } k_T \leq 0.22 \\ 0.9511 - 0.1604k_T + 4.388k_T^2 - 16.638k_T^3 + 12.336k_T^4 & \text{if } 0.22 < k_T \leq 0.80 \\ 0.165 & \text{if } k_T > 0.80 \end{cases}$$

Here, k_T is called the clearness index and quantifies the clearness of the atmosphere with a number between 0 and 1 and is given by:

$$K_T = \frac{\overline{G_E}}{\overline{G_o}}$$

A value of $K_T = 0.25$ represents a very cloudy time period, and a value of $K_T = 0.75$ a very sunny period of time. G_o is defined below.

Extraterrestrial solar radiation on horizontal surface The solar radiation on the top of the atmosphere at a surface normal to the radiation is in HOMER given by:

$$G_{on} = G_{sc}\left(1 + 0.033\cos\left(\frac{360d}{365}\right)\right)$$

Where $G_{sc} = 1.367\,\mathrm{kW/m^2}$ is the solar constant. The amount of radiation incident on a horizontal surface at the top of the atmosphere (not averaged over the time step) is then:

$$G_o = G_{on}\cos(\theta_z)$$

By using the expression for θ_z and integrating the above equation over one time step, the average can be found to be:

$$\overline{G_o} = \frac{12}{\pi}G_{on}\left(\cos(\phi)\cos(\delta)(\sin(HRA_2) - \sin(HRA_1)) + \frac{\pi(HRA_2 - HRA_1)}{180^\circ}\sin(\phi)\sin(\delta)\right)$$

Bibliography

[Aarrestad and Hatlen, 2015] Aarrestad, K. and Hatlen, L. M. (2015). Facts 2015 - energy and water resources in norway. Technical report, Norwegian Ministry of Petroleum and Energy. https://www.regjeringen.no/contentassets/fd89d9e2c39a4ac2b9c9a95bf156089a/facts_2015_energy_and_water_web.pdf.

[Al-Mohamad, 2004] Al-Mohamad, A. (2004). Efficiency improvements of photo-voltaic panels using a sun-tracking system. *Applied Energy*, 79(3):345–354.

[Andrews and Jelley, 2007] Andrews, J. and Jelley, N. (2007). *Energy Science - principles, technologies and impacts*. Oxford University Press.

[ASA,] ASA, D. Gjennomsnittskurser 2017. https://www.dnb.no/bedrift/markets/valuta-renter/valutakurser-og-renter/historiske/hovedvalutaer.html. Accessed 29 May 2017.

[Bhattacharyya, 2011] Bhattacharyya, S. C. (2011). *Energy Economics*. Springer-Verlag London Limited.

[Blæsterdalen, 2016] Blæsterdalen, T. (2016). Wind resource asssessment using mesoscale modelling. Master's thesis, UiT the Arctic University of Norway.

[Carvalho et al., 2012] Carvalho, D., Rocha, A., Gómez-Gesteira, M., and Santos, C. (2012). A sensitivity study of the {WRF} model in wind simulation for an area of high wind energy. *Environmental Modelling & Software*, 33:23 – 34.

[Diaf et al., 2008] Diaf, S., Notton, G., Belhamel, M., Haddadi, M., and Louche, A. (2008). Design and techno-economical optimization for hybrid pv/wind system under various meteorological conditions. *Applied Energy*, 85(10):968–987.

[Dudhia, 2017] Dudhia, J. (2017). Overview of wrf physics. http://www2.mmm.

ucar.edu/wrf/users/tutorial/201701/physics.pdf.

[Fang et al., 2017] Fang, W., Huang, Q., Huang, S., Yang, J., Meng, E., and Li, Y. (2017). Optimal sizing of utility-scale photovoltaic power generation complementarily operating with hydropower: A case study of the world's largest hydro-photovoltaic plant. *Energy Conversion and Management*, 136:161–172.

[Farret and Simões, 2006] Farret, F. A. and Simões, M. G. (2006). *Integration of Alternative Sources of Energy*, pages 301–332. John Wiley & Sons, Inc.

[Gerrard, 1990] Gerrard, J. (1990). *Mountain environments: An examination of the physical geography of mountains*. The MIT Press.

[Gildemeister, 2013] Gildemeister (2013). Treasure island. http://energy.gildemeister.com/en/company/news/pellworm-cellcube-installation/261096. Accessed 27 April 2017.

[Gipe, 2004] Gipe, P. (2004). *Wind Power - Renewable Energy for Home, Farm, and Business*. Chelsea Green Publishing Company.

[Godina et al., 2015] Godina, R., Rodrigues, E. M. G., Matias, J. C. O., and Catalão, J. P. S. (2015). Sustainable energy system of el hierro island. In *International Conference on Renewable Energies and Power Quality (ICREPQ'15)*, volume 1, pages 46–51.

[Green et al., 2017] Green, M. A., Emery, K., Hishikawa, Y., Warta, W., Dunlop, E. D., Levi, D. H., and Ho-Baille, A. W. Y. (2017). Solar cell efficiency tables (version 49). *Progress in Photovoltaics: Research and Applications*, 25(1):3–13.

[Hallam et al., 2012] Hallam, C. R. A., Alarco, L., Karau, G., Flannery, W., and Leffel, A. (2012). Hybrid closed-loop renewable energy systems: El hierro as a model case for discrete power systems. In *2012 Proceedings of PICMET '12: Technology Management for Emerging Technologies*, pages 2957–2969.

[Hansen et al., 2016] Hansen, C. W., Stein, J. S., Deline, C., MacAlpine, S., Marion, B., Asgharzadeh, A., and Toor, F. (2016). Analysis of irradiance models for bifacial pv modules. In *2016 IEEE 43rd Photovoltaic Specialists Conference (PVSC)*, pages 0138–0143.

[Hasanuzzaman et al., 2016] Hasanuzzaman, M., Malek, A., Islam, M., Pandey, A., and Rahim, N. (2016). Global advancement of cooling technologies for {PV} systems: A review. *Solar Energy*, 137:25–45.

[Hassaine et al., 2014] Hassaine, L., OLias, E., Quintero, J., and Salas, V. (2014).

Overview of power inverter topologies and control structures for grid connected photovoltaic systems. *Renewable and Sustainable Energy Reviews*, 30:796–807.

[Hernández-Moro and Martínez-Duart, 2013] Hernández-Moro, J. and Martínez-Duart, J. (2013). Analytical model for solar pv and csp electricity costs: Present lcoe values and their future evolution. *Renewable and Sustainable Energy Reviews*, 20:119–132.

[HOMER Energy, 2016] HOMER Energy (2016). *HOMER Pro Version 3.7 User Manual*.

[Honsberg and Bowden, 2015] Honsberg, C. and Bowden, S. (2015). Pv education. http://pveducation.org/pvcdrom. Accessed 4 Oct 2016.

[Howell,] Howell, M. Solar cells, modules, and arrays. https://pveducation.com/solar-concepts/solar-cells-modules-arrays/. Accessed 9 March 2017.

[(IEA), 2016] (IEA), I. E. A. (2016). World energy outlook. Technical report, IEA.

[IEC, 2012] IEC (2012). Grid integration of large-capacity renewable energy sources and use of large-capacity electrical energy storage. Technical report, IEC.

[(IHA), 2015] (IHA), I. H. A. (2015). 2015 hydropower status report. Technical report, IHA. `https://www.hydropower.org/2015-hydropower-status-report`.

[Instruments, 2016] Instruments, A. (2016). Owner's manual pyranometer - models sp-110 and sp-230. http://www.apogeeinstruments.co.uk/content/SP-110-manual.pdf. Accessed 7 Nov 2016.

[IRENA, 2015] IRENA (2015). Renewable power generation costs in 2014. Technical report, IRENA.

[ISET and SMA,] ISET and SMA. Kythnos island - 20 years' experience of system technology for renewable energies. `http://www.globalislands.net/greenislands/docs/greece_kythnos.pdf`.

[Jain and Jhunjhunwala, 2007] Jain, D. R. and Jhunjhunwala, B. (2007). *Business Statistics*. Tata McGraw-Hill Publishing Company Limited.

[Joge et al., 2002] Joge, T., Eguchi, Y., Imazu, Y., Araki, I., Uematsu, T., and Matsukuma, K. (2002). Applications and field tests of bifacial solar modules. In *Conference Record of the Twenty-Ninth IEEE Photovoltaic Specialists Conference, 2002.*, pages 1549–1552.

[Jordan and Kurtz, 2012] Jordan, D. C. and Kurtz, S. R. (2012). Photovoltaic degradation rates - an analytical review. Technical report, NREL.

[Kalogirou, 2014] Kalogirou, S. A. (2014). *Solar Energy Engineering - Processes and Systems*. Elsevier, second edition.

[Kjeller Vindteknikk, 2009] Kjeller Vindteknikk (2009). Vindkart for norge, aarsmiddelvind i 80m hoeyde. Technical report, Kjeller vindteknikk for NVE. Available from `https://www.nve.no/media/2462/vind_80m_kartbok1a_4140.pdf`.

[Koopmann et al., 2014] Koopmann, S., Nicolai, S., and Schnettler, A. (2014). Multifunctional operation of a virtual power plant in an active distribution grid: Modelling approaches and first field test experiences from the smartregion pellworm project. In *IEEE PES Innovative Smart Grid Technologies, Europe*, pages 1–6.

[Kreith, 2014] Kreith, F. (2014). *Principles of Sustainable Energy Systems*. CRC Press.

[Kropopski et al., 2006] Kropopski, B., Basso, T., Deblasio, R., and Friedman, N. R. (2006). *Interconnection of Alternative Energy Sources with the Grid*, pages 354–378. John Wiley & Sons, Inc.

[Li and Qiu, 2016] Li, F.-F. and Qiu, J. (2016). Multi-objective optimization for integrated hydro–photovoltaic power system. *Applied Energy*, 167:377–384.

[Manwell et al., 2009] Manwell, J. F., McGowan, J. G., and Rogers, A. L. (2009). *Wind Energy Explained - Theory, Design and Application*. John Wiley & Sons Ltd., second edition.

[Massey and Ward-Smith, 2006] Massey, B. and Ward-Smith, J. (2006). *Mechanics of Fluids*. Taylor and Francis.

[Mousazadeh et al., 2009] Mousazadeh, H., Keyhani, A., Javadi, A., Mobli, H., Abrinia, K., and Sharifi, A. (2009). A review of principle and sun-tracking methods for maximizing solar systems output. *Renewable and Sustainable Energy Reviews*, 13(8):1800–1818.

[Multiconsult, 2013] Multiconsult (2013). Kostnadsstudie, solkraft i norge 2013. Technical report, Enova SF.

[Nelson, 2003] Nelson, J. (2003). *The Physics of Solar Cells*. Imperial College Press.

[Niayifar and Porté-Agel, 2016] Niayifar, A. and Porté-Agel, F. (2016). Analytical modeling of wind farms: A new approach for power prediction. *Energies*, 9(9).

[NIBIO,] NIBIO. Landbruksmeteorologisk tjeneste. `lmt.bioforsk.no`. Accessed May 2017.

[Nord Pool,] Nord Pool. Historical market data. http://www.nordpoolspot.com/historical-market-data/. Accessed 21 April 2017. Excel-file named *Elspot Prices_2016_Hourly_NOK.xls*.

[NREL, 2017] NREL (2017). Best research-cell efficiencies. `https://www.nrel.gov/pv/assets/images/efficiency-chart.png`. Accessed May 2017.

[NVE, a] NVE. Nve kartsystem nettanlegg. http://gis3.nve.no/link/?link=nettanlegg. Accessed 8 Dec 2016.

[NVE, b] NVE. Utbygd og ikke utbygd vannkraft. http://gis3.nve.no/link/?link=vannkraft. Accessed 9 Dec 2016.

[NVE, 2017] NVE (2017). Et norsk-svensk elsertifikatmarked - aarsrapport for 2016. Technical report, NVE. Available at `https://www.nve.no/energiforsyning-og-konsesjon/elsertifikater/siste-nytt-om-elsertifikater/arsrapport-for-elsertifikater-2016/`.

[Osborne, 2008] Osborne, J. W., editor (2008). *Best Practices in Quantitative Methods*. SAGE Publications.

[Ovhed, 2016] Ovhed, M. (2016). Norske steder blant de toerreste i europa. `http://www.yr.no/artikkel/norske-steder-blant-de-torreste-i-europa-1.13096592`. Accessed May 2017.

[Patel, 2006] Patel, M. R. (2006). *Wind and Solar Power Systems: Design, Analysis, and Operation*. Taylor & Francis, second edition.

[Perez and Hoff, 2013] Perez, R. and Hoff, T. E. (2013). Solar resource variability. In Kleissl, J., editor, *Solar Energy Forecasting and Resource Assessment*, chapter 6. Elsevier.

[Peschel, 2015] Peschel, T. (2015). Germany's first large-scale photovoltaic plant is being refurbished. http://www.sunwindenergy.com/photovoltaics/germanys-first-large-scale-photovoltaic-plant-refurbished. Accessed 27 April 2017.

[Philips, 2017] Philips, T. (2017). China builds world's biggest solar farm in journey to become a green superpower. https://www.theguardian.com/environment/2017/jan/19/china-builds-worlds-biggest-solar-farm-in-journey-to-become-green-superpower. Accessed 25 April 2017.

[Plitt, 2015] Plitt, L. (2015). The greenest island in the world? http://www.bbc.com/news/magazine-34424606. Accessed 25 April 2017.

[Quaschning, 2005] Quaschning, V. (2005). *Understanding Renewable Energy Systems*. Earthscan.

[REN21, 2016] REN21 (2016). Renewables 2016 global status report. Technical report, REN21 Secretariat.

[Risso et al., 2017] Risso, A., Canales, F. A., Beluco, A., and Rossini, E. G. (2017). A pv wind hydro hybrid system with pumped storage capacity installed in linha sete, aparados da serre, southern brazil. In Kishor, N. and Fraile-Ardanuy, J., editors, *Modeling and Dynamic Behaviour of Hydropower Plants*, chapter 10, pages 205–221. The Institution of Engineering and Technology.

[Rizk and Chaiko, 2008] Rizk, J. and Chaiko, Y. (2008). Solar tracking system: More efficient use of solar panels. *World Academy of Science, Engineering and Technology*, (41):313–315.

[Roberts et al., 2017] Roberts, J. J., Zevallos, A. A. M., and Cassula, A. M. (2017). Assessment of photovoltaic performance models for system simulation. *Renewable and Sustainable Energy Reviews*, 72:1104–1123.

[Rodrigo et al., 2016] Rodrigo, P., Velázquez, R., and Fernández, E. F. (2016). Dc/ac conversion efficiency of grid-connected photovoltaic inverters in central mexico. *Solar Energy*, 139:650–665.

[Romero-Cadaval et al., 2013] Romero-Cadaval, E., Spagnuolo, G., Franquelo, L. G., Ramos-Paja, C.-A., Suntio, T., and Xiao, W.-M. (2013). Grid-connected photovoltaic generation plants: Components and operation. *IEEE Industrial Electronics Magazine*, 7(3):6–20.

[Ross, 2014] Ross, S. M. (2014). *Introduction to Probability and Statistics for*

Engineers and Scientists. Elsevier, fifth edition.

[Rosvold, 2016] Rosvold, K. A. (2016). Store norske leksikon: Skibotn kraftverk. http://snl.no/Skibotn_kraftverk. Accessed 9 Dec 2016.

[Sengupta et al., 2015] Sengupta, M., Habte, A., Kurtz, S., Dobos, A., Wilbert, S., Lorenz, E., Stoffel, T., Renné, D., Gueymard, C., Myers, D., Wilcox, S., Blanc, P., and Perez, R. (2015). Best practices handbook for the collection and use of solar resource data for solar energy applications. Technical report, National Renewable Energy Laboratory (NREL).

[Sharma, 2005] Sharma, A. K. (2005). *Text book of correlation and regression*. Discovery Publishing House.

[Sidelnikova et al., 2015] Sidelnikova, M., Weir, D. E., Groth, L. H., Nybakke, K., Stensby, K. E., Langseth, B., Fonneløp, J. E., Isachsen, O., Haukeli, I., Paulen, S.-L., Magnussen, I., Husabø, L. I., Ericson, T., and Qureishy, T. H. (2015). Kostnader i energisektoren - kraft, varme og effektivisering. Technical report, Norges vassdrags- og energidirektorat.

[Silvestre and Chouder, 2008] Silvestre, S. and Chouder, A. (2008). Effects of shadowing on photovoltaic module performance. *Progress in Photovoltaics: Research and Applications*, 16(2):141–149.

[Sinha and Chandel, 2014] Sinha, S. and Chandel, S. (2014). Review of software tools for hybrid renewable energy systems. *Renewable and Sustainable Energy Reviews*, 32:192–205.

[Skamarock et al., 2008] Skamarock, W. C., Klemp, J. B., Dudhia, J., Gill, D. O., Barker, D. M., Duda, M. G., Huang, X.-Y., Wang, W., and Powers, J. G. (2008). A description of the advanced research wrf version 3. Technical report, National Center for Atmospheric Research (NCAR).

[SMA Solar Technology AG,] SMA Solar Technology AG. Mv power station. `https://www.sma.de/en/products/system-solutions-packages/mv-power-station-2200sc-2500sc-ev.html`. Accessed May 2017.

[Solanki, 2015] Solanki, C. S. (2015). *Solar Photovoltaics - Dundamentals, Technologies and Applications*. PHI Learning Private Limited, third edition.

[SolarEdge Corporate,] SolarEdge Corporate. Power optimizer. http://www.solaredge.com/products/power-optimizer. Accessed 23 Mar 2017.

[Statnett, 2014] Statnett (2014). Energiskolen lærehefte. http://www.statnett.no/Global/Dokumenter/Milj

[Statnett, 2016a] Statnett (2016a). Balsfjord - skaidi - ny kraftledning. http://www.statnett.no/Nettutvikling/Balsfjord—Skaidi/. Accessed 9 Dec 2016.

[Statnett, 2016b] Statnett (2016b). Ofoten - balsfjord - ny kraftledning. http://www.statnett.no/Nettutvikling/Ofoten—Balsfjord/. Accessed 9 Dec 2016.

[Strauss and Kleinkauf, 2002] Strauss, P. and Kleinkauf, W. (2002). Re islands: Re hybrid systems integration. *Refocus*, 3(4):54–57.

[Taylor, 2012] Taylor, D. (2012). Wind energy. In Boyle, G., editor, *Renewable Energy - Power for a Sustainable Future*, chapter 7. Oxford University Press.

[Tiller, 2017] Tiller, C. (2017). Case study of a large-scale solar and wind power hybrid system at fakken wind farm, troms. Master's thesis, UiT the Arctic university of Norway.

[Troms Kraft, 2014] Troms Kraft (2014). Rieppi vindkraftverk og tilhoerende nettilknytning, konsesjonssoeknad med tekniske planer og konsekvensutredninger. Technical report, Troms Kraft.

[TromsKraft,] TromsKraft. Troms kraftforsyning og energi as. http://www.tromskraft.no/om/selskap/pronea. Accessed 9 Dec 2016.

[Wang et al., 2014] Wang, W., Bruyère, C., Duda, M., Dudhia, J., Gill, D., Kavulich, M., Keene, K., Lin, H.-C., Michalakes, J., Rizvi, S., and Zhang, X. (2014). Arw version 3 modeling system user's guide. Technical report, Mesoscale & Microscale Meteorology Division of National Center for Atmospheric Research.

[Weir, 2017] Weir, D. E. (2017). Vindkraft - produksjon i 2016. Technical Report 12, NVE.

[Wohlgemuth and Hermann, 2005] Wohlgemuth, J. and Hermann, W. (2005). Hot spot tests for crystalline silicon modules. In *Conference Record of the Thirty-first IEEE Photovoltaic Specialists Conference, 2005*, pages 1062–1063.

[Yaramasu et al., 2015] Yaramasu, V., Wu, B., Sen, P. C., Kouro, S., and Narimani, M. (2015). High-power wind energy conversion systems: State-of-the-art and emerging technologies. *Proceedings of the IEEE*, 103(5):740–788.

[Øystein Kleven,] Øystein Kleven. Conversations with Øystein Kleven.

[Zaitsev et al., 2016] Zaitsev, D., Rehbinder, E., Heimdal, K., and Abbas, A. (2016). Solkraft i norge - fremtidige muligheter for verdiskapning. Technical report, WWF and Accenture.

[Zipp, 2015] Zipp, K. (2015). The new age in solar inverter covnersion efficiency: 99%. http://www.solarpowerworldonline.com/2015/02/new-age-solar-inverter-conversion-efficiency-99/#. Accessed May 2017.